# ANALYSIS OF STRIP EXCITED WAVEGUIDE SLOT

By

APU SIVADAS

DEPARTMENT OF ELECTRICAL ENGINEERING

INDIAN INSTITUTE OF TECHNOLOGY KANPUR
OCTOBER, 1996

Analysis of Strip Excited Waveguide Slot

A Thesis Submitted
in Partial Fulfillment of the Requirements
for the Degree of
Doctor of Philosophy

by
Apu Sivadas

to the

Department of Electrical Engineering

Indian Institute of Technology, Kanpur

October, 1996.

EE-1996-D-SIV-ANA

CERTIFICATE

It is certified that the work contained in the thesis entitled **Analysis of strip excited waveguide slot** by **Apu Sivadas**, has been carried out under my supervision and that this work has not been submitted elsewhere for a degree.

Dr. M. Sachidananda

Professor

Department of Electrical Engineering,

Indian Institute of Technology, Kanpur.

October, 1996

Synopsis

Waveguide fed slot arrays are extensively used in many Radar and microwave communication systems. Though there exist many types of slots which could possibly be used as radiating elements in an array, the longitudinal broad wall slot and the inclined narrow wall slot have received extensive consideration. Two other slots, namely the centered longitudinal slot and the vertical narrow wall non-wrap-around slot are recognized as ideal candidates to build an array due to their properties of having no cross-polarization and the ability to build a true linear array. The vertical narrow wall waveguide slot in particular is preferred, specifically in all applications where scanning in E-plane is desired. There have been a number of attempts at making the narrow wall waveguide slot radiate, by attaching metallic wires in the neighborhood of the slot. Specifically, this technique makes use of either a bent screw or a pair of tilted wires, attached to the edges of the slot to achieve the necessary coupling from the incident wave.

This thesis introduces a fundamentally different method of exciting the vertical narrow wall slot. It makes use of a thin printed strip behind the slot to excite it. The strip can either be inclined with respect to the slot or can take up an L shape. The slot, along with the exciting strip, can be printed simultaneously on a dielectric substrate and can replace the narrow wall of the waveguide. This method possesses all the advantages of the printed circuit technique and

therefore can achieve good accuracy and square ended slots, which are generally hard to achieve by the conventional slot machining process. The coupling to the slot can be adjusted predominantly by varying the strip inclination with respect to the slot. There exist several possible parameters in the structure which could be made use of in achieving the desired excitation level.

For the analysis, this structure is modeled as a coupled integral equation and is solved by the Method of Moments (MoM). The integral equations are set up by making use of the Green's functions of an inhomogeneously filled waveguide. The required Green's functions are derived using the standard technique of normal mode expansions. The analysis of this structure via. MoM turns out to be extremely involved due to the $e^{-\gamma|z-z'|}$ dependence of the waveguide Green's functions. This, together with the inclination of the strip along the axis of the waveguide, makes all the source and field domain variables coupled, resulting in serious implementation problems in setting up the MoM matrix. This thesis presents a systematic quadrature scheme for making this problem tractable and computationally efficient. The thesis also introduces algorithms for solving the eigenvalues of LSE and LSM normal modes in an inhomogeneously filled waveguide.

Among the Green's functions made use of in the analysis, it is found that, the Green's function corresponding to the axial E field due to an axial electric current is a true distribution, due to the presence of the Dirac delta function. Method of computing the E_z field, in cases where one of the source domain quadratures are dropped, leads to divergence in the series representing the E_z field. This problem is identified as one involving the correct interpretation of distributions, and is solved by representing the singularity as an orthonormalized LSM series. Since the LSM eigenfunctions are not orthonormal to begin with, they are orthonormalized using Gram-Schmidt procedure. Algorithms for orthonormalization of functions through Gram-Schmidt procedure has been developed. This result will have implications in cases where an axial radiating

source in an inhomogeneously filled waveguide is considered.

A program is developed which computes the S parameters, equivalent circuit, slot voltage and higher order mode scattering coefficients etc. Extensive parametric studies are conducted by varying strip offset, strip angle, strip length, slot width, substrate thickness and substrate permittivity.

In order to validate the theoretical model, experiments are carried out at X-band. Waveguides with a part of the narrow wall machined off are used to fabricate the test pieces. A dielectric substrate, printed with the slot and the exciting strip on either side, is fitted into the waveguide in the region where the narrow wall is machined off. Through Reflect Line (TRL) calibration is used to establish the measurement plane at the center of the slot. The necessary TRL calibration standards are fabricated in the laboratory. The measurements are done on a HP8510C vector network analyzer. Experiments are also conducted to ascertain the effect of the ground plane.

The present study on the strip excited waveguide slot indicates the suitability of this structure in building planar arrays working at Ku-band and beyond. It is possible to build a planar array, by attaching, a printed dielectric substrate consisting of slots and exciting strips to a machined waveguide channel. An array of this type has all the slots along the array axis and does not suffer from the problem of cross-polarization.

●●●

to my father, mother and brother

Acknowledgments

I AM indebted to Dr M. Sachidananda for proposing this problem As my guide, he understood me completely in the sense that, he gave me the idea and let me free. To be precise, he let me think and do whatever I thought best for the thesis—a privilege few individuals can opt for. It was clear that he wanted me to develop the necessary analytical background and work myself up. Except when I had to make measurements, and he knew very well that I would need help. While on experiments, he set me into working systematically and even helped make measurements. Though I have not done much experiments, I wish I could do so, especially since I was with him.

Apart from Dr. M. Sachidananda, I was considerably been influenced by Dr. R. K. S. Rathore and Dr. P. C. Das of Mathematics Department. I learned matrix, approximation and boundary value problems from them. This, as well as the interaction with Prof. Rathore has influenced many sections of this thesis. Though I have not made use of any well known results in their repertoire, I managed to conduct myself well in the analytical part of the thesis primarily due to this training.

I would like to thank Dr. Bharathi Bhat and Dr. S. K. Koul of CARE, Indian Institute of Technology, Delhi for letting us use the network analyzer system. Dr. S. Rengarajan, Dr. J. Joubert, Dr. Hashemi-Yeganeh and Dr. Amlan Datta provided various related documents.

Dr. Anjan Ghosh, Dr. Sanjay. K. Bose and Dr. M. U. Siddiqi have been exceptionally helpful at various occasions.

I thank my colleagues Harish A. R and Chaitanya Babu for being there with me. Harish and Chaitanya can rightfully be regarded as my co-guides since I used to discuss with them before presenting myself in front of Dr. M. Sachidananda (Nevertheless, we met him for every little thing!). Harish helped me make the measurements since I was unfamiliar with the instrumentation.

I am indebted to these great friends of mine: Sajith, George, Puranjoy, Arun Kumar and Srikanth in whose company I was genuinely happy. Shaffi and Jitendra Das provided Gnuplot and Ghost-view. The staff of both microwave lab and precision shop helped me do the experimental work.

<div align="right">Apu Sivadas</div>

Contents

List of Figures

List of Tables

Glossary of Symbols

$2l_l$	Length of the strip.
$2l_s$	Length of the slot.
$2w_l$	Width of the strip.
$2w_s$	Width of the slot.
a	Broad wall dimension of the waveguide.
A_x	Magnetic vector potential along x.
a'_m	First derivative of a_m.
$\mathbf{Ax = b}$	MoM matrix equation.
b	Narrow wall dimension of the waveguide.
B_{10}	Amplitude of LSE_{10} mode.
B_{20}	Amplitude of LSE_{20} mode.
BVP	Boundary Value Problem.
c	$k_0 t\sqrt{\epsilon_r - 1}$ in Section 3.3.
cal.	Calibration
comp	Stands for "compute" in code description.
d	Width of the air region.
DEC	Digital Equipment Corp.
EM	Electromagnetics
$E_y(J_y)$	Waveguide Green's function. E_y field due to J_y current.
$E_z(J_z)$	Waveguide Green's function. E_z field due to J_z current.

$E_y\|_{M_y}$	E_y component due to M_y current.
f	Operating frequency in GHz.
$\langle f_i, f_j \rangle$	Real inner product between f_i and f_j.
f_{il}	ith basis function on the strip (longitudinal variation) .
f_{is}	ith basis function on the slot (longitudinal variation) .
f_{jl}	jth test function on the strip (longitudinal variation).
f_{js}	jth test function on the slot (longitudinal variation).
F_x	Electric vector potential along x.
F_y	Electric vector potential along y.
$f_{meas.}$	Measured resonant frequency.
f_{theory}	Computed resonant frequency.
$\|g_k\|$	Norm of g_k.
$H_y^{ext}\|_{M_y}$	H_y component due to M_y current via. slot exterior.
HP	Hewlett Packard.
$H_y^{ext}(M_y)$	Half space Green's function. H_y field due to M_y current.
$H_y\|_{J_z}$	H_y component due to J_z current.
$H_y(M_y)$	Waveguide Green's function. H_y field due to M_y current.
I	2×2 identity matrix.
i	Index to basis function: ith basis function.
I_0	Modified Bessel function of order 0.
I_1	Modified Bessel function of order 1.
j	$\sqrt{-1}$
j	Index to testing function. jth testing function.
k_0	$(\omega^2 \epsilon_0 \mu)^{1/2}$.
k	$(\omega^2 \epsilon_0 \epsilon_r \mu)^{1/2}$.
LSE_{mn}	The mnth LSE hybrid mode.
LSM_{mn}	The mnth LSM hybrid mode.
M_{max}	Number of modes summed in the x direction.

MoM	Method of Moment.
NAG	Numerical Algorithms Group.
N_l	Number of basis functions on the strip.
N_{max}	Number of modes summed in the y direction.
N_s	Number of basis functions on the slot.
O	Order notation.
PDE	Partial Differential Equation.
P_{rad}	Normalized radiated power.
r	d/t in Section 3.3.
s	Ratio of plate spacing to the distance below the iris.
R_{loss}	Resistance accounting for the losses in strip.
ROS	stRip On Slot interaction submatrix.
RSE	stRip SElf interaction submatrix.
S	Scattering matrix = $\begin{bmatrix} S_{11} & S_{12} \\ S_{21} & S_{22} \end{bmatrix}$.
$\mathcal{S}_{LSE}$	Term corresponding to LSE in $E_z\|_{J_z}$.
$\mathcal{S}_{LSM}$	Term corresponding to LSM in $E_z\|_{J_z}$.
SNT	Slot iNTernal interaction submatrix.
SOR	Slot On stRip interaction submatrix.
S'_R, S_R	Strip domain regarded for source/test.
S'_S, S_S	Slot domain regarded for source/test.
SSE	Slot SElf interaction submatrix.
SXT	Slot eXTernal interaction submatrix.
t	Thickness of substrate.
$[T]$	T-network.
$Tx = y$	Operator equation (first kind).
tr	tr stands for sin or cos. $\mathrm{tr}\,x$ stands for $\sin x$ or $\cos x$.
TRL	Thru-Reflect-Line (calibration standard).
UG-39/U	X Band brass flange designation.

(u', v')	Strip coordinate system as source domain.
(u, v)	Strip coordinate system as test domain.
u_1	LSE eigenvalue on air side.
u_2	LSE eigenvalue on dielectric side.
v_1	LSM eigenvalue on air side.
v_2	LSM eigenvalue on dielectric side.
VNA	Vector Network Analyzer.
V_s, V_k	Voltage at the slot center.
WR-90	X Band waveguide designation.
x_0	Starting value of LSE, LSM root finding.
x_N	$\sum_{i=1}^{N} I_i e_i$. The Nth approximate solution of $Tx = y$.
y_A	y coordinate of salient point labeled A. See Fig. 2.6
y_l	y coordinate of the strip center.
(y', z')	Global coordinate system as source domain.
y_s	y coordinate of the slot center.
y_t	Normalized T-network shunt admittance.
(y, z)	Global coordinate system as test domain.
Z	Normalized Z matrix $= \begin{bmatrix} z_{11} & z_{12} \\ z_{21} & z_{22} \end{bmatrix}$.
z_1	Normalized T-network series (left) impedance.
z_2	Normalized T-network series (right) impedance.
z_E	z coordinate of salient point labeled E. See Fig. 2.6
z_l	z coordinate of the strip center.
z_t	Normalized T-network shunt impedance.
α	$\sin \theta$
κ	Stands for regularizer in Section 3.6.
β	$\cos \theta$
ϵ_r	Relative permittivity of substrate.

ϵ_N	min $\left\|T\left(\sum_{i=1}^{N} I_i e_i\right) - y\right\|$ over $I_1, I_2, \ldots, I_N$.
ε	Maximum absolute error of MoM matrix entry.
γ	Propagation constant without reference to mode.
γ_e	Propagation constant of LSE mode.
γ_m	Propagation constant of LSM mode.
λ_0	Free space wavelength.
λ_g	Guide wavelength for LSE_{10} mode.
ϕ	Transverse variation without referring to domain.
ϕ_l	Transverse variation of strip basis.
ϕ_s	Transverse variation of slot basis.
$\Theta, \Theta(z - z')$	Heaviside signum function (sign of $z - z'$).
θ	Strip inclination.
θ_{max}	Maximum allowable strip inclination ($\tan^{-1}(l_l/w_l)$).
ω	$2\pi f$. Operating frequency in rad/s.

Chapter 1

Introduction

1.1 Introduction

Rectangular waveguide slot array antenna has been quite popular in large high power radars. Although a variety of slot configurations on a rectangular waveguide have been studied and reported in the literature, the broad wall offset slot and the narrow wall inclined slot have been the configurations chosen in most of the practical antennas, for their simplicity. For designing a high performance antenna with very low side-lobes, the accuracy of excitation control is of paramount importance. Thus, a very accurate evaluation of the characteristics of the slot has received considerable attention among the researchers.

There seems to be always a conflict between the slot geometry that can be analyzed relatively easily, and the slot geometry that can be fabricated easily. For example, a round ended slot is easier to machine than a square ended slot; but the analysis of a round ended slot is very difficult compared to the square ended one. Ultimately, from the cost considerations, the geometry that is easier

to fabricate is invariably chosen in practical antennas.

Assuming that accurate slot characterization is available, the rectangular waveguide slot array has some limitation, while using broad wall offset slots or inclined narrow wall slots in array configuration. In the first case, the array is no longer a linear array because of positive and negative offsets as well as the need to vary the offsets along the array. This introduces a second order perturbation in the pattern which can be troublesome while designing low side lobe antenna. In the second case, the slot inclinations produce a cross-polar component off axis, which cannot be reduced beyond a certain level.

The rectangular waveguide slot reported in this thesis is the result of a search for an ideal radiating element that can ameliorate most of the drawbacks mentioned earlier. However, this geometry is best suited for antenna arrays at higher microwave and millimeter wave frequencies, where the smaller size of the antenna allows the application of printed circuit technology in the fabrication.

The present work introduces a narrow wall vertical slot which is excited by a short strip, printed and kept behind the slot. The strip can be inclined with respect to the slot, or takes an L shape. The strip and the slot can be *printed* simultaneously on a dielectric substrate and can replace the narrow wall. Since the strip does not touch the waveguide walls, this excitation scheme can be regarded as electromagnetically coupled. The resonant frequency and the admittance level of the slot can be controlled, over a wide range, by changing the parameters of the strip. The use of printed circuit technique gives good dimensional accuracy, square ends and no wall thickness—features difficult to achieve with the conventional slot machining process.

1.2   Background and Motivation

1.2.1   Conventional Radiating Slots

A - Centered Longitudinal (Non Radiating)
B - Offset Longitudinal
C - Transverse
D - Centered Rotated
E - Offset Rotated (Compound)
F - Narrow wall vertical (Non Radiating)
G - Narrow wall inclined
H - Vertical Non wraparound (Non Radiating)
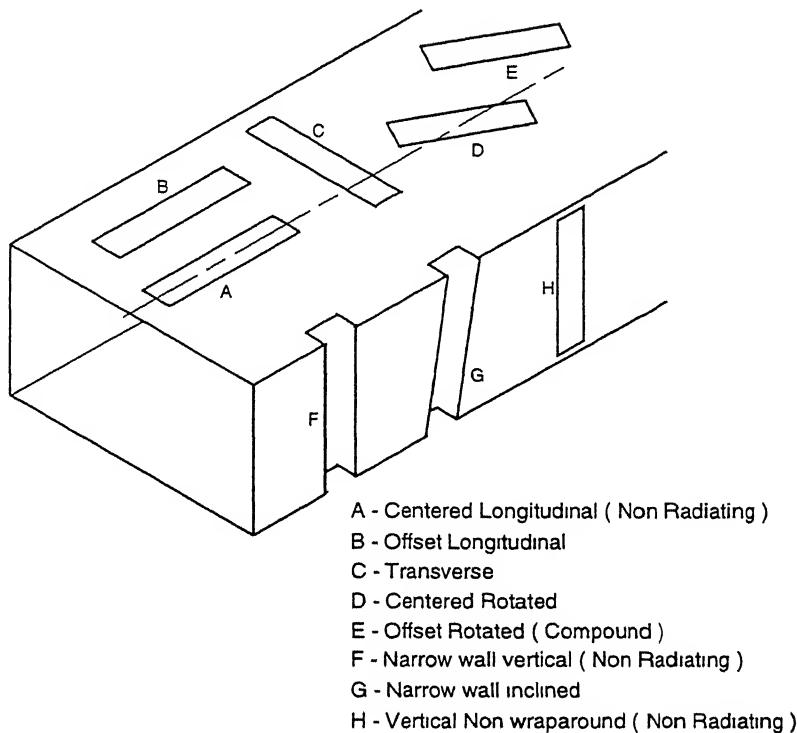
Figure 1.1: Types of waveguide slots.

A slot on a waveguide radiates if it is cut across the current flow lines of the dominant mode. Of the eight slots shown in Fig. 1.1, all the slots with the exception of (A), (F) and (H) are radiating. For example, the slot (A) does not radiate, because the TE_{10} wall currents are zero at the broad wall center line. The slots (F) and (H), do not radiate since they are cut *along* the current flow lines of the TE_{10} mode.

This principle, namely, *a slot radiates if it is cut across the current flow lines of the dominant mode*, can be used to identify the slots which radiate and the ones which do not. The same rule can be used, to decide how to perturb the

fields around the slot, so that a non-radiating slot is made radiating.

The wall current in the neighborhood of the slot decides the magnitude and phase of the radiated field. Consequently, the slot voltage can be adjusted in magnitude and phase, by changing the offset and/or inclination of the slot. For example, in the longitudinal offset slot (B), the radiated power goes up with the offset from the center line. For the compound slot (E), both the rotation and the location of the slot decides the slot voltage.

A waveguide with a series of slots is a good approximation to a linear array. A planar array is formed by stacking several linear arrays and feeding them appropriately. Since the voltage across each slot radiator is adjustable, an array of slots can synthesize a variety of radiation patterns.

The slots shown in Fig. 1.1, with the exception of the non-radiating ones, belong to the conventional slot repertoire. These slots, especially the longitudinal offset slot (B) has received wide attention and is well understood. The research on slot antennas began with Stevenson [1], and can be traced along the works of Oliner [2], Vu Khac [3], Yee [4], Lyon and Sangster [5], Park [6], Elliott [7], Joseffson [8], Rengarajan [9] and Joubert [10].

The literature on conventional slots is not surveyed here, since the present work falls in the class on non-radiating slots, and the attempts at making them radiating. A brief survey of longitudinal slots can be found in [7, 11]. Certain significant developments which are not mentioned in these references are discussed below.

The compound slot (E) can achieve any complex slot voltage, since the location and the angle can be varied. This property makes it attractive as a coupling and radiating element in a planar array. The principles of compound slots are now sufficiently well developed [12, 13, 14], so that compound slots can be used for realizing a variety of patterns.

The effect of TE_{20} mode, on the performance of arrays have been studied by Rengarajan [15] and Elliott [16]. The array design methodology of Elliott [16,

17, 18] is capable of incorporating the internal and external mutual coupling.
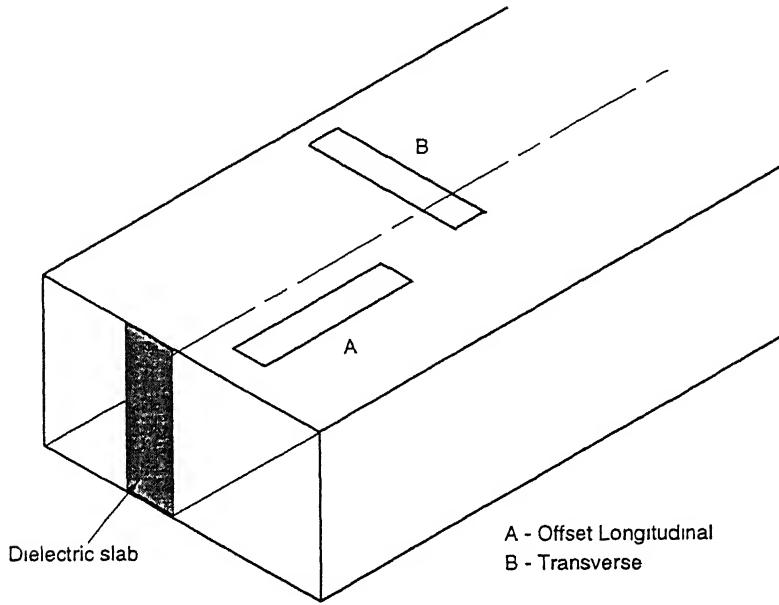
Figure 1.2: Slots on inhomogeneously filled waveguides [10].

For a weakly excited slot, two standard assumptions on the longitudinal offset slot analysis were shown to be erroneous by Espino [19] and Mc Namara [20]. It was shown that, the longitudinal component of the slot E-field cannot be ignored, and the transverse variation of the transverse E-field is not necessarily even about the slot center line.

Joubert [11] has analyzed slots on inhomogeneously filled waveguides. [See Fig. 1.2]. This work is relevant to the thesis, because the analysis of the strip excited slot also involves an inhomogeneously filled waveguide.

1.2.2   Broad Wall Slots that do not Radiate

In an array of centered slots, all the slots, line up along the broad wall center line. Therefore, the array is strictly linear unlike an array of longitudinal offset slots. Since all the slots are identical, the external mutual coupling can be
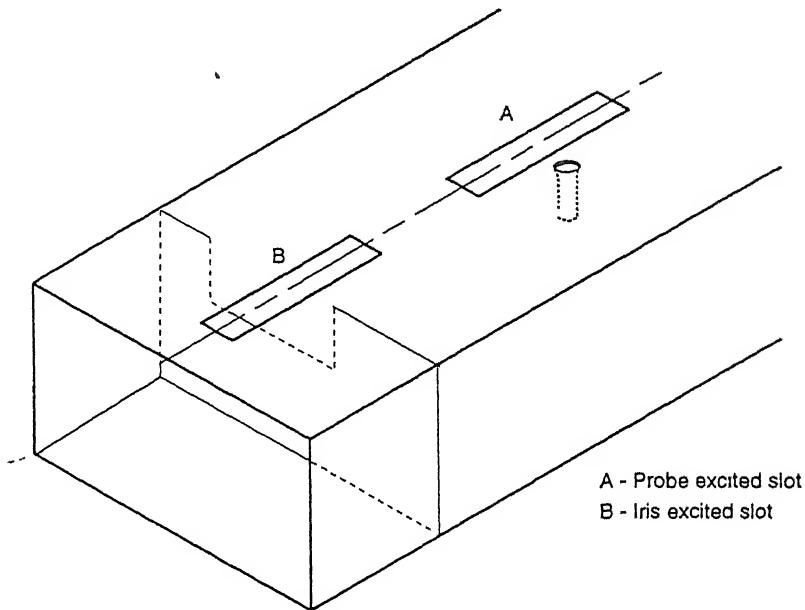
Figure 1.3: Excitation schemes for centered longitudinal slots [21, 22, 23].

incorporated once for all in the array design. These properties have prompted the following attempts for exciting the centered longitudinal slot.

Fig. 1.3 shows two methods of exciting the longitudinal centered slot. In method (A), which is due to Clapp [21], a vertical screw or a post introduces the necessary asymmetry in the TE_{10} mode fields. The coupling can be increased by increasing the depth of the screw. The polarity of the slot E-field can be flipped, if the screw is changed to the other side of the slot.

A. Datta et al. [23] have analyzed a variant of the Clapp method, where they consider two flat strips on either side of the slot. The analysis incorporates the waveguide wall thickness and can take care of arbitrary strip locations.

The method (B) in Fig. 1.3 has been proposed by Tang [22]. In this technique, an iris is introduced into the waveguide, such that, the waveguide fields are made asymmetrical. The slot radiates if the iris is offset from the broad wall center line.

This method combines various interesting features. The slot is a series

R–L–C circuit in shunt, while the iris is a parallel L–C circuit in shunt. Consequently, the reactances of the slot and the iris tend to cancel each other around the resonance. Therefore, the iris excited slot is noticeably broad band. The susceptance is relatively insensitive to the the iris offset, so that coupling and resonance are somewhat independent. The range of slot voltage control is significant that the author is able to achieve patterns with side lobes levels from 10–34 dB.

1.2.3   Narrow Wall Slots that do not Radiate

The attempts on the centered longitudinal slots remain limited to the iris and probe excited geometries or the variants thereof. However, the narrow wall vertical slots have received better attention. This is partly because narrow wall slots are preferred, if the beam is to be scanned in the E-plane.

Conventional narrow wall slot arrays consist of the inclined slots (G) shown in Fig. 1.1. The inclination of the slot leads to a cross-polar component in the radiated field. The presence of the cross polarization restricts the maximum achievable side lobe level, in a narrow wall inclined slot array. The cross-polar effects are more serious, if the slots are made more inclined as in an efficient array.

The narrow wall slots are generally cut through the narrow wall, so that a part of the slot lies on the broad wall, wrapped around. This happens because the resonant length of the slot usually exceeds the narrow wall dimension of the guide. The wrap around is undesirable for making a planar array since the adjacent waveguides cannot be stacked together. It also produces a discontinuous ground plane so that a standard mutual coupling evaluation cannot be carried out. The vertical slots considered up to the year 1989 were of the wrap-around type.

The vertical non-wrap around slot emerges as the ideal choice for a narrow
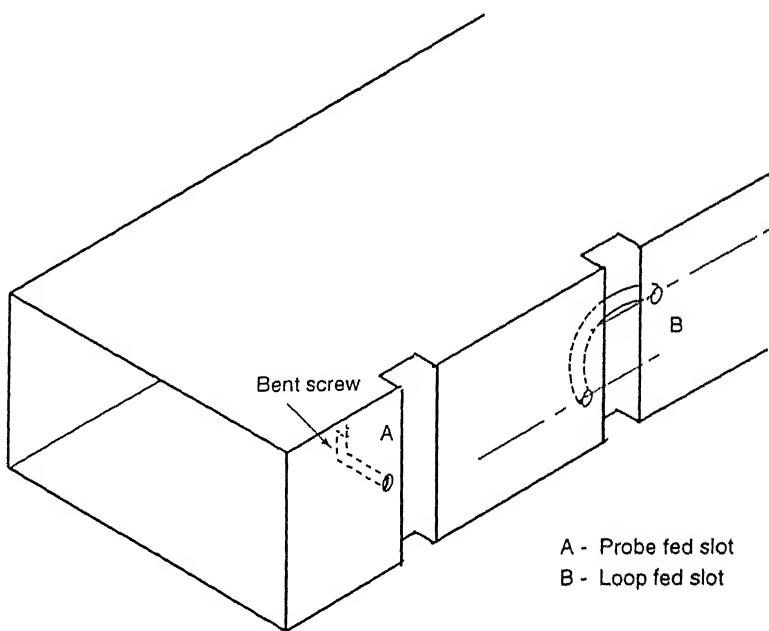
Figure 1.4: Excitation schemes for narrow wall slots from Clapp [21].

wall slot array. The attempts on vertical slot excitation also began with Clapp
[21]. Apart from certain variations, the ideas on narrow wall slot excitations
can be traced back to the following ideas of Clapp.

Fig. 1.4 shows the two well known methods of Clapp. In (A) a bent screw is
used to couple from the TE_{10} mode. In (B) a loop links the two sides of the slot.
We shall call these as probe fed and loop fed respectively. In the probe method,
the location and the length of the vertical part of the screw decides the coupling
to the slot. For the loop fed slot, the effective loop area in the transverse plane
decides the coupling. Therefore, rotating the screw, or twisting the loop changes
the radiated power. The polarity of the induced slot voltage can be flipped in
both cases.

J. S. Ajioka [24] introduced a method which came to be known as the Ajioka
element. With reference to Fig. 1.5, the Ajioka element consists of two inclined
metallic rods attached to the sides of the slot. The other end of the rods are at-
tached to the upper and lower broad walls respectively. The element is referred
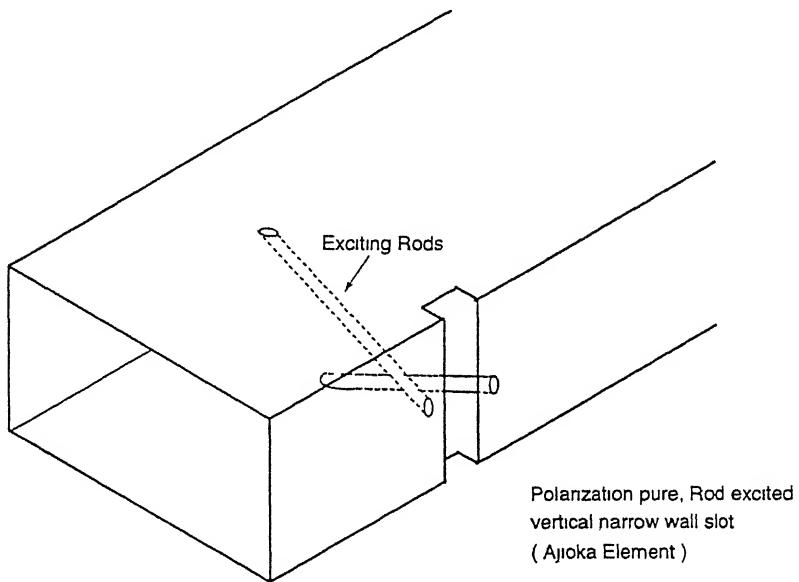
Figure 1.5: The Ajioka element [24].

to as "Polarization pure, rod excited transverse slot element". The inclination of the rods make them couple from the TE_{10} mode so that the slot is radiating.

Ajioka describes the design and implementation of a −40 dB side lobe, 15% bandwidth, 41 dB gain planar array at S-band. The coupling level was adjusted in this array, by altering the position of the rods on the narrow wall. The Ajioka element is the first reported use of a vertical narrow wall slot for a practical application.

Hashemi-Yeganeh and Elliott [25] modeled the Ajioka element with thin strips instead of rods. Method of moments with pulse and point matching were used for the analysis. They showed that, the slot in the Ajioka element need not be wrap-around, and can be confined to the narrow wall. That is, a slot which is shorter than the resonant length, can be made resonant via. loading by the rods. On one hand, this observation leads one to consider non-wrap around slots made resonant via. suitable loading. But the non-wrap around slots have lower bandwidth than full length slots. Thus the advantages of being non-wrap around comes at a loss of bandwidth.
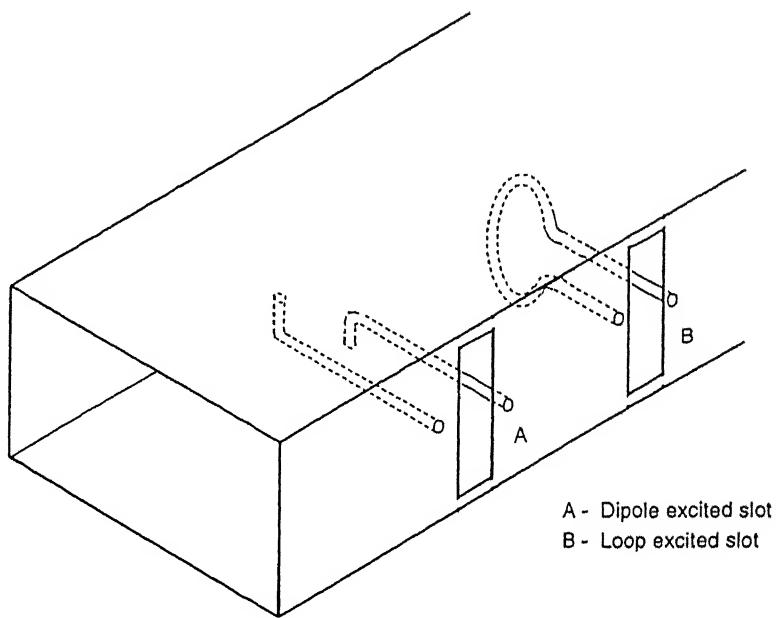
Figure 1.6: Variants to Ajioka and Clapp methods [26].

Two variants of the methods envisaged by Clapp and Ajioka are considered in [26]. As shown in Fig. 1.6, the slot is excited by a dipole or a loop kept within the waveguide. A pair of horizontal wires attach the dipole/loop to the slot. In the method described in this reference, the structure is viewed as a dipole/loop within the waveguide, loaded by a slot via. a two wire transmission line. Since the dipole cannot interact with the slot except via. the transmission line, the problem is decoupled and solved. That is, the impedance of the slot is found, which is then transferred to the dipole. The problem is thus reduced to that of the scattering by a loaded dipole within a waveguide.

There have been attempts at modifying the slot geometry itself, to counter the problems of wrap-around. The C-slot [28] and the I-slot [27] fall into this category. As shown in Fig. 1.7, the C-slot and the I-slot fit entirely into the narrow wall. It is possible to meet the resonant length due to the essential shape of the slot. Both C-slot and the I-slot has cross polar radiation and C-slot in particular, suffers from a poorly defined phase center.
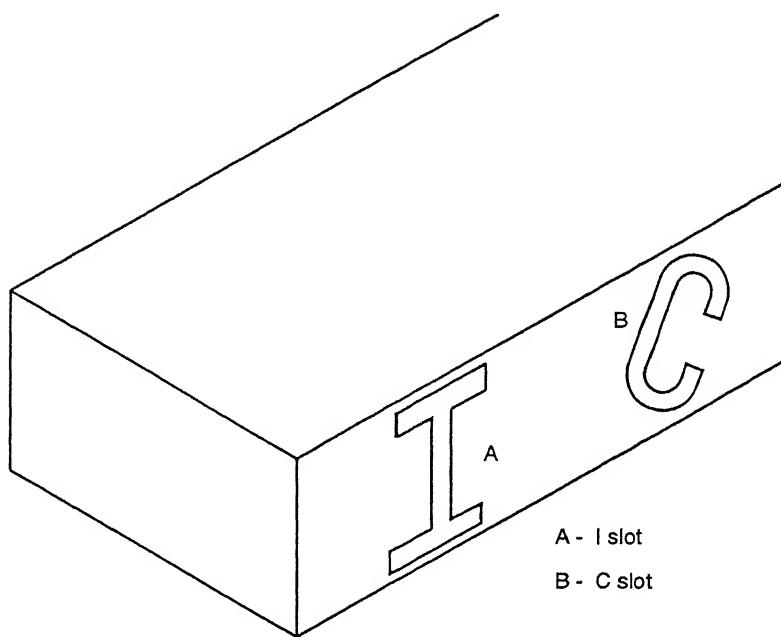
Figure 1.7: The I and C type narrow wall slots [27, 28].

A modification of Ajioka element has appeared recently as a patent [29]. They consider vertical wrap-around slots, excited by flat vertical plates. Each plate is right triangular such that the base and the height are kept fused to the waveguide walls. The technique appears close to the Ajioka element in the sense that the inclined wires are replaced by triangular plates.

1.3   Strip Excited Waveguide Slot

In this thesis, a fundamentally different method for exciting the narrow wall vertical non-wrap around slot is considered. Fig. 1.8 to 1.9 shows two views of the strip excited slot. The slot is excited by a metallic strip printed and kept behind the slot. The element can be viewed as an inhomogeneously filled waveguide with an inclined strip at the air-dielectric interface.

It is possible to fabricate this element by etching the strip and the slot,
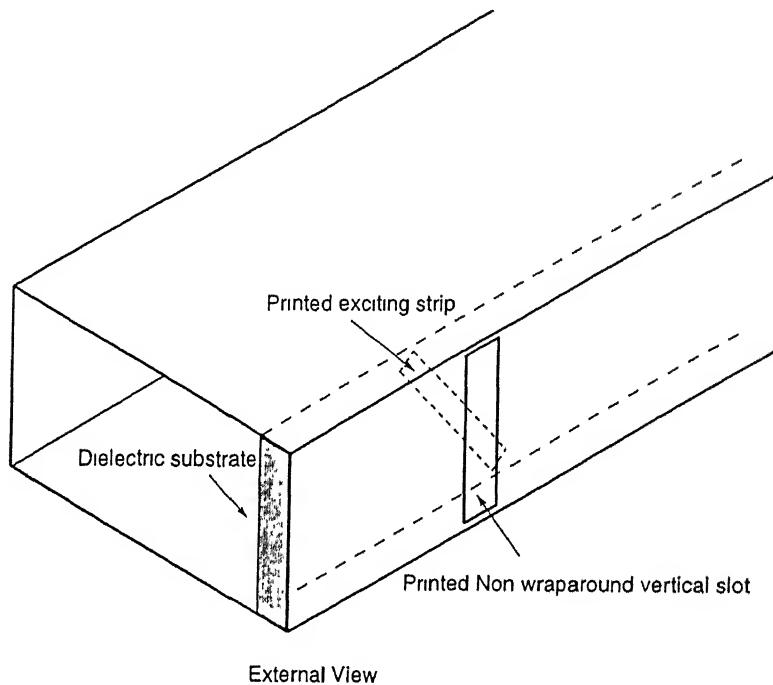
Figure 1.8: Printed strip excited narrow wall slot.
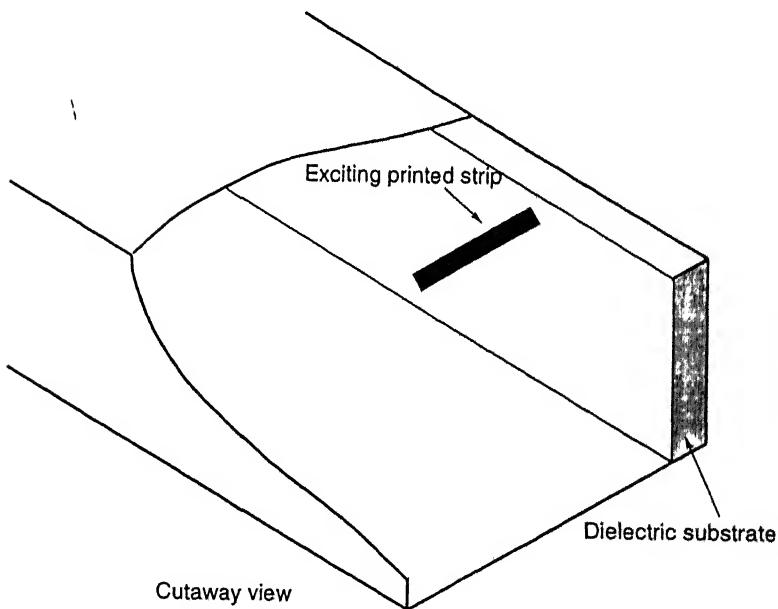
Figure 1.9: Cutaway view of printed strip excited slot.

simultaneously on a dielectric substrate. The use of printed circuit technique gives good dimensional accuracy and square ended slots. These are difficult and expensive to achieve with the conventional slot machining process.

The dominant mode of a guide with an E-plane dielectric slab is the LSE_{10} mode. The presence of a thin, low ϵ_r substrate does not significantly alter the mode structure of the waveguide. Therefore, the LSE_{10} mode is very close to the TE_{10} mode of the homogeneously filled waveguide.

The behavior of the strip excited slot can be explained making use of the following intuitive ideas. The LSE_{10} mode electric field is vertical and it drives a current along the strip. The strip current scatters on its own and alters the current flow pattern in the neighborhood of the slot. Note that, for exciting the vertical slot, it is sufficient to generate a vertical magnetic field. Thus, the incident wave couples to the vertical slot via. the inclined strip.

A - Inclined centered
B - Inclined offset vertical
C - Inclined offset horizontal
D - Inclined compound offset
E - L shaped
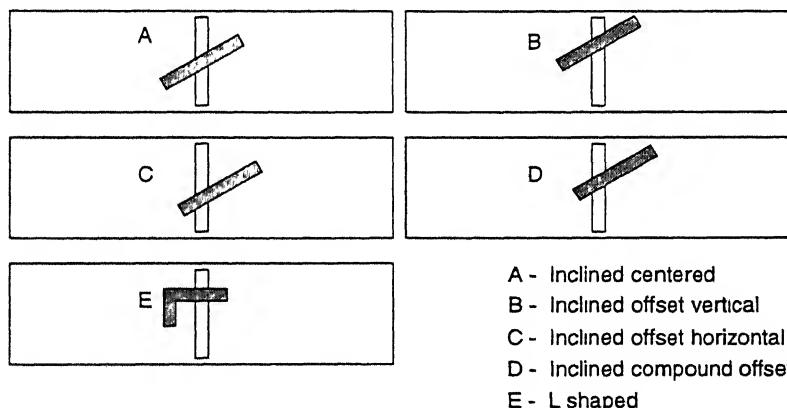
Figure 1.10: Different types of exciting strips.

The strip excited slot has numerous parameters that can be used to change the coupling level and the resonant frequency. The behavior of this element can be altered, by changing any of the following parameters: strip dimensions, slot dimensions, position of the strip with respect to the slot, substrate thickness or substrate permittivity.

If the slot dimensions and the substrate parameters are kept unaltered, a

substantial range of coupling can be achieved, by changing the strip inclination alone. The resonant frequency and the coupling are not independently controllable. However, a specific admittance at a given frequency can be achieved, by adjusting the strip length and the strip inclination together. It is also possible to flip the slot voltage by altering the strip inclination from positive to negative.

The slot can also excited by an L shaped strip instead of an inclined strip. Fig. 1.10 shows an L shaped strip, exciting the slot. The L-strip couples from the incident wave through the vertical part, while the strip to slot coupling takes place along the horizontal part. The inclined strip can also be moved relative to the slot, vertically, horizontally or both ways, as shown in Fig. 1.10. The slot radiates a little even in the extreme when the strip does not overlap the slot anywhere.

Fig. 1.11 shows the details of a suggested planar array schematic. The array is composed of a machined waveguide channel and a printed dielectric substrate. The upper side of the substrate is etched with radiating slots, whereas the bottom side consists of the exciting strips. The strips and the slots can be etched together as in a standard printed circuit fabrication. The substrate can be attached to the waveguide bottom channel, with screws via. the set of plated through holes on the substrate. This configuration is ideally suited for higher microwave frequencies including the millimeter waves.

1.4   Organization of the Thesis

This thesis investigates the behavior of the strip excited slot using both theoretical and experimental techniques. The strip excited slot has numerous parameters—nine parameters: strip and slot dimensions, strip angle, strip offsets, substrate thickness and permittivity—that affect its behavior. Therefore, theoretical results are made use of for an extensive parameter wise characteri-
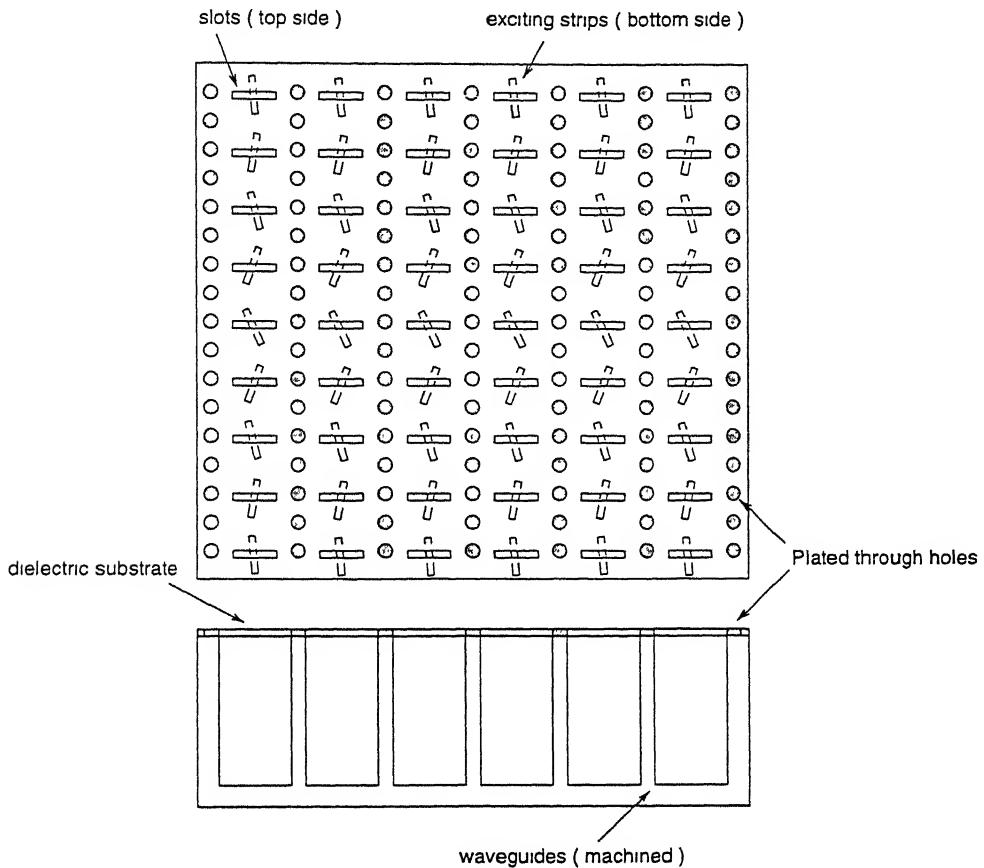
Figure 1.11: A suggested planar array configuration.

zation. The experimental results are used, primarily to validate the computed results. However, experimental results are used wherever computed results are unavailable. This includes the effect of the ground plane, losses etc.

In chapter 2, the strip excited slot is modeled as a boundary value problem in an inhomogeneously filled waveguide. A pair of coupled integral equations are used to enforce the boundary conditions, with Green's functions as kernels. Green's functions, for an inhomogeneously filled waveguide, and the half space are derived and elaborated upon in Chapter 3.

The implementation of this problem via. MoM is considerably involved, since the waveguide Green's functions contain the $e^{-\gamma|z-z'|}$ factor. For an inclined strip

in the axial direction, all the variables participating in the MoM matrix quadratures gets tied up. Since a total of 9 distinct Green's function are necessary for the solution, the closed form evaluation of MoM matrix entries becomes formidable.

An algorithm has been developed for implementing the MoM matrix quadratures. It is based on the identification of a multiple integral as a binary tree, and the exponential representation of trigonometric functions. This chapter also contains the computation of secondary parameters before dealing with coding and runtime details.

Chapter 3 deals with two kinds of topics: supplementary results necessary for the analysis of Chapter 2 and topics of an independent nature. Green's functions in an inhomogeneously filled waveguide are derived using the method of normal mode expansions. Since, the Green's function is a series in terms of the LSE and LSM modes, the solution of the LSE and LSM eigenvalues are dealt with subsequently. The eigenvalues are found using a combined Newton-Raphson-Bisection algorithm with good starting values and tight bounds.

Section 3.4 deals with a topic which has not been done elsewhere. The $E_z(J_z)$ Green's function is identified as a distribution since it contains a Dirac delta term, in addition to the LSE and LSM series. For a thin strip, the source domain quadrature along the thickness of the strip is neglected. This makes the E_z field to remain as a distribution. This problem manifests itself as a divergent LSM summation. It is shown that, for the E_z expressions to make sense (classically), it is necessary to represent the Dirac delta in terms of an orthonormalized LSM series. An algorithm for implementing the Gram-Schmidt procedure is developed in this connection. The numerical subtraction of Dirac delta is also shown to be an intrinsically unstable operation.

Method of moment (MoM) is widely used for solving integral equations in electromagnetics (EM). A careful evaluation of MoM as *numerical* method has not been carried out so far. MoM involves the straightforward implementation

of a very naive idea: the direct solution of the first kind integral equation. Since this problem belongs to the class of ill-posed problems, the solution becomes unstable after reaching a certain accuracy. In EM, this problem does not show up often (or goes unreported) partly because the right-hand-side is very smooth and known analytically while the kernel is not so smooth.

In Section 3.6, we illustrate the instability in MoM based on our examples as well as the works of S. W. Lee, R. Mittra and M. Leroy [30, 31, 32] in connection with the relative convergence phenomenon. The results indicate that the computed results depend on a parameter κ, and that the optimum choice of κ is a compromise between accuracy and stability. The instability in MoM is interpreted from the point of Tikhonov regularization.

Chapter 4 is on fabrication, measurements and the design of appropriate calibration standards. The test pieces are fabricated using a standard X-band waveguide with a part of the narrow wall machined off. The substrate is kept pressed from inside the waveguide, and is attached to the guide wall via. soldering. The S parameters are measured using a vector network analyzer using TRL standards, since the conventional waveguide standards are inconvenient for setting up the measurement plane in an inhomogeneously filled waveguide. This chapter contains the design and implementation of the appropriate TRL calibration standards. The effects of the ground plane and losses in the element are also illustrated.

Chapter 5 summarizes the behavior of the strip excited slot based on the computed and measured results of the previous chapters. The computed results are validated by comparing it with a select set of measurement. It is shown that the strip excited slot is a shunt discontinuity which goes through a series resonance. It is also shown that, the strip length and strip inclination can be used to realize a wide range of operating points. The effect of all the parameters in the strip excited slot are presented and interpreted qualitatively.

Chapter 6 deals with the conclusions and the ideas for future work.

Chapter 2

Analysis of Strip Excited

Waveguide Slot

2.1 Introduction

This chapter contains the complete discussion on the formulation, setting up and the solution of the strip excited slot as a boundary value problem. The formulation begins with the geometrical descriptions and the coordinate systems, and proceed to model the strip excited slot as a pair of coupled integral equations. The integral equations enforce the boundary conditions, and the Green's functions act as the kernels. The analysis requires 9 waveguide Green's functions and one external half space Green's function. These are derived and elaborated upon in the next chapter. Chapter 3 contains various issues related to the present analysis that it serves as a companion chapter to the present. Method of Moments is used to approximate the integral equations to a matrix

equation. Throughout the discussion, the structural aspect of the problem is emphasized and the necessary symbolism is developed.

The major problem in implementing the MoM lies in being able to do the MoM matrix quadratures analytically. The presence of the factor $e^{-\gamma|z-z'|}$ and the inclination of the strip along the waveguide axis lead to serious difficulties in representing the quadratures. An algorithm is developed for implementing these quadratures based on the realization that it is a problem in developing the requisite symbolism. The algorithm is based on 2 key ideas: the exponential representation of trigonometric functions, and the identification of a multiple integral with a binary tree. The major exceptions (division by zero, underflow etc.) and the restrictions of the algorithm are discussed. The number of function evaluations in the quadrature are estimated which indirectly suggest the simplifications possible in the implementation.

A systematic investigation of the secondary parameters that can be computed with the present analysis has been carried out. The set of useful parameters include—S matrix, T equivalent network, Slot voltage, LSE_{10} and LSE_{20} mode coefficients etc. A simplified model is put forward for evaluating the external mutual coupling to a first order. A brief discussion on the structure and organization of the code is included along with the details of CPU time requirements.

2.2   Geometry and Coordinate Systems

Fig. 2.1 shows the notations and the coordinate systems used for the analysis. The antenna consists of an infinite inhomogeneously filled waveguide. The dielectric substrate is printed with a slot and a strip as shown in the figure. The inhomogeneously filled waveguide is a rectangular waveguide of size $a \times b$ with an E-plane dielectric slab of thickness t and relative permittivity ϵ_r. The (x, y) coordinate system is used to specify quantities related to the waveguide.
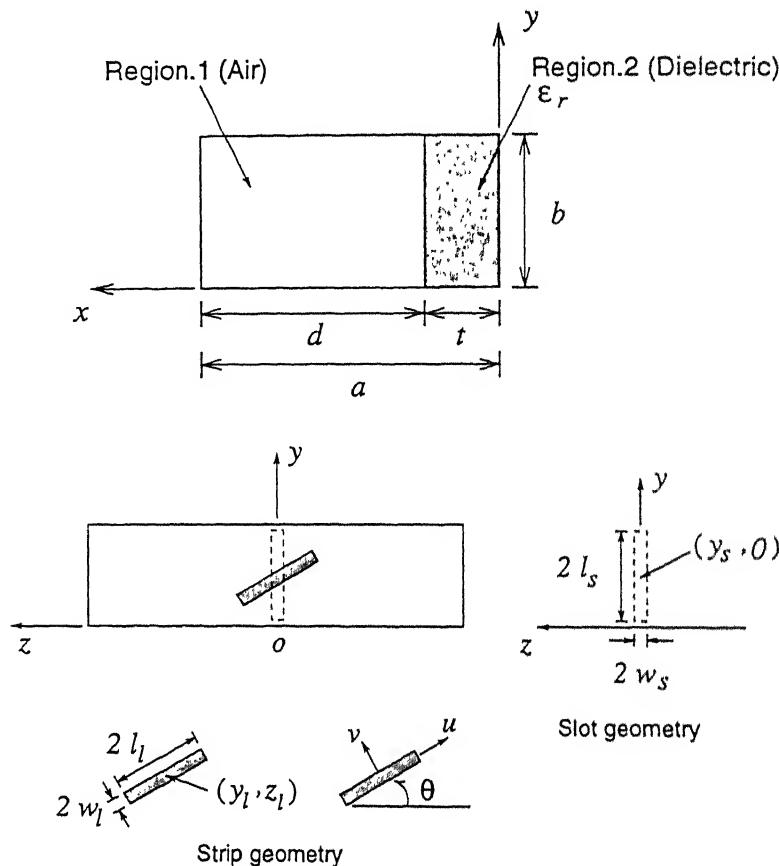
Figure 2.1: Geometry and coordinate systems

The strip of size $2w_l \times 2l_l$ makes an angle θ with the waveguide axis. Since it is possible to translate the strip with respect to the slot, we specify the coordinates of the center of the strip as (y_l, z_l). The (u, v) coordinate system is introduced at the center of the strip in order to facilitate the evaluation of various MoM matrix entries related to the strip. The transformation between (u, v) and (y, z) coordinates are given by,

$$y = y_l + \alpha u + \beta v \tag{2.1}$$

$$z = z_l - \beta u + \alpha v \tag{2.2}$$

$$u = \alpha(y - y_l) - \beta(z - z_l) \tag{2.3}$$

$$v = \beta(y - y_l) + \alpha(z - z_l) \tag{2.4}$$

where $\beta = \cos\theta$ and $\alpha = \sin\theta$.

The slot is vertical and has dimensions $2w_s \times 2l_s$. It is assumed to be centered at $z = 0$. The slot is generally kept centered on the narrow wall of the waveguide. However, the slot can be slightly offset on the narrow wall in practice. The parameter y_s specify the position of the center of the slot on the narrow wall. y_s is usually $b/2$ except when the slot is offset on the narrow wall.

2.3 Formulation of the Boundary Value Problem

2.3.1 Introduction

The strip excited slot can be fed by a propagating LSE_{10} mode from one end of the waveguide. It can also be excited by a plane wave incident externally on the slot. The first case corresponds to the case when the antenna is used for transmission, whereas the latter corresponds to the case when the antenna is used for reception. In general, the strip excited slot can be excited by any valid mode of the inhomogeneously filled waveguide. It can also be excited by another slot kept excited in the neighborhood. This is the approximate model used for computing the external mutual coupling in an array. One can thus identify various instances of exciting the element depending on the context in which the element is used. A formulation of the strip excited slot should be able to compute all the parameters of interest in any of these situations.

While formulating the strip excited slot as a boundary value problem, it is not necessary to pay attention to any specific method of excitation. Using the MoM, it will be shown that a boundary value problem can be reduced to the

solution of a matrix equation of the form $\mathbf{Ax} = \mathbf{b}$. The specific nature of the excitation decides the structure of $\mathbf{b}$, and the matrix $\mathbf{A}$ remains independent of the excitation scheme. Once the $\mathbf{A}$ matrix is formulated it is possible to compute any parameter of interest for any specific excitation. For the convenience of further discussion, we shall assume that the element is excited by a propagating LSE_{10} mode incident from $z = -\infty$. This is the primary method of excitation and the one that is used while making an S-parameter measurement. The alternate methods of excitation and the results therein are discussed in Section 2.5.

Consider an infinite inhomogeneously filled uniform rectangular waveguide containing the strip excited slot. The narrow wall containing the slot is assumed to be unbounded, so that the slot is part of an infinite ground plane. We shall assume the conductor and dielectric losses to be zero and no thickness whatsoever for the strip and the slot.

The incident wave causes a current flow on the strip and an E-field distribution in the slot. These sources can be regarded as induced sources causing a scattered field. (The electric field distribution can also be regarded as an induced source, by modeling it as a magnetic current, making use of Equivalence Theorem [33].) The scattered field together with the incident field has to satisfy all the necessary boundary conditions. In a boundary value problem, the boundary conditions are enforced to solve for the induces sources.

The following definitions will be adhered to throughout the discussion—J denote the electric current, whereas M denote the magnetic current; E stands for the electric field and H stands for the magnetic field; J_u and M_y denote the induced current in the directions indicated by the subscript; E_u and H_y denote the fields in the specified directions.

If the length to width ratio of the strip (slot) is large, it is generally acceptable to make certain approximations on the induced currents. It can be assumed that the strip current is entirely axial, whereas the slot E-field is entirely transverse. Note that, this amounts to considering only J_u and M_y and neglecting J_v and M_z
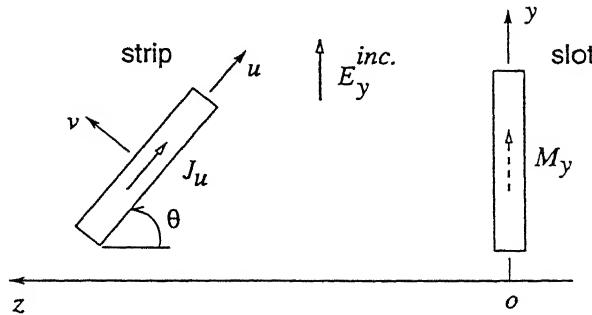
Figure 2.2: Induced currents and the incident field

components. [See Fig. 2.2]. Therefore, it is necessary to consider two induced sources, namely the electric current J_u on the strip, and the magnetic current M_y in the slot.

The total tangential E-field has to be zero on the strip, whereas the total tangential magnetic field has to be continuous across the slot. We introduce further approximations and enforce the boundary conditions only on the axial field components. That is, the total E_u field has to be zero on the strip, whereas the total H_y field has to be continuous at the slot. If the symbol $E|_M$ (for example) denote the E-field due to the source type M, then the boundary conditions can be stated as,

$$E_u|_{J_u} + E_u|_{M_y} = -E_u^{inc} \quad \text{on the strip} \tag{2.5}$$

$$H_y|_{J_u} + H_y|_{M_y} - H_y^{ext}|_{M_y} = 0 \quad \text{at the slot} \tag{2.6}$$

Equation 2.5 is a condition on E_u at the strip, whereas Equation 2.6 is a condition on H_y at the slot. The equations have been arranged such that, they suggest the matrix partitioning it will lead to, on application of MoM. The excitation is kept on the RHS of Equation 2.5 to 2.6, while the self and mutual interactions are on the LHS. Since the incident field does not have an H_y component the RHS of Equation 2.6 is zero. Had the slot been excited externally, the RHS of Equation 2.6 would be non-zero, while that of Equation 2.5 would

RSE - stRip SElf interaction
SOR - Slot On stRip
ROS - stRip On Slot
SNT - Slot iNTernal interaction
SXT - Slot eXTernal interaction
SSE - Slot SElf interaction
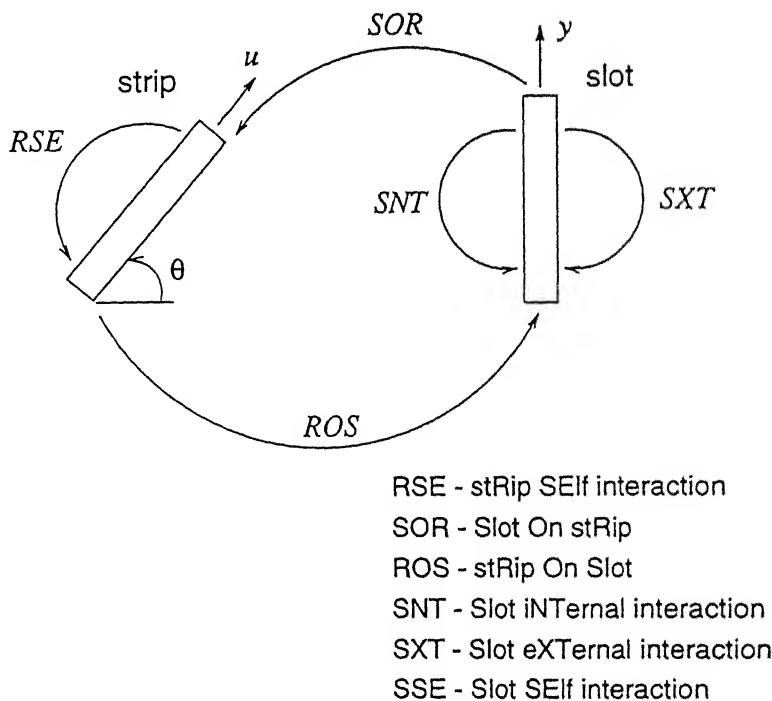
Figure 2.3: Illustrating the interactions

be zero.

Note that $E_u|_{J_u}$ is the E_u component at the strip due to the strip current J_u. $H_y|_{J_u}$ is the H_y component at the slot due to the strip current J_u and so on. Therefore, $E_u|_{J_u}$ is the strip's self interaction, whereas $H_y|_{J_u}$ is the strip's effect on the slot. Fig. 2.3 illustrates all the interactions between the strip and the slot. The abbreviations RSE, ROS etc. explained in Fig. 2.3 will be used to denote the submatrices resulting from MoM formulation. All the field components in Equations 2.5–2.6 except the $H_y^{ext}|_{M_y}$ are within the waveguide. $H_y^{ext}|_{M_y}$ is the H_y component due to the slot current M_y via. the external half space. Each term in Fig. 2.3 can be associated with the terms in Equations 2.5 to 2.6, so that

$$\underbrace{E_u|_{J_u}}_{RSE} + \underbrace{E_u|_{M_y}}_{SOR} = \underbrace{-E_u^{inc}}_{\text{source term}} \qquad \text{on the strip} \qquad (2.7)$$

$$\underbrace{H_y|_{J_u}}_{ROS} + \underbrace{\underbrace{H_y|_{M_y}}_{SNT} - \underbrace{H_y^{ext}\big|_{M_y}}_{SXT}}_{SSE} = 0 \qquad \text{at the slot} \qquad (2.8)$$

The scattered field components can be related to their respective sources via. Green's functions. Two types of Green's functions will be used, namely, the internal waveguide Green's functions and the external half space Green's function. Since, Green's functions relate the E, H fields to the sources in the (y, z) coordinate system, it is necessary to express (2.5–2.6) in terms of the (y, z) coordinate system.

With reference to Fig. 2.2, we have

$$J_y = \alpha J_u \qquad (2.9)$$

$$J_z = -\beta J_u \qquad (2.10)$$

$$E_u = \alpha E_y - \beta E_z \qquad (2.11)$$

so that

$$E_u|_{J_u} = \alpha E_y|_{J_u} - \beta E_z|_{J_u} \qquad (2.12)$$

$$E_y|_{J_u} = E_y|_{J_y} + E_y|_{J_z}$$

$$E_z|_{J_u} = E_z|_{J_y} + E_z|_{J_z}$$

$$E_u|_{M_y} = \alpha E_y|_{M_y} - \beta E_z|_{M_y} \qquad (2.13)$$

$$H_y|_{J_u} = H_y|_{J_y} + H_y|_{J_z} \qquad (2.14)$$

where $\alpha = \sin\theta$ and $\beta = \cos\theta$. By substituting (2.12–2.14) in (2.5–2.6), we get,

$$\alpha \left[E_y|_{J_y} + E_y|_{J_z} \right] - \beta \left[E_z|_{J_y} + E_z|_{J_z} \right] + \left[\alpha E_y|_{M_y} - \beta E_z|_{M_y} \right] = -\alpha E_y^{inc}$$

$$(2.15)$$

$$\left[H_y|_{J_y} + H_y|_{J_z} \right] + \left[H_y|_{M_y} - H_y^{ext}\big|_{M_y} \right] = 0 \qquad (2.16)$$

Section 3.1 contains the derivation and properties of the waveguide Green's functions. These relate the 3 field components E_y, E_z and H_y, to the 3 source types namely J_y, J_z and M_y. Section 3.5 discusses the external half space Green's function. The waveguide Green's functions $E_y(J_y)$, $E_y(J_z)$, ..., $H_y(M_y)$ and the external half space Green's function $H_y^{ext}(M_y)$ are defined such that,

$$E_y|_{J_y} = \int_{S'} E_y(J_y) \, J_y \, dS' \tag{2.17}$$

$$E_y|_{J_z} = \int_{S'} E_y(J_z) \, J_z \, dS' \tag{2.18}$$

$$\vdots$$

$$H_y|_{M_y} = \int_{S'} H_y(M_y) \, M_y \, dS' \tag{2.19}$$

$$H_y^{ext}\big|_{M_y} = \int_{S'} H_y^{ext}(M_y) \, M_y \, dS' \tag{2.20}$$

where $\int_{S'}$ stands for the integration in the respective source domain. By substituting (2.17–2.20) etc. in (2.15–2.16), we get the coupled integral equations in J_u and M_y.

$$\alpha \left[\int_{S'_R} E_y(J_y) \, J_y \, dS' + \int_{S'_R} E_y(J_z) \, J_z \, dS' \right] - \beta \left[\int_{S'_R} E_z(J_y) \, J_y \, dS' \right.$$

$$+ \int_{S'_R} E_z(J_z) \, J_z \, dS' \Bigg] + \left[\alpha \int_{S'_S} E_y(M_y) \, M_y \, dS' - \beta \int_{S'_S} E_z(M_y) \, M_y \, dS' \right]$$

$$= -\alpha \, E_y^{inc} \tag{2.21}$$

$$\left[\int_{S'_R} H_y(J_y) \, J_y \, dS' + \int_{S'_R} H_y(J_z) \, J_z \, dS' \right] + \Bigg[\int_{S'_S} H_y(M_y) \, M_y \, dS'$$

$$- \int_{S'_S} H_y^{ext}(M_y) \, M_y \, dS' \Bigg] = 0 \tag{2.22}$$

where $\int_{S'_R}$ represent quadrature over the strip, whereas $\int_{S'_S}$ represent quadrature over the slot. The prime on a domain (say S'_R) indicate that it is a source

domain.

2.3.2 Method of Moment Solution

Method of Moments (MoM) is used to solve the coupled integral equations in (2.21–2.22). A rigorous discussion of MoM can be found Section 3.6. The application of MoM to an integral equation of this type involves two distinct approximations: restricting the induced currents to a finite dimensional space, and enforcing the boundary conditions on a finite grid. We introduce a basis for J_u and M_y and assume the currents to be approximated by finite linear combinations. The choice of basis for strip and slot currents are governed by the boundary conditions the currents are to satisfy. The currents are such that,

strip basis functions   strip testing functions
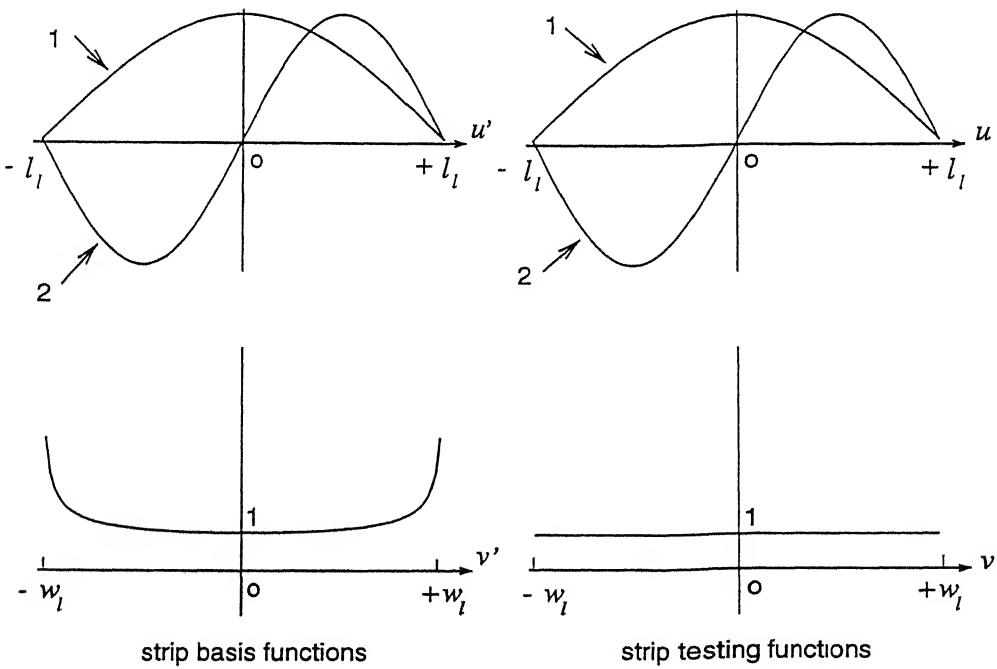
Figure 2.4: Basis and testing functions for the strip

$$J_u = 0 \quad \text{at} \quad u' = \pm l_l \tag{2.23}$$
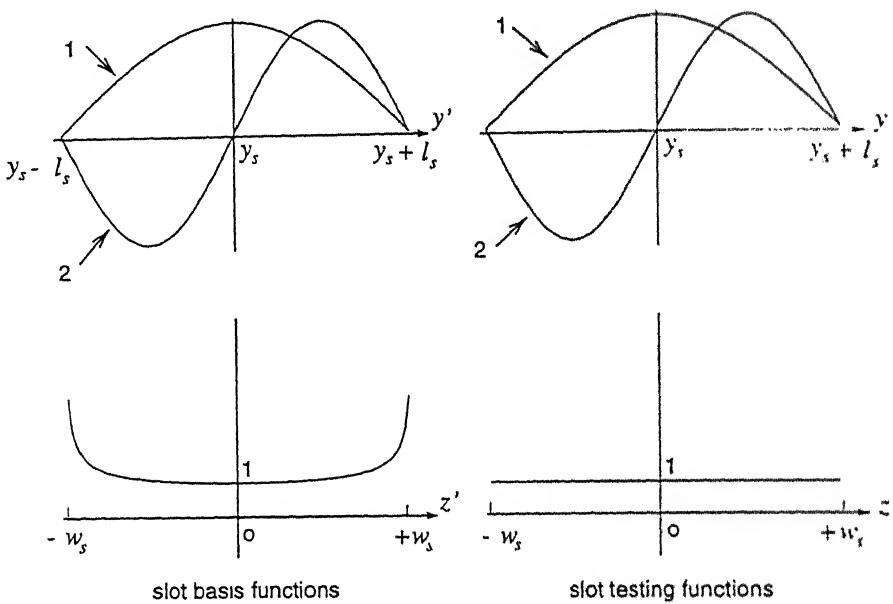
Figure 2.5: Basis and testing functions for the slot

$$M_y = 0 \quad \text{at} \quad y' = y_s \pm l_s \tag{2.24}$$

$$|J_u| \sim \left[1 - (v'/w_l)^2\right]^{-1/2} \quad \text{as} \quad v' \to \pm w_l \tag{2.25}$$

$$|M_y| \sim \left[1 - (z'/w_s)^2\right]^{-1/2} \quad \text{as} \quad z' \to \pm w_s . \tag{2.26}$$

(2.23–2.24) indicate that the currents vanish at the end points of their respective domains, whereas (2.25–2.26) describe the edge condition. The currents should have the inverse square root growth at the strip (slot) edges. Fig. 2.4 to 2.5 show the basis functions used for the strip and slot currents. Entire domain sinusoids are used in the axial direction, whereas an even edge current distribution is used along the transverse direction. The subscript "s" is used for the basis functions on the slot, while the subscript "l" is used for the basis functions on the strip. Therefore,

$$J_u = \sum_{i=1}^{N_l} I_i^l f_{il} \, \phi_l \tag{2.27}$$

$$M_y = \sum_{i=1}^{N_s} I_i^s f_{is} \phi_s \qquad (2.28)$$

where

$$f_{il} = \begin{cases} \cos k_{il} u', & \text{for} \quad i = 1, 3, \ldots \\ \sin k_{il} u', & \text{for} \quad i = 2, 4, \ldots \end{cases}$$

$$\phi_l = 1 \Big/ \sqrt{1 - (v'/w_l)^2}$$

$$k_{il} = i\pi \Big/ 2\, l_l$$

$$f_{is} = \begin{cases} \cos k_{is}(y' - y_s), & \text{for} \quad i = 1, 3, \ldots \\ \sin k_{is}(y' - y_s), & \text{for} \quad i = 2, 4, \ldots \end{cases}$$

$$\phi_s = 1 \Big/ \sqrt{1 - (z'/w_s)^2}$$

$$k_{is} = i\pi \Big/ 2\, l_s\,.$$

N_l and N_s are the number of strip and slot basis functions respectively. Note that both even and odd bases (f_i for all i) are used along the axial direction. This choice of bases accommodates every possible current distribution along the axial direction of the strip(slot), but constrain the transverse variation to be even symmetric. In general, it is necessary to have flexibility in the transverse direction as well. This choice of basis functions is widely used in slot discontinuity problems [7, 11].

Fig. 2.4 to 2.5 also show the test functions used in reducing the integral equations to matrix form. Entire domain sinusoids with constant transverse variation are used as test functions. The coupled integral equations are reduced to a matrix system $\mathbf{Ax = b}$, by substituting the expansions for J_u and M_y in (2.21–2.22), and taking inner product with the test functions. Equations (2.9–2.10) are used for expressing J_y and J_z in terms of J_u. Equation 2.21 gives rise to N_l equations via. inner product with N_l strip test functions, whereas Equation 2.22 gives rise to N_s equations via. inner product with N_s slot test

functions. The resulting matrix equation can be arranged as,

$$\underbrace{\begin{bmatrix} \text{RSE} & \text{SOR} \\ \text{ROS} & \text{SSE} \end{bmatrix}}_{A} \underbrace{\begin{bmatrix} \text{I}^l \\ \text{I}^s \end{bmatrix}}_{x} = \underbrace{\begin{bmatrix} -\text{E}^{\text{inc}} \\ 0 \end{bmatrix}}_{b}. \tag{2.29}$$

Each of the submatrices derives their name from the interaction diagram of Fig. 2.3. In the following expressions, primed quantities denote source level variables, whereas unprimed quantities represent field (test) level variables. The index i is used on basis functions whereas j is used for testing functions. The strip is indicated as S_R' or S_R depending on whether it is a basis/test domain. The slot is indicated as S_S' or S_S depending on whether it is a basis/test domain. A quadrature like $\int_{S_S', S_R}$ indicates a 4-D quadrature with the source level integration on the slot followed by the field level integration on the strip. All bold quantities represent intermediate submatrices. The following definitions hold good for the matrix partitioning.

- **RSE**= stRip SElf interaction matrix of size $N_l \times N_l$

$$\text{RSE} = \alpha\,\text{RSE}_y - \beta\,\text{RSE}_z$$

$$\text{RSE}_y = \alpha\,\text{RSE}_{yy} - \beta\,\text{RSE}_{yz}$$

$$\text{RSE}_z = \alpha\,\text{RSE}_{zy} - \beta\,\text{RSE}_{zz}$$

$$RSE_{yy}(j,i) = \int_{S_R', S_R} E_y(J_y)\, f_{il}\, \phi_l\, f_{jl}\, dS'\, dS$$

$$RSE_{yz}(j,i) = \int_{S_R', S_R} E_y(J_z)\, f_{il}\, \phi_l\, f_{jl}\, dS'\, dS$$

$$RSE_{zy}(j,i) = \int_{S_R', S_R} E_z(J_y)\, f_{il}\, \phi_l\, f_{jl}\, dS'\, dS$$

$$RSE_{zz}(j,i) = \int_{S_R', S_R} E_z(J_z)\, f_{il}\, \phi_l\, f_{jl}\, dS'\, dS$$

- **SOR**= Slot On stRip cross interaction matrix of size $N_l \times N_s$

$$\text{SOR} = \alpha\,\text{SOR}_y - \beta\,\text{SOR}_z$$

$$SOR_y(j,i) = \int_{S'_S, S_R} E_y(M_y)\, f_{is}\, \phi_s\, f_{jl}\, dS'\, dS$$

$$SOR_z(j,i) = \int_{S'_S, S_R} E_z(M_y)\, f_{is}\, \phi_s\, f_{jl}\, dS'\, dS$$

- **ROS**= stRip On Slot cross interaction matrix of size $N_s \times N_l$

$$\mathbf{ROS} = \alpha\,\mathbf{ROS}_y - \beta\,\mathbf{ROS}_z$$

$$ROS_y(j,i) = \int_{S'_R, S_S} H_y(J_y)\, f_{il}\, \phi_l\, f_{js}\, dS'\, dS$$

$$ROS_z(j,i) = \int_{S'_R, S_S} H_y(J_z)\, f_{il}\, \phi_l\, f_{js}\, dS'\, dS$$

- **SSE**= Slot SElf interaction matrix of size $N_s \times N_s$

$$\mathbf{SSE} = \mathbf{SNT} - \mathbf{SXT}$$

$$SNT(j,i) = \int_{S'_S, S_S} H_y(M_y)\, f_{is}\, \phi_s\, f_{js}\, dS'\, dS$$

$$SXT(j,i) = \int_{S'_S, S_S} H_y^{ext}(M_y)\, f_{is}\, \phi_s\, f_{js}\, dS'\, dS$$

- $\mathbf{I}^l$ and $\mathbf{I}^s$ are the vectors of expansion coefficients.

$$\mathbf{I}^l = \begin{bmatrix} I_1^l \\ I_2^l \\ \vdots \\ I_{N_l}^l \end{bmatrix} \quad \text{and} \quad \mathbf{I}^s = \begin{bmatrix} I_1^s \\ I_2^s \\ \vdots \\ I_{N_s}^s \end{bmatrix}$$

- $\mathbf{E}^{inc}$ is the incident field vector of size $N_l \times 1$

$$E^{inc}(j) = \alpha \int_{S_R} E_y^{inc}\, f_{jl}\, dS$$

If the incident field is LSE_{10}, E_y^{inc} can be taken as $e^{-j\gamma z}$, where γ is the propagation constant of the LSE_{10} mode.

- $\mathbf{0}$ is the zero vector of size $N_s \times 1$

In the next subsection, the problem of evaluating the submatrices **RSE**, **SOR**, **ROS** and **SNT** are taken up. The evaluation of **SXT** is discussed in

Section 3.5. The matrices $\mathbf{A}$ and $\mathbf{b}$ can be computed to solve for the coefficient matrix $\mathbf{x}$. Any parameter of interest can be computed once the current distributions J_u and M_y are reconstructed from $\mathbf{I^l}$ and $\mathbf{I^s}$.

2.4 Quadrature Schemes for MoM Matrix Entries

2.4.1 Introduction

Algorithms for implementing the internal MoM element quadratures are developed here. For simple MoM problems, it is possible to give closed form expressions for the MoM matrix entries. However, the expressions for MoM matrix entries for this problem are extremely involved and voluminous. It is therefore impractical to quote such expressions, for the reason that, the expressions can neither be coded efficiently nor does it provide any insight into the structure of the integrals.

Our discussion of quadrature methods will be based on the stRip SElf interaction (RSE) formulation, since this presents the most difficult case. All the other matrices, namely **SOR**, **ROS** and **SNT** can be evaluated based on the method developed for **RSE** evaluation. Consider the definition of two typical RSE intermediate matrices.

$$RSE_{yy}(j,i) = \int_{S'_R, S_R} E_y(J_y)\, f_{il}\, \phi_l\, f_{jl}\, dS'\, dS \qquad (2.30)$$

$$RSE_{yz}(j,i) = \int_{S'_R, S_R} E_y(J_z)\, f_{il}\, \phi_l\, f_{jl}\, dS'\, dS \qquad (2.31)$$

where the Green's functions (See Section 3.1 for derivation and details) are given by,

$$E_y(J_y) = \sum C^e_{E_y (J_y)} \sin u_1(a - x') \cos k_y y' \sin u_1(a - x) \cos k_y y \, e^{-\gamma_e | z-z' |} \; +$$

$$\sum C^m_{E_y (J_y)} \sin v_1(a - x') \cos k_y y' \sin v_1(a - x) \cos k_y y \, e^{-\gamma_m | z-z' |}$$

$$E_y(J_z) = \sum C^e_{E_y (J_z)} \sin u_1(a - x') \sin k_y y' \sin u_1(a - x) \cos k_y y \, e^{-\gamma_e | z-z' |} \; \Theta \; +$$

$$\sum C^m_{E_y (J_z)} \sin v_1(a - x') \sin k_y y' \sin v_1(a - x) \cos k_y y \, e^{-\gamma_m | z-z' |} \; \Theta$$

These Green's functions, namely $E_y(J_y)$ and $E_y(J_z)$ represent two generic cases, so that we can make the following observation regarding the structure of Green's functions in inhomogeneously filled waveguides. Each Green's function consists of 2 double indexed series, one through the LSE modes and the other through the LSM modes. Each series has a coefficient part, say $C^m_{E_y (J_z)}$ and a function part. The function part depends on both primed and unprimed variables. It is composed of the product of four trigonometric functions and an exponential factor which depends on $|z - z'|$. On some Green's functions, we also have the signum function $\Theta(z - z')$, which merely changes sign based on $z - z'$. Since the source (field) level integrations are to be carried out over the strip (slot), the variables x or x' does not appear in the quadratures. If "tr" stands ("tr" denotes the word trigonometric) for sin or cos, then, we are looking at integrals of the form,

$$\mathcal{I} = \int_{S'_R, \; S_R} \mathrm{tr}\, (k_y \, y) \, \mathrm{tr}\, (k_y \, y') \, \mathrm{tr}\, (k_{jl} \, u) \, \mathrm{tr}\, (k_{il} \, u') \, e^{-\gamma|z-z'|} \; \phi_l \; \Theta \; dS' \, dS \; . \quad (2.32)$$

In (2.32), we have replaced the basis and testing functions with their definitions in terms of "tr". The evaluation of the entire MoM matrix requires 9 waveguide Green's functions which amounts to the evaluation of 18 double series. The integral $\mathcal{I}$ or the variants thereof appear within each of these series.

Therefore, these integrals gets evaluated once every mode, and 10,000 modes or more are generally used to get convergence with respect to modes. This necessitates a very efficient method for *representing* and coding these integrals.
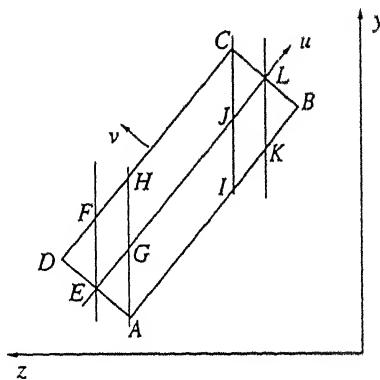
Figure 2.6: Salient points on the strip

The integral in (2.32) cannot be evaluated in the present form due to the presence of the factors $|z - z'|$ and Θ. It is necessary to get rid of the $|z - z'|$ dependence of the integrand by partitioning the strip into regions of trapezoids, where either $z > z'$ or $z < z'$. Fig. 2.7 illustrates the partitioning scheme used on the strip, whereas Fig. 2.6 indicates certain salient points on the strip. It will be proved later in the discussion that the integral for $\mathcal{I}$ can be computed by evaluating the integrand at these 12 points on the strip. The symbols z_A, z_D, y_C,... stand for the coordinates of the points A, D, C and so on. Since the primed and unprimed variables are on the strip, one can identify 3 cases of z', namely $z_D > z' \geq z_A$, $z_A > z' \geq z_C$ and $z_C > z' \geq z_B$. For each of these z' ranges, we can subdivide the test domain into a set of 2 or 3 trapezoids. (Triangles and rectangles can also be regarded as trapezoids in general). Therefore, the quadrature for $\mathcal{I}$ can be split over these 8 domains as follows.

$$\int_{S_R', \, S_R} = \underbrace{\int_{S_1', \, S_1} \pm \left[\int_{S_1', \, S_2} + \int_{S_1', \, S_3} \right]}_{\text{case a}}$$
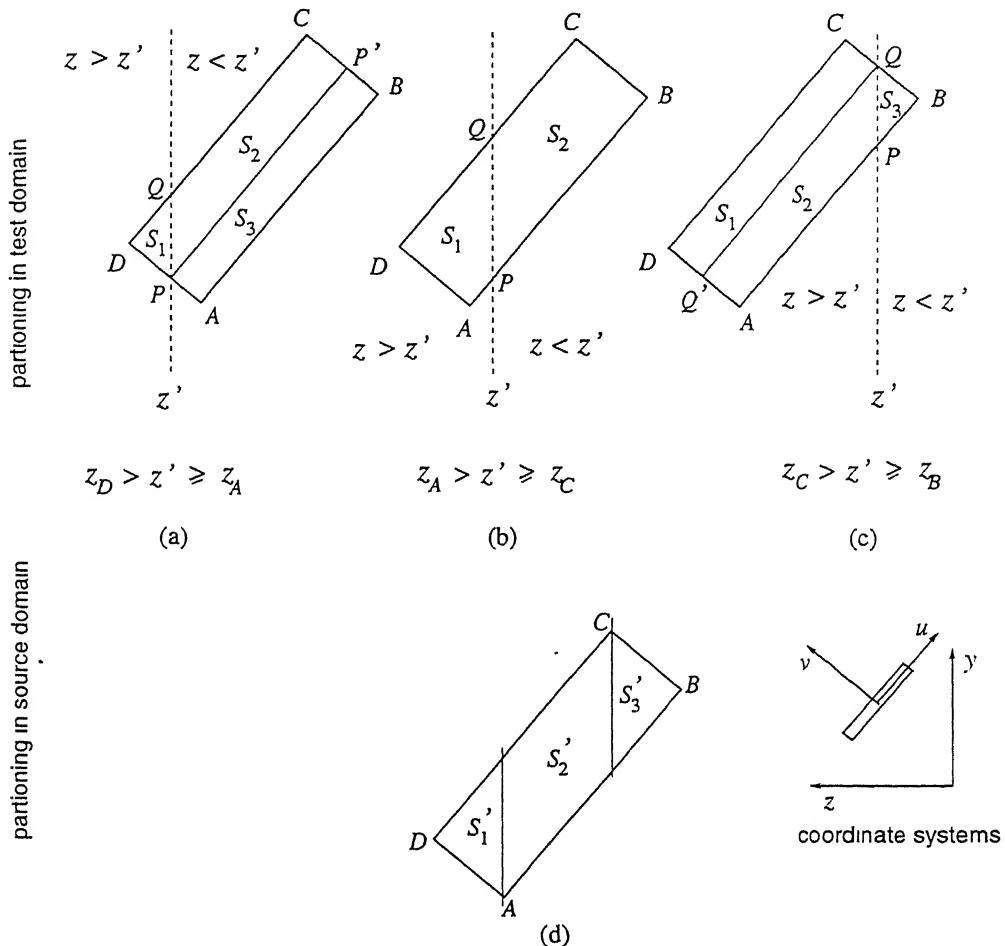
Figure 2.7: Partitioning the strip into trapezoids

$$+ \underbrace{\int_{S_2', \, S_1} \pm \int_{S_2', \, S_2}}_{\text{case b}}$$

$$+ \underbrace{\left[\int_{S_3', \, S_1} + \int_{S_3', \, S_2} \right] \pm \int_{S_3', \, S_3}}_{\text{case c}} \tag{2.33}$$

The meaning of an integral like $\int_{S_1', \, S_1}$ is as follows. Assuming $z_D > z' \geq z_A$, evaluate the field point integral $\int_{S_1}$. This integral depends on both y' and z' because of two reasons: the domain of integration depends on z', and the

integrand is a function of y' and z'. Evaluate this over the source domain S_1' to get $\int_{S_1', S_1}$. In (2.33), the $+$ sign is chosen if Θ is absent and $-$ sign otherwise.

The evaluation of any integral in (2.33) is similar. Therefore, we choose a typical term and continue the discussion. $\mathcal{I}$ is redefined as the part of the integral over S_1 and S_1'. Therefore,

$$\mathcal{I} = \int_{S_1', S_1} \text{tr}(k_y\, y)\, \text{tr}(k_y\, y')\, \text{tr}(k_{jl}\, u)\, \text{tr}(k_{il}\, u')\, e^{-\gamma(z-z')}\, \phi_l\, dS'\, dS \quad (2.34)$$

It is possible (in theory) to carry out the integration in (2.34) analytically. However it will turn out to be an arduous task for the following reason. A 4-D quadrature of this kind is evaluated as a sequence of 4 iterated integrals. Each intermediate quadrature will be referred to as a partial quadrature. Therefore, there exist an order for the quadrature say u, v, u' and v'. Since the function ϕ_l depends only on v', and the partial quadrature with respect to v' is done at the end, we can ignore ϕ_l until the last integral. For doing a partial quadrature, say in u, we have to use trigonometric product to sum formulae and express the integral in the form,

$$\int_{u_1}^{u_2} e^{au}\, \text{tr}(bu)\, du . \quad (2.35)$$

Note that, the application of trigonometric product to sum formulae for n terms lead to 2^{n-1} terms in the integrand. The indefinite integral of (2.35) doubles the number of terms and the limit substitution again doubles the terms. Therefore, at the completion of just one partial quadrature we are left with an elaborate number of integrals. The situation is made worse because the domain of integration depends on the variables awaiting for the quadrature. One has to keep track of this interaction between the terms of the integrand to get the parameters a and b. If we continue this thought experiment, it is obvious that the expressions becomes unmanageable. In fact, it can be shown that the integrand becomes the sum of $8 \times 4^3 = 512$ terms prior to the v' quadrature.

This a fundamental problem in evaluating the waveguide Green's functions on inclined domains [34].

There is yet another problem which is intrinsic to the integrand in (2.34). Since the integrand is a product of 4 functions of the "tr" type, there exist $2^4 = 16$ possibilities for the integrand. Even if the integral for one specific case is evaluated, there remains the task of evaluating the rest 15 cases.

Note that, apart from the inability to keep track of this large number of terms, this problem does not present any profound mathematical puzzles. An attempt at evaluating this quadrature is discussed in [35]. The method makes use of an integral representation of the waveguide Green's function such that the factor $e^{-\gamma|z-z'|}$ is absent. This technique however is applicable only to a select set of integrands and cannot be applied if the edge current distribution is used. The method also necessitates the investigation of the complex plane behavior of the integral (poles, branch cut etc.). The algorithm that is proposed here is based on the conviction that, this is a problem in clever book keeping and one that eventually needs a coding solution, than the mathematical niceties the author suggests.

2.4.2 Algorithm and Illustration

The algorithm for the evaluation of integrals of the type (2.34) are presented here. Let bold j denote $\sqrt{-1}$ since j is already used for indexing the test functions. Consider the definition of $\mathcal{I}$ with a few modifications,

$$\mathcal{I} = \int_{S_1', S_1} \operatorname{tr}(k\,y)\operatorname{tr}(k_j\,u)\operatorname{tr}(k\,y')\operatorname{tr}(k_i\,u')\,e^{-\gamma\,(z - z')}\,\phi\,dS'\,dS \quad (2.36)$$

where

$$k = \frac{n\,\pi}{b}, \quad \text{for} \quad n = 1, 2, 3, \ldots$$

$$k_j = \frac{j\pi}{2\,l_l}, \quad \text{for} \quad j = 1, 2, 3, \ldots$$

$$\phi = \phi(v') = 1\big/\sqrt{1 - (v'/u_l)^2}$$

and γ is assumed to be real and non-negative. The steps of the algorithm evolves naturally from the following step: replace the four term trigonometric product in the integrand of (2.36) by the exponential representation. That is, we regard the term $\text{tr}\,(ky)\,\text{tr}\,(k_ju)\,\text{tr}\,(ky')\,\text{tr}\,(k_lu')$ as a linear combination of $e^{j\,(k\,y\,\pm\,k_j\,u\,\pm\,k\,y'\,\pm\,k_l\,u')}$. If we define,

$$\mathcal{E} = \int_{S_1',\,S_1} e^{j\,(k\,y\,\pm\,k_j\,u\,\pm\,k\,y'\,\pm\,k_l\,u')}\,e^{-\gamma\,(z-z')}\,\phi\;dS'\,dS \quad (2.37)$$

then there exist 8 possibilities in the integral for $\mathcal{E}$. Let $\mathcal{E}^0, \mathcal{E}^1, \ldots, \mathcal{E}^7$ denote the corresponding integrals such that,

$$\mathcal{E}^0 = \int_{S_1',\,S_1} e^{j\,(k\,y\,-\,k_j\,u\,-\,k\,y'\,-\,k_l\,u')}\,e^{-\gamma(z-z')}\,\phi\;dS'\,dS$$

$$\mathcal{E}^1 = \int_{S_1',\,S_1} e^{j\,(k\,y\,-\,k_j\,u\,-\,k\,y'\,+\,k_l\,u')}\,e^{-\gamma(z-z')}\,\phi\;dS'\,dS$$

$$\vdots$$

$$\mathcal{E}^7 = \int_{S_1',\,S_1} e^{j\,(k\,y\,+\,k_j\,u\,+\,k\,y'\,+\,k_l\,u')}\,e^{-\gamma(z-z')}\,\phi\;dS'\,dS \;.$$

It then follows that,

$$\mathcal{I} = \frac{1}{\pm 16\,j}\Big[\,(\mathcal{E}^0 \pm \mathcal{E}^1 \pm \mathcal{E}^2 \pm \mathcal{E}^3 \pm \mathcal{E}^4 \pm \mathcal{E}^5 \pm \mathcal{E}^6 \pm \mathcal{E}^7)\,\pm$$

$$(\bar{\mathcal{E}}^0 \pm \bar{\mathcal{E}}^1 \pm \bar{\mathcal{E}}^2 \pm \bar{\mathcal{E}}^3 \pm \bar{\mathcal{E}}^4 \pm \bar{\mathcal{E}}^5 \pm \bar{\mathcal{E}}^6 \pm \bar{\mathcal{E}}^7)\,\Big] \quad (2.38)$$

for some choice of signs. *The term j is absent in some cases.* In this representation $\bar{\mathcal{E}}^n$ stands for the complex conjugate of $\mathcal{E}^n$. The first implication of this result is as follows. Once we evaluate the 8 integrals $\mathcal{E}^0, \mathcal{E}^1, \ldots, \mathcal{E}^7$ it is possible

to evaluate $\mathcal{I}$ for any of the 16 choices in the integrand. For example, if the integrand is composed of "$\cos(k\,y)\,\cos(k_j\,u)\,\sin(k\,y')\,\sin(k_i\,u')$", then we have the following choice of signs.

$$
\mathcal{I} \;=\; \frac{1}{-16}\Big[\,(\mathcal{E}^0 - \mathcal{E}^1 - \mathcal{E}^2 + \mathcal{E}^3 + \mathcal{E}^4 - \mathcal{E}^5 - \mathcal{E}^6 + \mathcal{E}^7) + \\
(\bar{\mathcal{E}}^0 - \bar{\mathcal{E}}^1 - \bar{\mathcal{E}}^2 + \bar{\mathcal{E}}^3 + \bar{\mathcal{E}}^4 - \bar{\mathcal{E}}^5 - \bar{\mathcal{E}}^6 + \bar{\mathcal{E}}^7)\,\Big]
$$

Therefore, the type of tr's involved in $\mathcal{I}$ can be ignored, and one can concentrate on an integral of the generic form,

$$
\mathcal{E} \;=\; \int_{S_1',\,S_1} \mathcal{X}\,\phi\;dS'\,dS \tag{2.39}
$$

$$
\mathcal{X} \;=\; e^{j\,(k\,y\,+\,s_1\,k_j\,u\,+\,s_2\,k\,y'\,+\,s_3\,k_i\,u')}\;e^{-\gamma\,(z\,-\,z')} \tag{2.40}
$$

where s_1, s_2 and s_3 are ± 1.

Two observations can be made regarding the integral in (2.39): one regarding the structure of the integrand, and the other related to the domain of integration.

- The integrand is a complex function of 4 real variables: two primed variables and 2 unprimed variables. The integrand is the product of an exponential function $\mathcal{X}$ and the edge current function ϕ. The function $\mathcal{X}$ can be regarded as _one_ exponential function of a composite argument. The argument is a complex linear combination of the integration variables.

- The domain of integration is a sequence of 2 trapezoids. Each trapezoid is defined by a set of 4 straight lines. These bounding lines are linear functions of the variables awaiting for the quadrature.

For example, the domain of integration for the quadrature $\int_{S_1',S_1}$ is defined
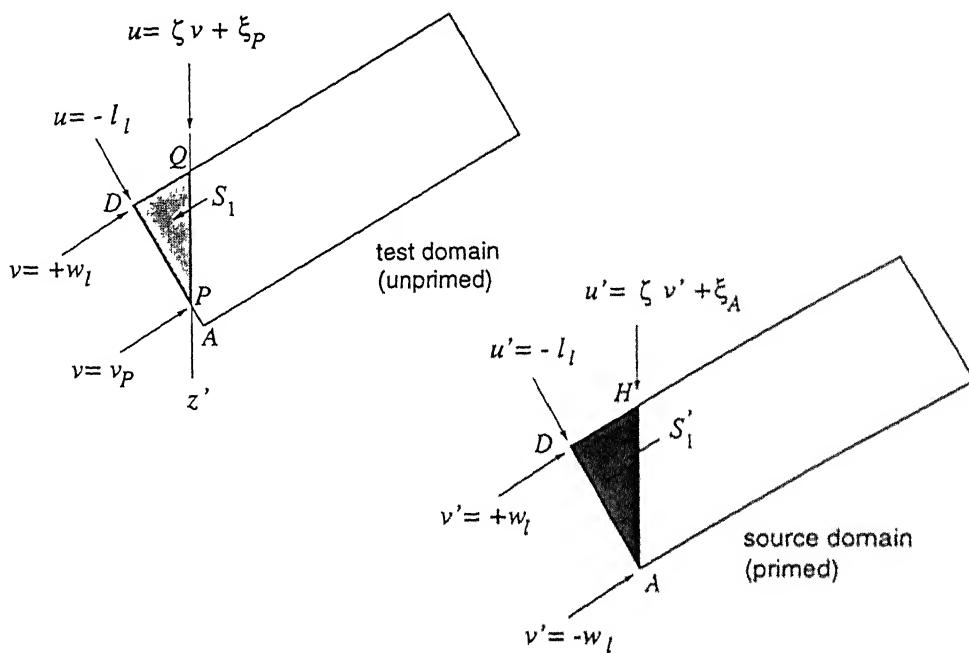
Figure 2.8: Descriptions of the domains S_1' and S_1

as, [See Fig. 2.8]

$$S_1 \; : \quad \begin{array}{ccccc} -l_l & < & u & < & \zeta v + \xi_P \\ v_P & < & v & < & +w_l \end{array}$$

$$S_1' \; : \quad \begin{array}{ccccc} -l_l & < & u' & < & \zeta v' + \xi_A \\ -w_l & < & v' & < & +w_l \end{array}$$

where

$$\zeta = \alpha/\beta$$
$$\xi_P = -\frac{z' - z_l}{\beta}$$
$$\xi_A = -\frac{z_A - z_l}{\beta}$$
$$v_P = \frac{+(z' - z_l) - \beta l_l}{\alpha}$$

The quadrature is done after choosing a quadrature sequence. For *RSE* matrix evaluation, it is necessary to do the partial quadratures in the sequence

$$X \xrightarrow[k_u]{u} \begin{cases} X_1 \xrightarrow[k_{v_1}]{v} \begin{cases} X_3 \xrightarrow[k_{u'_3}]{u'} \begin{cases} X_7 \xrightarrow[k_{v'_7}]{v'} \pi w_l\, I_0^7\, \tilde{X}_7 \\ X_6 \xrightarrow[k_{v'_6}]{v'} \pi w_l\, I_0^6\, \tilde{X}_6 \end{cases} \\ X_2 \xrightarrow[k_{u'_2}]{u'} \begin{cases} X_5 \xrightarrow[k_{v'_5}]{v'} \pi w_l\, I_0^5\, \tilde{X}_5 \\ X_4 \xrightarrow[k_{v'_4}]{v'} \pi w_l\, I_0^4\, \tilde{X}_4 \end{cases} \end{cases} \\ X_0 \xrightarrow[k_{v_0}]{v} \begin{cases} X_1 \xrightarrow[k_{u'_1}]{u'} \begin{cases} X_3 \xrightarrow[k_{v'_3}]{v'} \pi w_l\, I_0^3\, \tilde{X}_3 \\ X_2 \xrightarrow[k_{v'_2}]{v'} \pi w_l\, I_0^2\, \tilde{X}_2 \end{cases} \\ X_0 \xrightarrow[k_{u'_0}]{u'} \begin{cases} X_1 \xrightarrow[k_{v'_1}]{v'} \pi w_l\, I_0^1\, \tilde{X}_1 \\ X_0 \xrightarrow[k_{v'_0}]{v'} \pi w_l\, I_0^0\, \tilde{X}_0 \end{cases} \end{cases} \end{cases}$$
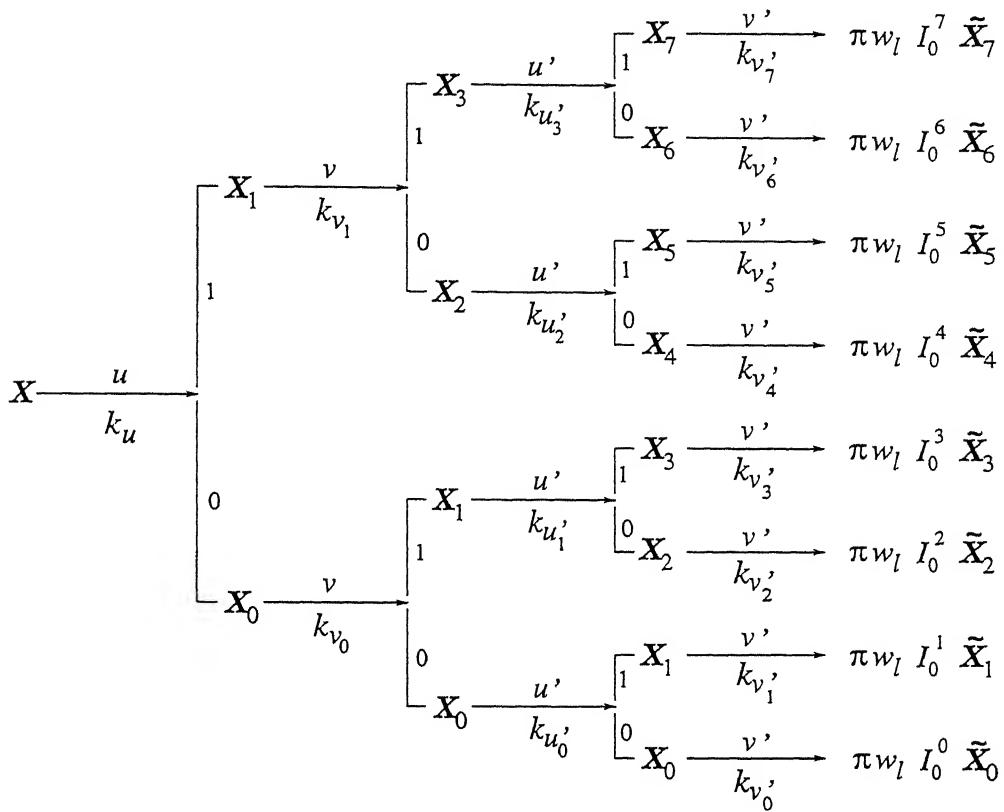
Figure 2.9: Quadrature sequence as a binary tree

u, v, u' and v'. Since the quadrature in v' is done at the end, the term ϕ can be ignored from the integrand until the integrations with respect to u, v and u' are completed. Consider the quadrature with respect to u. If we regard the integrand $\mathcal{X}$ as $e^{k_u u}$ then the integral consists of 2 terms of similar structure evaluated at the upper and lower limits of the integration variable. That is,

$$\mathcal{X} \xrightarrow{u} \frac{1}{k_u}[\mathcal{X}_1 - \mathcal{X}_0] \tag{2.41}$$

where $\mathcal{X}_1$ stands for $\mathcal{X}$ evaluated at the upper limit of the integration variable and $\mathcal{X}_0$ stands for $\mathcal{X}$ evaluated at the lower limit of the integration variable. Note that, the integrand retains this structure after every partial quadrature because of the nature of the integrand as well as the domain of integration.

Thus every integration splits the integrand into the above form. A sequence of partial quadratures thus forms a binary tree. Fig. 2.9 shows a detailed view of this evolution.

One begins with the integrand $\mathcal{X}$, perform the quadrature in u leading to terms $\mathcal{X}_1$ and $\mathcal{X}_0$. We associate the term arising out of the upper limit substitution as the upper branch of the tree (designated 1). The term arising out of the lower limit substitution is traced along the lower branch (designated 0). Therefore at the end of 3 quadratures there are just 8 terms $\mathcal{X}_0, \mathcal{X}_1, \ldots, \mathcal{X}_7$.

The state of the integrand is specified by tracing down the branch in binary. For example, the term $\mathcal{X}_6$ corresponds to the term $\mathcal{X}$ evaluated at the upper limit of u (1), upper limit of v (1) and the lower limit of u' (0). Similar numbering scheme is used for the coefficients of the quadrature variables.

The quadrature in v' is different from its predecessors. At the completion the 3 previous quadratures, we are left with an integral of the following form,

$$\int_{-w_l}^{+w_l} e^{k_{v'} v'} \phi(v') \, dv' \; . \tag{2.42}$$

Using the transformation $v' = w_l \cos\varphi$, this integral can be reduced to this known form,

$$\pi w_l \underbrace{\left[\frac{1}{\pi} \int_0^\pi e^{k_{v'} w_l \cos\varphi} \, d\varphi \right]}_{I_0(k_{v'} w_l)} \tag{2.43}$$

where $I_0(k_{v'} w_l)$ is the modified Bessel function of the complex argument $k_{v'} w_l$. Thus the effect of the quadrature in v' is to replace the integrand $\mathcal{X}$ by $\pi w_l I_0 \widetilde{\mathcal{X}}$. $\widetilde{\mathcal{X}}$ stands for $\mathcal{X}$ evaluated at $v' = 0$. Note that this operation does not increase the number of terms. This procedure is sufficiently systematic that it is possible to write down the sequence (by inspection) as follows:

$$\mathcal{X} \xrightarrow{u} \frac{1}{k_u} (\mathcal{X}_1 - \mathcal{X}_0) \xrightarrow{v} \frac{1}{k_u} \left[\frac{1}{k_{v1}} (\mathcal{X}_3 - \mathcal{X}_2) - \frac{1}{k_{v0}} (\mathcal{X}_1 - \mathcal{X}_0) \right] \xrightarrow{u'}$$

$$\frac{1}{k_u} \left\{ \frac{1}{k_{v1}} \left[\frac{1}{k_{u'_3}} (\mathcal{X}_7 - \mathcal{X}_6) - \frac{1}{k_{u'_2}} (\mathcal{X}_5 - \mathcal{X}_4) \right] - \right.$$

$$\left. \frac{1}{k_{v0}} \left[\frac{1}{k_{u'_1}} (\mathcal{X}_3 - \mathcal{X}_2) - \frac{1}{k_{u'_0}} (\mathcal{X}_1 - \mathcal{X}_0) \right] \right\} \xrightarrow{v'}$$

$$\frac{\pi \, w_l}{k_u} \left\{ \frac{1}{k_{v1}} \left[\frac{1}{k_{u'_3}} (I_0^7 \, \widetilde{\mathcal{X}}_7 - I_0^6 \, \widetilde{\mathcal{X}}_6) - \frac{1}{k_{u'_2}} (I_0^5 \, \widetilde{\mathcal{X}}_5 - I_0^4 \, \widetilde{\mathcal{X}}_4) \right] - \right.$$

$$\left. \frac{1}{k_{v0}} \left[\frac{1}{k_{u'_1}} (I_0^3 \, \widetilde{\mathcal{X}}_3 - I_0^2 \, \widetilde{\mathcal{X}}_2) - \frac{1}{k_{u'_0}} (I_0^1 \, \widetilde{\mathcal{X}}_1 - I_0^0 \, \widetilde{\mathcal{X}}_0) \right] \right\}$$

If all the quadrature limits are distinct, then the case illustrated in Fig. 2.9 is valid. That is, there are eight coefficients for v', four coefficients for u', two coefficients for v and one coefficient for u quadratures. However, if the domains are not distinct like this case (Note that the RSE domain, (See Fig. 2.7–2.8) is bounded by lines having only 3 distinct slopes), not all the coefficients are distinct. It can be shown that there exist the following (distinct) coefficients in the entire RSE quadrature.

- Distinct coefficients for k_u

    1. $\pm \gamma_2 + j \, (k_1 + s_1 \, k_j)$

- Distinct coefficients for k_v

    1. $j \, (k + s_1 \, k_j \, \alpha)/\beta$

    2. $\mp \gamma_1 + j \, k_2$

- Distinct coefficients for $k_{u'}$

    1. $j [(1 + s_2) \, k_1 + (s_1 \, k_j + s_3 \, k_i)]$

    2. $j \, [-k(\beta^2/\alpha) + s_2 \, k_1 + s_3 \, k_i]$

    3. $\mp \gamma_2 + j \, (s_2 \, k_1 + s_3 \, k_i)$

- Distinct coefficients for $k_{v'}$

1. $j\left[-k(\alpha^2/\beta) - s_1 k_j(\alpha/\beta) + s_2 k_2\right]$

2. $j(1 + s_2) k_2$

3. $\pm\gamma_1 + j s_2 k_2$

4. $j(s_2 k + s_3 k_i \alpha)/\beta$

where

$$k_1 = k\alpha$$
$$k_2 = k\beta$$
$$\gamma_1 = \gamma\alpha$$
$$\gamma_2 = \gamma\beta$$

In the above expressions, the choice of the sign $\pm$ is to be made based on whether $z > z'$ or $z < z'$.

The terms $\widetilde{\mathcal{X}}_0$ to $\widetilde{\mathcal{X}}_7$ can be evaluated using a simple idea. The definition of $\widetilde{\mathcal{X}}_k$ is repeated once again. $\widetilde{\mathcal{X}}_k$ is the value of $\mathcal{X}$ evaluated at the kth stage of the binary tree, with $v' = 0$. For example, the value of $\widetilde{\mathcal{X}}_6$ is evaluated as follows. We identify the set of points on the strip domain [See Figs 2.6–2.8] which belongs to the intersection of the 4 lines.

$$u = \zeta v + \xi_P, \quad \text{upper limit of } u$$
$$v = +w_l, \quad \text{upper limit of } v$$
$$u' = -l_l, \quad \text{lower limit of } u'$$
$$v' = 0$$

With reference to the Fig. 2.6, this takes the unprimed variables to the point F and the primed variables to to the point E. We list the value of $\widetilde{\mathcal{X}}_0$ to $\widetilde{\mathcal{X}}_7$ for $\int_{S_1', S_1}$.

$$\widetilde{\mathcal{X}}_7 = 1 \; HHGG$$

$$\widetilde{\mathcal{X}_6} = 1 \; FFEE$$

$$\widetilde{\mathcal{X}_5} = 1 \; AAGG$$

$$\widetilde{\mathcal{X}_4} = 1 \; EEEE$$

$$\widetilde{\mathcal{X}_3} = e_{DG} \; DDGG$$

$$\widetilde{\mathcal{X}_2} = e_{DE} \; DDEE$$

$$\widetilde{\mathcal{X}_1} = 1 \; AAGG$$

$$\widetilde{\mathcal{X}_0} = 1 \; EEEE$$

where

$$e_{DG} = e^{-\gamma |z_D - z_G|}$$

$$e_{DE} = e^{-\gamma |z_D - z_E|}$$

$$\vdots$$

$$HHGG = e^{j\left(k\,y_H + s_1\,k_j\,u_H + s_2\,k\,y'_G + s_3\,k_i\,u'_G\right)}$$

$$FFEE = e^{j\left(k\,y_F + s_1\,k_j\,u_F + s_2\,k\,y'_E + s_3\,k_i\,u'_E\right)}$$

$$AAGG = e^{j\left(k\,y_A + s_1\,k_j\,u_A + s_2\,k\,y'_G + s_3\,k_i\,u'_G\right)}$$

$$\vdots$$

2.4.3   Exception Handling and Restrictions

In this section, we discuss certain miscellaneous topics related to the quadrature. These include some important exceptions, restrictions and limitations of the algorithm.

Exception Handling

(1) Modes other than LSE_{mn}/LSM_{mn} $(m, n > 1)$

While developing the quadrature scheme, the propagation constant γ is assumed to be real and k to be nonzero. However, for LSE_{m0} modes, we have

$k = 0$ and, in particular for LSE_{10} mode γ is imaginary. The algorithm does not need any modification for the case of LSE_{m0} mode with $m > 1$, except that (2.38) is valid in the following simplified form.

$$\mathcal{I} = \frac{1}{\pm 4\,j} \left[(\mathcal{E}^0 \pm \mathcal{E}^1) \pm (\bar{\mathcal{E}}^0 \pm \bar{\mathcal{E}}^1) \right] \tag{2.44}$$

If γ is imaginary it is necessary to change (2.38) substantially as follows. If γ is imaginary and $k = 0$, we are dealing with an integral of the form,

$$\mathcal{I} = \int_{S_1',\,S_1} \mathrm{tr}\,(k_j\,u)\,\mathrm{tr}\,(k_i\,u')\,e^{-\gamma(z-z')}\,\phi\,dS'\,dS \tag{2.45}$$

Define,

$$\mathcal{E}^0 = \int_{S_1',\,S_1} e^{j\,(k_j\,u\,-\,k_i\,u')}\,e^{-\gamma(z-z')}\,\phi\,dS'\,dS$$

$$\mathcal{E}^1 = \int_{S_1',\,S_1} e^{j\,(k_j\,u\,+\,k_i\,u')}\,e^{-\gamma(z-z')}\,\phi\,dS'\,dS$$

$$\mathcal{E}'^0 = \int_{S_1',\,S_1} e^{j\,(k_j\,u\,-\,k_i\,u')}\,e^{+\gamma(z-z')}\,\phi\,dS'\,dS$$

$$\mathcal{E}'^1 = \int_{S_1',\,S_1} e^{j\,(k_j\,u\,+\,k_i\,u')}\,e^{+\gamma(z-z')}\,\phi\,dS'\,dS$$

Then,

$$\mathcal{I} = \frac{1}{\pm 4\,j} \left[(\mathcal{E}^0 \pm \mathcal{E}^1) \pm (\bar{\mathcal{E}}'^0 \pm \bar{\mathcal{E}}'^1) \right] \tag{2.46}$$

(2) Division by Zero

A division by zero occurs if any of the coefficients k_u, k_v or $k_{u'}$ becomes zero for some combination of parameters. However all the distinct coefficients have already been listed in page 43 that it is possible to identify such cases and avoid them. The 6 coefficients can be thought of as belonging to 3 distinct groups depending on the possibility of becoming zero. For example, the coefficient $k_v =$

$\mp \gamma_1 + j\, k_2$ can never become zero. However the coefficient $k_v = j\, (k + s_1\, k_j\, \alpha)/\beta$ becomes zero only if $k = k_j\, \alpha$. Such cases can be ignored because it requires a strange coincidence of parameters to make it zero. This case can definitely be avoided either by computing with extended precision or using parameters with an infinite-small offset. For example, we can use $\theta = 30\,0001^0$ instead of 30^0. The coefficient

$$k_{u'} = j\left[(1 + s_2)\, k_1 + (s_1\, k_j + s_3\, k_i)\right]$$

however becomes zero for the condition,

$$\imath = j$$

$$s_2 = -1$$

$$s_1 = -s_3\,.$$

This case *definitely* occurs on the principal diagonal of the RSE matrix and needs to be taken care of. The quadrature scheme illustrated in Fig. 2.9 will go through the following changes in this case. If $k_{u'} = 0$ at the completion of the quadrature in v, then it is necessary to evaluate an integral of the form, [See Fig. 2.8]

$$\int_{u'} e^{k_{u'}\, u'}\, du' = u'\Big|_{-l_i}^{\zeta v' + \xi_A} = \zeta\, v' + \xi_A + l_i \tag{2.47}$$

Therefore the v' quadrature becomes,

$$\int_{-w_l}^{+w_l} \left[\zeta\, v' + (\xi_A + l_i)\right] e^{k_{v'}\, v'}\, dv' =$$

$$\pi\, w_l \left(\zeta\, w_l\, \underbrace{\frac{1}{\pi} \int_0^\pi \cos\varphi\, e^{k_{v'}\, w_l\, \cos\varphi}\, d\varphi}_{I_1(k_{v'}\, w_l)} + (\xi_A + l_i)\, \underbrace{\frac{1}{\pi} \int_0^\pi e^{k_{v'}\, w_l\, \cos\varphi}\, d\varphi}_{I_0(k_{v'}\, w_l)}\right)$$

Therefore, the integral can be reduced to a closed form for this case. The modified Bessel functions I_n has the property that,

$$|I_n(z)| \le I_0(x) = O(e^{+x}), \quad \text{for} \quad n \ge 0$$

for $x = |Re(z)|$. Since the arguments to the Bessel functions grow indefinitely with respect to the modes, it is necessary to keep the term I_n bounded in the quadrature expressions. This can be done by combining the term arising from $e^{-\gamma|z-z'|}$ with the Bessel functions. For example, the term $\pi\, w_l\, I_0^2\, \mathcal{X}_2$ in $\int_{S_1, S_1'}$ consists of

$$\pi\, w_l\, I_0^2\, \widetilde{\mathcal{X}_2} \;=\; \pi\, w_l\, I_0(\overline{\gamma_1 + j\, s_2\, k_2}\; w_l)\, e^{-\gamma(z_0 - z_K)}\; DEEE$$
$$=\; \pi\, w_l\, \underbrace{e^{-\gamma_1\, w_l}\, I_0}\; DEEE$$

Note that, it is necessary to treat $e^{-\gamma_1\, w_l}\, I_0$ together so as to avoid floating point overflow at large γ. All standard mathematical libraries return $I_n(z)$ as $e^{-|x|}\, I_n(z)$ to avoid overflow [36].

Restrictions in the Algorithm

The restrictions in the algorithm arise from our inability to carry out the v' quadrature in terms of the Bessel functions, I_n. For the cases that has been considered so far, it was possible to partition the domain such that the v' quadrature could be cast in one of the following forms.

$$(1)\qquad \int_{-w_l}^{+w_l} e^{k_{v'}\, v'}\, \phi(v')\, dv'$$
$$(2)\qquad \int_{-w_l}^{+w_l} v'\, e^{k_{v'}\, v'}\, \phi(v')\, dv'$$

Fig. 2.10 shows 2 cases where such a partitioning scheme does not hold good. If the strip inclinations exceeds θ_{max}, then the partitioning scheme of Fig. 2.7 cannot be applied for RSE formulation. Therefore, the quadrature in v' cannot be reduced to one of the standard forms, and we have a limit on the maximum allowable strip inclination. However, θ_{max} is of the order of 80^0 if the length to width ratio of the strip is more than 7.

Similar results hold good if the strip is partially overlapped over the slot.
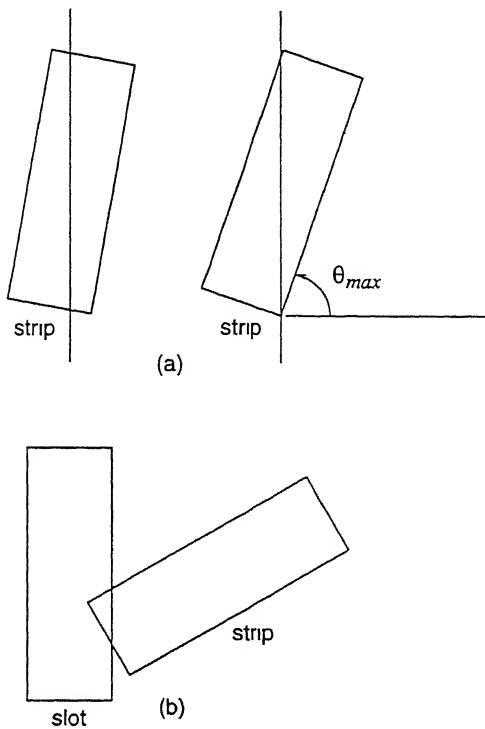
Figure 2.10: Restrictions in the algorithm

This is shown in Fig. 2.10b. Therefore, cases having arbitrary horizontal offsets between strip and the slot cannot be handled. In fact, the offset should be such that,

$$z_A \geq +w_s$$
$$z_C \leq -w_s$$

Certain Simplifications in the Algorithm

It was shown in the discussion of the quadrature that the integral in (2.39) is evaluated as a linear combination of $\widetilde{\mathcal{X}_0}$ to $\widetilde{\mathcal{X}_7}$ evaluated at the salient points of Fig. 2.6. If we observe the partition scheme of Fig. 2.7 and Equation (2.33), it can be seen that the contribution from S_2 and S_3 are added together in case(a). Therefore, it so happens that the contribution from the point P' cancels while

combining the integrals over S_2 and S_3. That is, one need not retain the term
arising from P' in v quadrature for $\int_{S_1', S_2}$. Therefore, there need to be only 6
terms in the final integral. Similar observations can be made regarding point
Q' while combining $\int_{S_3', S_1}$ and $\int_{S_3', S_2}$ in case(c).

A substantial reduction in computation is achieved by introducing some
symmetry assumptions. Note however that the result mentioned above does
not need any symmetry assumptions. If the strip is assumed to be centered on
the narrow wall, the following results hold good.

$$\text{RSE}(j, i) \;=\; 0\,, \quad \text{for} \quad |j - i| = \text{odd}$$

This brings about 50% reduction in the number of matrix elements to be
computed. There are further simplifications resulting from the symmetry of
the partitioning scheme. With respect to Fig. 2.7 and (2.33) it can be shown
that we need to evaluate only the first 4 quadratures. That is, the quadratures
$\int_{S_2', S_2}$, $\int_{S_3', S_1}$, $\int_{S_3', S_2}$, $\int_{S_3', S_3}$ can be shown to be the complex conjugates of $\int_{S_2', S_1}$,
$\int_{S_1', S_3}$, $\int_{S_1', S_2}$, $\int_{S_1', S_1}$ respectively.

The cost of a quadrature scheme is specified in terms of the number of
function evaluations, and not by the multiplication count. For this quadrature
algorithm, the number of function evaluations are very small. The algorithm
requires the evaluation of $\widetilde{\mathcal{X}}_0$ to $\widetilde{\mathcal{X}}_7$ and I_0^0 to I_0^7 for 8 sign factors (s_1, s_2 and
s_3) over the 8 partitioned domains. However, not all functions are distinct in
the sense that one can evaluate them from a canonical set, by forming the
conjugates, taking products etc. An exact estimate of the number of function
evaluations in (2.32), for the case of $i \neq j$, is given in Table 2.1.

This is the cost of function evaluations for each mode. However, the evalua-
tion of e^{jky} and $e^{jk_j u}$ need not be repeated after it has been evaluated for a
mode because of the curious structure of k and k_j. Note that,

$$k \;=\; \frac{n\pi}{b}, \quad \text{for} \quad n = 0, 1, \ldots$$

Table 2.1: Function evaluations in the quadrature method

Function type:	$e^{-\gamma |z - z'|}$	I_0	e^{jky}	$e^{jk_j u}$
No of evaluations:	2	8	12	3

$$k_j = \frac{j\pi}{2 l_l}, \quad \text{for} \quad j = 1, 2, \ldots$$

Therefore, one can evaluate them recursively using relations of the type,

$$e^{j(n\pi/b)y} = e^{j(\overline{n-1}\pi/b)y} e^{j(\pi/b)y}$$

If we regard the integral (2.32) as being evaluated alone, the cost per quadrature is not substantial. However, since the integrals appear within double indexed series, the cost of MoM matrix evaluation is substantial, mostly because of the large multiplication count.

2.5 Computation of Secondary Parameters

It is possible to compute various parameters of interest once the boundary value problem is formulated in the matrix form. The most important parameter is the S matrix with respect to the propagating LSE_{10} mode because it can be measured and can be used for validating the theory. However, other parameters such as slot voltage (V_s), normalized radiated power (P_{rad}), LSE_{10} and LSE_{20} mode coefficients etc. are of interest for array design purpose. Once the induced currents are computed, the evaluation of these parameters follows automatically from their definitions. Therefore, the formulas for the evaluation of the secondary parameters are not quoted, but the relevant implementation aspects are explained.
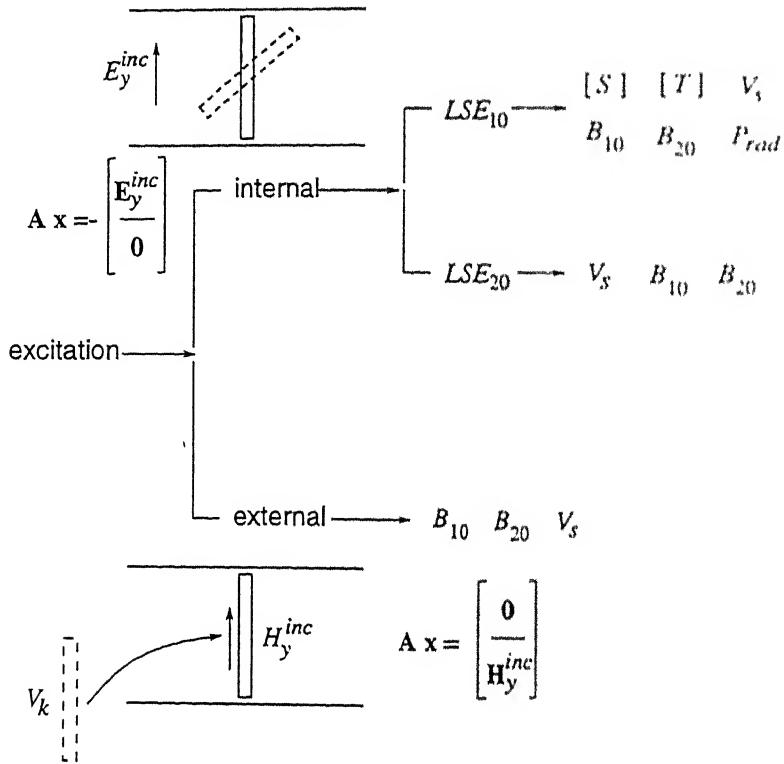
Figure 2.11: Secondary parameter computation schematic

Fig. 2.11 shows the complete schematic of computing the secondary parameters. We regard $z = -\infty$ as port 1 while $z = +\infty$ is regarded as port 2. In order to compute the S matrix, an LSE_{10} mode is assumed to be incident from port 1 and the reflected and transmitted dominant mode amplitudes are computed. This gives S_{11} and S_{21}. S_{22} and S_{12} are computed by assuming an LSE_{10} mode from port 2. Since each excitation leads to a column b, it is possible to solve the S matrix in one step by solving $A x = b$ with multiple right-hand side. Standard $A x = b$ solvers allows multiple right-hand sides [36]. The LSE_{10} mode coefficient B_{10} is identical with S_{11}, whereas the LSE_{20} mode coefficient B_{20} can be evaluated by extracting the amplitude of the LSE_{20} mode.

The S matrix can be converted to normalized Z matrix via. the transformation $(I + S)(I - S)^{-1}$. The T network representation is preferred if the discon-

tinuity is a shunt admittance. The T network is defined by three impedances,

$$z_1 = z_{11} - z_{12}$$

$$z_2 = z_{22} - z_{12}$$

$$z_t = z_{12}$$

where z_1, z_2 are the series arms and z_t is the shunt arm. The quantity $1 - |S_{11}|^2 - |S_{21}|^2$ represents the ratio of the radiated power to the incident power from port 1. We shall refer to it as the normalized radiated power P_{rad}.

If the internal excitation is via. the LSE_{20} mode, it is possible to proceed exactly as in the case of LSE_{10} mode incidence and solve for B_{10}, B_{20}. The slot voltage is obtained by integrating the slot E-field across the width of the slot. The slot voltage is evaluated at the center of the slot with assumption that the incident wave has a certain magnitude at some reference point.

The computation of external mutual coupling between two strip excited slots is an exceptionally difficult problem. The analysis is considerably simplified, by considering it as an *excitation* problem from a slot kept excited at the voltage V_k. The extraneous slot is regarded as causing an external magnetic field H_y^{inc}. The column **b** will have zero entries corresponding to the rows which enforce conditions on the strip. [See Fig. 2.11]. The lower nonzero part of **b** can be computed using the half space Green's function.

2.6 Aspects of Coding

Referring to Fig. 2.12, the code is organized into various translational units and kept in different directories[1]. The Unix utility **make** is used to compile and link various units. Though subroutines have been used wherever necessary, they were avoided while writing the quadrature routines fill_matrix_RSE etc.

---

[1]The source code can be made available upon request. It takes about 174 kB memory

```
program main        subroutine do_MoM          subroutine greens function
set frequency       solve LSE LSM roots        do Gram Schmidt
read specks         comp Green's function      get δ representation
 do MoM             fill matrix RSE            return
stop                fill matrix SOR            end
end                 fill matrix ROS
                    fill matrix SNT
                    fill matrix SXT
                    fill column b              subroutine comp results
                    assemble A                 comp S-parameters
                    solve Ax= b                comp Z-parameters
                    compute results            make T network equivalent
                    return                     comp slot voltage
                    end                        comp power radiated
                                               comp 10, 20 mode coeff.
                                               return
                                               end
```

Figure 2.12: Code structure

because of the following reasons. It is found that the quadrature algorithm uses all the variables at some stage or other. Therefore, in the strict sense, there are no intermediate variables. If a modular structure were opted for the quadrature routines, it would require massive storage via. **common** locations. The variables in **common** are static and cannot be forced to automatic storage. Therefore, this algorithm was implemented as one complete code. The compiler utility **include** is used to make the code structured. The compiler option **automatic** can be used to force dynamic storage of all the variables.

Table 2.2: Specification of the Computing Environment

Machine	DEC 3000/500
Operating System	DEC OSF/1 2.0
Compiler	DEC Fortran 77 v 3.3
Numeric Precision	Double

Table 2.2 shows the relevant details of the computing environment. A typical run at a frequency takes about 9.0 minutes of CPU time for $M_{max} = 100$, $N_{max} = 100$, $N_l = 9$, $N_s = 9$ and $y_s = b/2$. If the strip is assumed to be centered with respect to the slot, then the execution time comes down to 3.3 minutes because of the savings due to the symmetry.

2.7   Summary and Conclusions

This chapter contained a complete account of the analysis of the strip excited slot as a boundary value problem. The discussion began with the development of the necessary symbolism as notations, coordinate systems etc. The boundary value problem was set up using a pair of coupled integral equations in terms of the induced currents. The transverse currents were neglected and the boundary conditions were enforced only on the axial field components. This simplified the model. Suitable acronyms were coined to model the strip and slot interactions which were consistently used up to the stage of code organization.

An algorithm was developed for implementing the MoM matrix quadratures. The development of the algorithm was based on the conviction that the method should be systematic enough for programming. The operation count of the algorithm was made which indicate a surprisingly small number of function evaluations. However, the number of multiplications were found to be large enough which tend to make the problem computationally intensive. The major exceptions in the algorithm were discussed. The method was found to be applicable only below a critical angle for the strip. It also could not handle arbitrary horizontal offsets between the strip and the slot. These two restrictions do not seriously limit the operating range of the analysis.

A brief discussion on the structure of the code and programming practices were made. The run time information was dealt with along with a discussion of the computing environment.

Chapter 3

On Green's functions and Method of Moment

3.1 Introduction

This is an extraordinarily big chapter which contains nearly all the theoretical work done in this thesis. The topics dealt here do not have a continuous theme, but they are related to the topic of Green's functions in some way or other. Certain sections such as (3.2) and (3.5) are essentially an elaboration or an extension of well known works [33, 7], but all other sections are by and large original contribution by the author.

Many sections of this chapter are of independent interest though this is meant primarily as a companion to Chapter 2. Here is a section-wise summary of the contents. In Section 3.2, the Green's functions in an inhomogeneously filled waveguide are derived using the method of normal mode expansions from

Collin [33]. The structure and properties of waveguide Green's functions decide the subject matter of the next two sections. Section 3.3 discusses the solution of LSE/LSM eigenvalues based on a combined Newton-Raphson and Bisection algorithm.

Section 3.4 is an illustration of a fundamental problem while handling a Green's function which is a *distribution*. The $E_z(J_z)$ Green's function is taken as an example to illustrate the subtleties in computing E_z, if one of the source domain quadratures are dropped. The results are interpreted from the point of view of distributions and a solution is proposed based on the LSM representation of Dirac delta. Section 3.5 contains a method of computing with the half space Green's function. This work is partly based on the work of R. S. Elliott [7].

In Section 3.6 we deal with the theory and practice of method of moment. MoM is a numerical method which is based on a very naive idea—the direct solution of a first kind integral equation. Since this problem is intrinsically illconditioned, the sequence of approximate solutions becomes unstable after reaching a certain accuracy. In this section, this issue is brought to the limelight along with an attempt to consolidate various MoM thumb rules from the point of regularization theory.

3.2 Waveguide Green's Functions

3.2.1 Introduction

The purpose of this section is to derive the waveguide Green's functions necessary in setting up the boundary value problem of Chapter 2. The Green's functions in an inhomogeneously filled rectangular waveguide has already been derived by [37, 38]. However, it will be re-derived in a form which suits the requirement of our analysis. We shall use a method from "Field Theory of

Guided Waves" by R. E. Collin [33] which is popular and simple. The principle of derivation is briefly as follows.

By a normal mode of a waveguide, we understand a valid solution of Maxwell's equation inside the waveguide having $e^{-\gamma z}$ dependence. The set of normal modes are countable and have distinct[1] propagation constants γ. If the wave guide is homogeneously filled, the normal modes are degenerate and there are two modes with the same propagation constant, namely the TE and TM mode. For the inhomogeneously filled waveguide, one can identify two distinct sets to which the normal modes belong to: the LSE and LSM modes. The normal modes are significant because they form a complete orthonormal set among the valid solutions inside the waveguide. There also exist suitable orthogonality relations between the normal modes which enable us to express the Green's function as a series of normal modes. Some Green's functions such as $E_z(J_z)$ do not fit into this form, and contain terms other than the normal modes. The outline of this section is to derive the normal modes, and assume the Green's function as a series in terms of them. The coefficients of the normal mode series are evaluated by applying the reciprocity theorem.

3.2.2 Derivation of Normal Modes

Consider an inhomogeneously filled waveguide as shown in Fig. 3.1. We desire to derive the LSE and LSM normal modes of this waveguide. This is done by making use of the vector potentials F_x and A_x and the relationship between the fields and the potentials as enumerated below.

$$\left(\nabla^2 + k^2 \right) F_x = 0 \tag{3.1}$$

$$\mathbf{E} = -\frac{1}{\epsilon} \nabla \times \mathbf{F} \tag{3.2}$$

---

[1] Waveguide is assumed to be inhomogeneously filled unless otherwise stated.
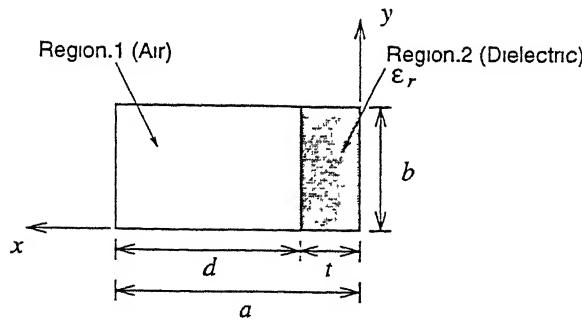
Figure 3.1: Inhomogeneously filled waveguide.

$$\mathbf{H} = +\frac{1}{\jmath\omega\epsilon\mu}\left(\nabla\nabla\cdot\mathbf{F} + k^2\mathbf{F}\right) \tag{3.3}$$
$$\mathbf{F} = F_x\,\mathbf{x}$$

and

$$\left(\nabla^2 + k^2\right)A_x = 0 \tag{3.4}$$

$$\mathbf{H} = +\frac{1}{\mu}\nabla\times\mathbf{A} \tag{3.5}$$

$$\mathbf{E} = +\frac{1}{\jmath\omega\epsilon\mu}\left(\nabla\nabla\cdot\mathbf{A} + k^2\mathbf{A}\right) \tag{3.6}$$

$$\mathbf{A} = A_x\,\mathbf{x}.$$

(3.1–3.3) will be used to derive the *LSE* modes, while (3.4–3.6) will be used to derive the *LSM* modes. The potentials F_x and A_x are defined suitably, such that the boundary conditions at the waveguide walls are satisfied, in addition to satisfying (3.1) and (3.4) respectively. This is done by the choice,

$$F_x = f(x)\,\cos(k_y\,y)\,e^{\pm\gamma z} \tag{3.7}$$

$$\text{where}\quad f(x) = \begin{cases} A\,\sin u_1(a-x), & a \geq x > t \\ B\,\sin u_2 x, & t \geq x \geq 0 \end{cases}$$

$$\gamma^2 + k_0^2 - k_y^2 - u_1^2 = \gamma^2 + k^2 - k_y^2 - u_2^2 = 0$$

$$k_y = \frac{n\pi}{b} \text{ for } n = 0, 1, \ldots$$

$$A_x = a(x) \sin(k_y y) e^{\pm \gamma z} \tag{3.8}$$

$$\text{where} \quad a(x) = \begin{cases} C \cos v_1(a - x), & a > x > t \\ D \cos v_2 x, & t > x > 0 \end{cases}$$

$$\gamma^2 + k_0^2 - k_y^2 - v_1^2 = \gamma^2 + k^2 - k_y^2 - v_2^2 = 0$$

$$k_y = \frac{n\pi}{b} \text{ for } n = 1, 2, \ldots$$

The constants A, B, C and D and u_1, u_2, v_1 and v_2 will be related making use of further conditions. The potentials F_x and A_x should satisfy the continuity conditions for E_z and H_z at the interface at $x = t$. This leads to the characterization of LSE and LSM modes as shown below.

For LSE modes, we have

$$A \sin u_1 d = \frac{B}{\epsilon_r} \sin u_2 t \tag{3.9}$$

$$-A u_1 \cos u_1 d = \frac{B}{\epsilon_r} u_2 \cos u_2 t \tag{3.10}$$

$$-u_1^2 - k_y^2 + k_0^2 + \gamma^2 = 0 \tag{3.11}$$

$$-u_2^2 - k_y^2 + k^2 + \gamma^2 = 0. \tag{3.12}$$

For LSM modes, we have

$$C v_1 \sin v_1 d = -\frac{D}{\epsilon_r} v_2 \sin v_2 t \tag{3.13}$$

$$C \cos v_1 d = D \cos v_2 t \tag{3.14}$$

$$-v_1^2 - k_y^2 + k_0^2 + \gamma^2 = 0 \tag{3.15}$$

$$-v_2^2 - k_y^2 + k^2 + \gamma^2 = 0. \tag{3.16}$$

The equations which characterize the modes can be expressed more concisely,

by taking the ratio of the first two equations, while subtracting the last two equations from each set. This leads to (3.17–3.18) as the characterization of LSE roots, and (3.19–3.20) as the characterization of LSM roots.

$$\frac{\tan(u_1 d)}{u_1} = -\frac{\tan(u_2 t)}{u_2} \tag{3.17}$$

$$u_2^2 - u_1^2 = k_0^2 (\epsilon_r - 1) \tag{3.18}$$

$$\epsilon_r v_1 \tan(v_1 d) = -v_2 \tan(v_2 t) \tag{3.19}$$

$$v_2^2 - v_1^2 = k_0^2 (\epsilon_r - 1) \tag{3.20}$$

Equations 3.17–3.20 admit a countably infinite number of solutions, which grow monotonically. The roots can be ordered by indexing with m. We shall refer to the roots, later, as the mth LSE/LSM root. The detailed algorithm for solving them will be dealt with in the next section. However, some properties of the roots are worth emphasizing. If the waveguide is homogeneously filled, then,

$$u_1 = u_2 = v_1 = v_2 = \frac{m \pi}{a}.$$

For an inhomogeneously filled waveguide, all the roots tend to $m\pi/a$ asymptotically. For low filling factors, the LSE and LSM roots are very close to each other and are only slightly different from $m\pi/a$.

The constants B and D can be eliminated from the definition of normal modes using (3.9) and (3.14), and put $A = C = 1$, so that,

$$F_x = \begin{cases} \sin u_1 (a - x) \, \cos(k_y y) \, e^{\pm \gamma z}, & a \geq x > t \\ \epsilon_r R_{te} \, \sin u_2 x \, \cos(k_y y) \, e^{\pm \gamma z}, & t \geq x \geq 0 \end{cases} \tag{3.21}$$

$$\text{where} \quad R_{te} = \frac{\sin(u_1 d)}{\sin(u_2 t)}$$

$$A_x = \begin{cases} \cos v_1 (a - x) \; \sin(k_y y) \, e^{\cdots} , & a \cdots r \cdots t \\ R_{tm} \; \cos v_2 x \; \sin(k_y y) \, e^{\cdots} , & t \cdots r \cdots 0 \end{cases} \qquad (3.22)$$

$$\text{where} \quad R_{tm} = \frac{\cos(v_1 d)}{\cos(v_2 t)}$$

LSE normal modes propagating in the $+z$ direction will be derived from (3.21) with $-\gamma z$ dependence using (3.2–3.3). LSM normal modes propagating in the $+z$ direction will be derived from (3.22) with $-\gamma z$ dependence using (3.5–3.6). If the mth mode in the $+z$ direction is represented as,

$$\mathbf{E}_m = \left(\overline{\mathcal{E}}_t + \mathcal{E}_z \mathbf{z} \right) e^{-\gamma z} = \vec{\mathcal{E}}_m^{+} e^{\cdots} \qquad (3.23)$$

$$\mathbf{H}_m = \left(\overline{\mathcal{H}}_t + \mathcal{H}_z \mathbf{z} \right) e^{-\gamma z} = \vec{\mathcal{H}}_m^{+} e^{\cdots} \qquad (3.24)$$

then the mode propagating in the $-z$ direction is given by,

$$\mathbf{E}_m = \left(\overline{\mathcal{E}}_t - \mathcal{E}_z \mathbf{z} \right) e^{+\gamma z} = \vec{\mathcal{E}}_m^{-} e^{+\gamma z} \qquad (3.25)$$

$$\mathbf{H}_m = \left(-\overline{\mathcal{H}}_t + \mathcal{H}_z \mathbf{z} \right) e^{+\gamma z} = \vec{\mathcal{H}}_m^{-} e^{+\gamma z} \qquad (3.26)$$

The caligraphic letters $\overline{\mathcal{E}}_t$, $\mathcal{H}_z$ etc. will be used to denote the normal mode field components without the $e^{\pm \gamma z}$ dependence.

3.2.3   Orthogonality Relations

The orthogonality relations between the normal modes will be introduced at this stage. General orthogonality relations between modes in uniform cylindrical guides with arbitrary filling is discussed in Bresler [39]. For an inhomogeneously filled waveguide, the following (restricted) form of orthogonality is available. That is,

$$\int_S \mathbf{E}_m \times \mathbf{H}_n \cdot \mathbf{z} \ dS \ = \ 0 \ . \tag{3.27}$$

$\mathbf{E}_m$ is the electric field of the mth normal mode and $\mathbf{H}_n$ is the magnetic field of the nth normal mode. If $\mathbf{E}$ and $\mathbf{H}$ belong to distinct sets such as LSE and LSM, then the above relation is valid for all m and n. However, if both the vectors belong to the same set say LSE, the relation is valid only when $m \neq n$. Since the integrand is a scalar triple product involving $\mathbf{z}$, and the integration domain is the transverse cross-section, the above relation can be reduced to one involving the transverse components only. That is,

$$\int_S \overline{\mathcal{E}}_{t,m} \times \overline{\mathcal{H}}_{t,n} \cdot \mathbf{z} \ dS \ = \ 0 \ . \tag{3.28}$$

3.2.4 Derivation of Green's Functions

We shall adopt the notion of Green's function as the *field due to an elementary source (Dirac delta)*. For the analysis of Chapter 2, it is necessary to consider 3 source types namely J_y, J_z and M_y. It is also necessary to consider 3 field types caused by the aforesaid sources, namely E_y, E_z and H_y. This amounts to 9 Green's functions which we shall indicate as $E_y(J_y)$, $H_y(J_z)$ etc. The rule for getting the fields from the sources will be (3.29) without any scale factors such as $-\jmath\omega\mu$ because of the above definition. Thus,

$$E_y \ = \ \int_{S'} E_y(\,J_y\,) \ J_y \ dS' \ . \tag{3.29}$$

Let the field radiated by the elementary source of concerned type at (x', y', z') be represented as a series of LSE and LSM modes,

$$\mathbf{E} \ = \ \sum_m a_m \ \overline{\mathcal{E}}^+_{m,LSE} \ e^{-\gamma(z-z')} \ + \ \sum_n b_n \ \overline{\mathcal{E}}^+_{n,LSM} \ e^{-\gamma(z-z')} \tag{3.30}$$

$$H = \sum_m a_m \overline{\mathcal{H}}^+_{m,LSE} \; e^{-\gamma(z-z')} + \sum_n b_n \, H_{n,LSM} \quad \quad \quad (3.31)$$

for $z > z'$ and,

$$E = \sum_m a'_m \overline{\mathcal{E}}^-_{m,LSE} \; e^{+\gamma(z-z')} + \sum_n b'_n \, \mathcal{E}_{n,LSM} \quad \quad \quad (3.32)$$

$$H = \sum_m a'_m \overline{\mathcal{H}}^-_{m,LSE} \; e^{+\gamma(z-z')} + \sum_n b'_n \, \mathcal{H}_{n,LSM} \quad \quad \quad (3.33)$$

for $z < z'$.
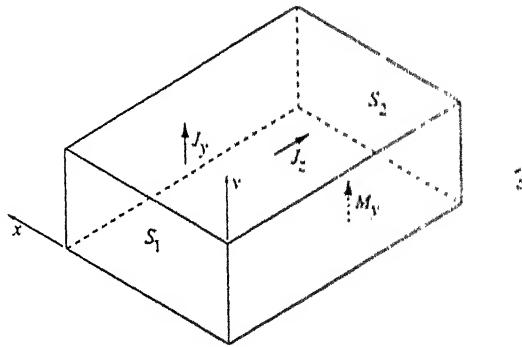
Figure 3.2: Radiating sources inside waveguide.

The coefficients a_m, b_n, a'_m, b'_n can be evaluated by applying reciprocity theorem to a suitably defined volume. Fig. 3.2 shows the volume containing the radiating sources to which reciprocity theorem is applied. Note that this region is bounded by the surfaces S_1, S_2 and the waveguide walls.

Consider the following pair of source-field situations:

• The source pair **J**, **M** producing the fields **E**, **H** as defined in (3.30–3.33).

• The source free solutions $\mathbf{E}_n$, $\mathbf{H}_n$, which corresponds to one of the normal modes in $\pm z$ direction.

The reciprocity relation between this pair of fields, $(\mathbf{E}_n, \mathbf{H}_n)$ and $(\mathbf{E}, \mathbf{H})$ is given by,

$$\oint_S \left(\mathbf{E} \times \mathbf{H}_n - \mathbf{E}_n \times \mathbf{H} \right) \cdot \mathbf{n} \, dS \;=\; \int_V \left(\mathbf{J} \cdot \mathbf{E}_n - \mathbf{M} \cdot \mathbf{H}_n \right) dV \,. \quad (3.34)$$

Note that $(\mathbf{E}_n, \mathbf{H}_n)$ satisfies source free Maxwell's equations while $(\mathbf{E}, \mathbf{H})$ satisfies Maxwell's equations with the concerned source type. That is,

$$\nabla \times \mathbf{E} \;=\; -j\omega\mu\, \mathbf{H} - \mathbf{M} \quad\quad (3.35)$$

$$\nabla \times \mathbf{H} \;=\; +j\omega\epsilon\, \mathbf{E} + \mathbf{J} \quad\quad (3.36)$$

The reciprocity relation reduces to the following form on applying to this volume and for this pair of fields.

$$\underbrace{\int_{S_2} \left(\mathbf{E} \times \mathbf{H}_n - \mathbf{E}_n \times \mathbf{H} \right) \cdot \mathbf{z} \, dS}_{I_2} - \underbrace{\int_{S_1} \left(\mathbf{E} \times \mathbf{H}_n - \mathbf{E}_n \times \mathbf{H} \right) \cdot \mathbf{z} \, dS}_{I_1} =$$

$$\int_V \left(\mathbf{J} \cdot \mathbf{E}_n - \mathbf{M} \cdot \mathbf{H}_n \right) dV \quad\quad (3.37)$$

One can choose $\mathbf{E}_n$, $\mathbf{H}_n$ as *LSE/LSM* mode fields with 2 choices on the direction of propagation. By making use of the orthogonality relation (3.28), and the 4 choices on $\mathbf{E}_n$, $\mathbf{H}_n$, we have the following results.

• $\mathbf{E}_n$, $\mathbf{H}_n$ are the *LSE* fields propagating in $+z$ direction.

$$I_2 \;=\; 0$$
$$I_1 \;=\; +2\, a'_m \, P_{LSE} \, e^{-\gamma z'}$$

• $\mathbf{E}_n$, $\mathbf{H}_n$ are the *LSE* fields propagating in $-z$ direction.

$$I_1 \;=\; 0$$
$$I_2 \;=\; -2\, a_m \, P_{LSE} \, e^{+\gamma z'}$$

• $\mathbf{E}_n$, $\mathbf{H}_n$ are the *LSM* fields propagating in $+z$ direction.

$$I_2 = 0$$

$$I_1 = +2\, b_n'\, P_{LSM}\, e^{-\gamma z'}$$

- E_n, H_n are the *LSM* fields propagating in $-z$ direction.

$$I_1 = 0$$

$$I_2 = -2\, b_n\, P_{LSM}\, e^{+\gamma z'}$$

where

$$P_{LSE} = \int_S \left(\overline{\mathcal{E}}_{t,LSE} \times \overline{\mathcal{H}}_{t,LSE} \right) \cdot z \; dS$$

$$P_{LSM} = \int_S \left(\overline{\mathcal{E}}_{t,LSM} \times \overline{\mathcal{H}}_{t,LSM} \right) \cdot z \; dS.$$

The coefficients a_m, b_n, a_m' and b_n' can be evaluated by computing the right-hand-side of (3.37) in the above 4 cases, leading to the following results.

- J_y as source.

$$a_m = \frac{\mathcal{E}_{y,LSE}(x',y')}{-2\,P_{LSE}} \tag{3.38}$$

$$b_n = \frac{\mathcal{E}_{y,LSM}(x',y')}{-2\,P_{LSM}} \tag{3.39}$$

$$a_m' = +a_m$$

$$b_n' = +b_n$$

- J_z as source.

$$a_m = \frac{\mathcal{E}_{z,LSE}(x',y')}{+2\,P_{LSE}} \tag{3.40}$$

$$b_n = \frac{\mathcal{E}_{z,LSM}(x',y')}{+2\,P_{LSM}} \tag{3.41}$$

$$a_m' = -a_m$$

$$b_n' = -b_n$$

- M_y as source.

$$a_m = \frac{\mathcal{H}_{y,LSE}(x', y')}{-2\,P_{LSE}} \tag{3.42}$$

$$b_n = \frac{\mathcal{H}_{y,LSM}(x', y')}{-2\,P_{LSM}} \tag{3.43}$$

$$a'_m = -a_m$$

$$b'_n = -b_n$$

(3.38–3.43) can be substituted in (3.30–3.31) to obtain the following 9 Green's functions.

$$
\begin{aligned}
E_y(J_y) &= \sum C^e_{E_y(J_y)} \sin u_1(a-x') \cos k_y y' \sin u_1(a-x) \cos k_y y\, e^{-\gamma_e\,|z-z'|} \\
&+ \sum C^m_{E_y(J_y)} \sin v_1(a-x') \cos k_y y' \sin v_1(a-x) \cos k_y y\, e^{-\gamma_m\,|z-z'|}
\end{aligned}
$$

$$
\begin{aligned}
E_z(J_y) &= \sum C^e_{E_z(J_y)} \sin u_1(a-x') \cos k_y y' \sin u_1(a-x) \sin k_y y\, e^{-\gamma_e\,|z-z'|}\,\ominus \\
&+ \sum C^m_{E_z(J_y)} \sin v_1(a-x') \cos k_y y' \sin v_1(a-x) \sin k_y y\, e^{-\gamma_m\,|z-z'|}\,\ominus
\end{aligned}
$$

$$
\begin{aligned}
H_y(J_y) &= \sum C^e_{H_y(J_y)} \sin u_1(a-x') \cos k_y y' \cos u_2 x \sin k_y y\, e^{-\gamma_e\,|z-z'|}\,\ominus \\
&+ \sum C^m_{H_y(J_y)} \sin v_1(a-x') \cos k_y y' \cos v_2 x \sin k_y y\, e^{-\gamma_m\,|z-z'|}\,\ominus
\end{aligned}
$$

$$
\begin{aligned}
E_y(J_z) &= \sum C^e_{E_y(J_z)} \sin u_1(a-x') \sin k_y y' \sin u_1(a-x) \cos k_y y\, e^{-\gamma_e\,|z-z'|}\,\ominus \\
&+ \sum C^m_{E_y(J_z)} \sin v_1(a-x') \sin k_y y' \sin v_1(a-x) \cos k_y y\, e^{-\gamma_m\,|z-z'|}\,\ominus
\end{aligned}
$$

$$
\begin{aligned}
E_z(J_z) &= \sum C^e_{E_z(J_z)} \sin u_1(a-x') \sin k_y y' \sin u_1(a-x) \sin k_y y\, e^{-\gamma_e\,|z-z'|} \\
&+ \sum C^m_{E_z(J_z)} \sin v_1(a-x') \sin k_y y' \sin v_1(a-x) \sin k_y y\, e^{-\gamma_m\,|z-z'|}
\end{aligned}
$$

$$
H_y(J_z) = \sum C^e_{H_y(J_z)} \sin u_1(a-x') \sin k_y y' \cos u_2 x \sin k_y y\, e^{-\gamma_e\,|z-z'|}
$$

$$+ \sum C^m_{H_y(J_z)} \sin v_1(a - x') \sin k_y y' \cos v_2 x \sin k_y y \, e^{-\gamma_m |z - z'|}$$

$$E_y(M_y) = \sum C^e_{E_y(M_y)} \cos u_2 x' \sin k_y y' \sin u_1(a - x) \cos k_y y \, e^{-\gamma_e |z - z'|} \, (-)$$

$$+ \sum C^m_{E_y(M_y)} \cos v_2 x' \sin k_y y' \sin v_1(a - x) \cos k_y y \, e^{-\gamma_m |z - z'|} \, (-)$$

$$E_z(M_y) = \sum C^e_{E_z(M_y)} \cos u_2 x' \sin k_y y' \sin u_1(a - x) \sin k_y y \, e^{-\gamma_e |z - z'|}$$

$$+ \sum C^m_{E_z(M_y)} \cos v_2 x' \sin k_y y' \sin v_1(a - x) \sin k_y y \, e^{-\gamma_m |z - z'|}$$

$$H_y(M_y) = \sum C^e_{H_y(M_y)} \cos u_2 x' \sin k_y y' \cos u_2 x \sin k_y y \, e^{-\gamma_e |z - z'|}$$

$$+ \sum C^m_{H_y(M_y)} \cos v_2 x' \sin k_y y' \cos v_2 x \sin k_y y \, e^{-\gamma_m |z - z'|}$$

where,

$$C^e_{E_y(J_y)} = \frac{1}{-2 P_{LSE}} \left(\frac{\gamma_e}{\epsilon_0} \right)^2$$

$$C^m_{E_y(J_y)} = \frac{1}{-2 P_{LSM}} \left(\frac{k_y v_1}{j \omega \epsilon_0 \mu} \right)^2$$

$$C^e_{E_z(J_y)} = \frac{1}{-2 P_{LSE}} \left(\frac{-k_y \gamma_e}{\epsilon_0^2} \right)$$

$$C^m_{E_z(J_y)} = \frac{1}{-2 P_{LSM}} \frac{-k_y v_1^2 \gamma_m}{(j \omega \epsilon_0 \mu)^2}$$

$$C^e_{H_y(J_y)} = \frac{1}{-2 P_{LSE}} \frac{-u_2 k_y \gamma_e}{j \omega \epsilon_0^2 \mu} R_{te}$$

$$C^m_{H_y(J_y)} = \frac{1}{-2 P_{LSM}} \frac{-v_1 k_y \gamma_m}{j \omega \epsilon_0 \mu^2} R_{tm}$$

$$C^e_{E_z(J_z)} = \frac{1}{+2 P_{LSE}} \left(\frac{k_y}{\epsilon_0} \right)^2$$

$$C^m_{E_z(J_z)} = \frac{1}{+2 P_{LSM}} \left(\frac{v_1 \gamma_m}{j \omega \epsilon_0 \mu} \right)^2$$

$$C^e_{H_y(J_z)} = \frac{1}{+2 P_{LSE}} \frac{u_2 k_y^2}{j \omega \epsilon_0^2 \mu} R_{te}$$

$$C^m_{H_y(J_z)} \;=\; \frac{1}{+2\,P_{LSM}}\,\frac{v_1\gamma_m^2}{\jmath\omega\epsilon_0\,\mu^2}\,R_{tm}$$

$$C^e_{H_y(M_y)} \;=\; \frac{1}{-2\,P_{LSE}}\left(\frac{u_2\,k_y}{\jmath\omega\epsilon_0\,\mu}\right)^2 R_{te}^2$$

$$C^m_{H_y(M_y)} \;=\; \frac{1}{-2\,P_{LSM}}\left(\frac{\gamma_m}{\mu}\right)^2 R_{tm}^2$$

$$C^e_{E_y(J_z)} \;=\; -C^e_{E_z(J_y)}$$

$$C^m_{E_y(J_z)} \;=\; -C^m_{E_z(J_y)}$$

$$C^e_{E_y(M_y)} \;=\; +C^e_{H_y(J_y)}$$

$$C^m_{E_y(M_y)} \;=\; +C^m_{H_y(J_y)}$$

$$C^e_{E_z(M_y)} \;=\; -C^e_{H_y(J_z)}$$

$$C^m_{E_z(M_y)} \;=\; -C^m_{H_y(J_z)}$$

$$P_{LSE} \;=\; \frac{1}{\jmath\omega\,\epsilon_0^2\,\mu}\,\frac{b}{\delta_n}\,S_{te}\,\gamma_e\,\left(\dot{\gamma}_e^2 - k_y^2\right)$$

$$P_{LSM} \;=\; \frac{1}{\jmath\omega\epsilon_0\,\mu^2}\,\frac{b}{2}\,S_{tm}\,\gamma_m\,\left(\gamma_m^2 - k_y^2\right)$$

$$S_{te} \;=\; \frac{t}{2}\left(1 - \frac{\sin 2u_2 t}{2u_2 t}\right)R_{te}^2 + \frac{d}{2}\left(1 - \frac{\sin 2u_1 d}{2u_1 d}\right)$$

$$S_{tm} \;=\; \frac{t}{2}\left(1 + \frac{\sin 2v_2 t}{2v_2 t}\right)\frac{R_{tm}^2}{\epsilon_r} + \frac{d}{2}\left(1 + \frac{\sin 2v_1 d}{2v_1 d}\right)$$

$$\Theta \;=\; \Theta\,(z - z') \;=\; \begin{cases} +1, & z > z' \\ -1, & z < z' \end{cases}$$

$$\delta_n \;=\; \begin{cases} 1, & n = 0 \\ 2, & n > 0 \end{cases}$$

Of the 9 waveguide Green's functions listed above, the source point (x', y', z') and the field point (x, y, z) are *restricted* to be in either the dielectric region or the air region of the inhomogeneously filled waveguide. Green's functions of the $E(J)$ type has both source and field point on the air side, whereas the type $H(M)$ has both points on the dielectric side. Green's functions of the $H(J)$

type has source point on the air side and the field point on the dielectric side, whereas the $E(M)$ type has it vice versa.

It is possible to (partially) verify the Green's functions, by reducing them to the case of homogeneously filled guide. Therefore, substituting $\epsilon_r = 1$ or $t = 0$ should lead to $E_y(M_y) = 0$ and $H_y(J_y) = 0$. All the summations on Green's functions are double indexed from $m = 1$, $n = 1$ (to $m = +\infty$, $n = +\infty$), except for the LSE part of $E_y(J_y)$ Green's function. For this case, the sum starts from $m = 1$, $n = 0$ through the dominant mode. In the above expressions γ_e and γ_m represent the LSE and LSM propagation constants.

The Green's function $E_z(J_z)$ as given above is valid only if the field point does not coincide with the source point. In cases where this is not true, it is necessary to add a Dirac delta function to the above expansion. Therefore, the $E_z(J_z)$ valid at all points is given by [40],

$$E_z(J_z) \;=\; E_z(J_z) \;+\; \frac{-1}{\jmath\omega\epsilon_0}\,\delta(\mathbf{r} - \mathbf{r}') \tag{3.44}$$

This result has significant implications throughout the present work and Section 3.4 is dedicated entirely to this Green's function.

3.3   LSE and LSM Propagation Constants

3.3.1   Introduction

The LSE/LSM eigenvalues u_1, u_2, v_1 and v_2 appear throughout the Green's functions at various places. It is necessary to solve these values at every frequency in order to evaluate the Green's functions. This section deals with the construction of robust algorithms for solving these roots.

The set (u_1, u_2) which satisfy (3.17–3.18) simultaneously are defined as the

LSE roots, whereas the set (v_1, v_2) which satisfy (3.19–3.20) simultaneously are defined as the LSM roots. We make the substitutions $x = u_2 t$, $y = u_1 d$ in (3.17–3.18) and $x = v_2 t$, $y = v_1 d$ in (3.19–3.20). The LSE/LSM defining equations gets transformed to,

$$\frac{\tan x}{x} = -r \frac{\tan y}{y} \qquad \text{LSE family} \qquad (3.45)$$

$$x \tan x = -\frac{\epsilon_r}{r} y \tan y \qquad \text{LSM family} \qquad (3.46)$$

$$x^2 - \frac{y^2}{r^2} = c^2 \qquad \text{Hyperbola} \qquad (3.47)$$

where

$$r = \frac{d}{t}$$

$$c = k_0 t \sqrt{\epsilon_r - 1} \ .$$

The solutions of (3.45) and (3.46) are disjoint family of curves which are sketched in Fig. 3.3. (3.47) is a hyperbola whose positive asymptote is the line $y = rx$. We shall investigate the salient properties of the 3 set of curves, such as the trajectory, slopes etc. in order to construct a solution scheme.

We shall make use of a modified form of the algorithm $rtsafe$ from [41]. This uses both Newton-Raphson and bisection so that it is necessary to provide both a starting value and an interval for the root. The algorithm makes use of Newton-Raphson for a fixed number of times. It then switches to bisection if the root wanders off the interval, or if Newton-Raphson is unable to achieve the accuracy within a certain number of iterations. This scheme is necessary for the present problem because the functions involved are multiple valued and the solution may fall into another possible region. The idea of the following discussion is to provide good starting values and safe bounds for the roots so that solution scheme is robust.
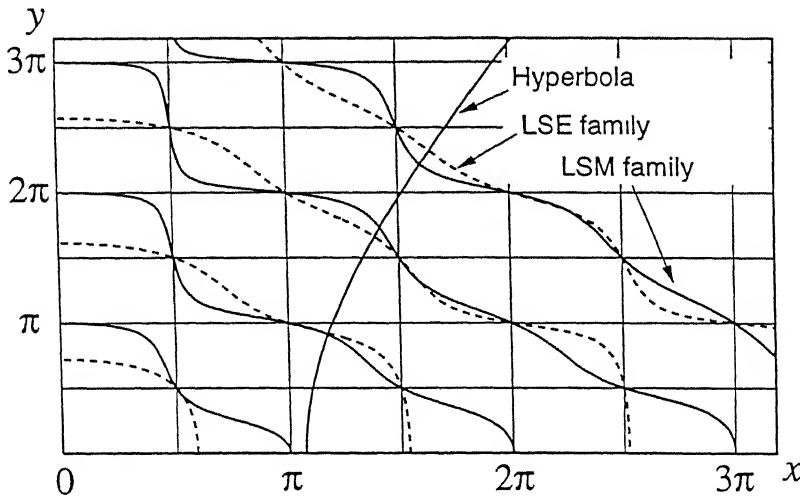
Figure 3.3: LSE/LSM family of curves

3.3.2   Concept of a Root Square

With Reference to Fig. 3.3, the region of interest, namely $x > 0$ and $y > 0$ can be divided into squares of size $\pi \times \pi$ centered at $(m\pi, n\pi)$ where $m, n = 0, 1, \ldots$. Each such square will be defined as a *root square*. The squares with $m, n > 0$ will be called *proper root squares*, while squares with $m = 0$ or $n = 0$ will be called *improper root squares* [See Fig. 3.4]. A root square centered at $(m\pi, n\pi)$ will be referred as "(m, n)th root square".

For each root square we identify 3 points, namely bottom right $A(x_r, y_b)$, center $B(x_c, y_c)$ and top left $C(x_l, y_t)$. For improper root squares, either C or A will be outside the region of interest depending on whether $m = 0$ or $n = 0$.

The LSE/LSM curves pass diagonally across each root square such that it passes through A, B and C. It is this property that prompts us to introduce the notion of a root square. Note that in $(m, 0)$ root squares, the LSE curve does not pass through B. This is because $\tan x / x = 1$ when $y = 0$. Therefore, in improper root squares LSE curves does not pass through B.

We can view the root finding problem as one of identifying the sequence of root squares through which the hyperbola passes. Each such root square will
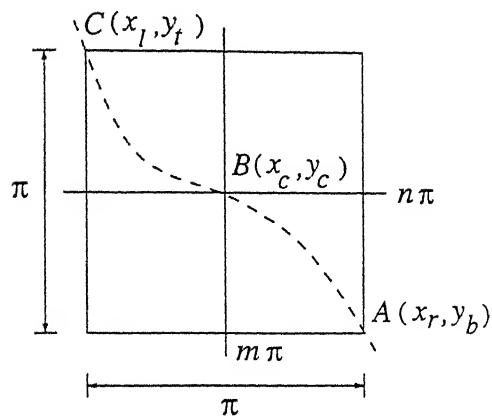
Figure 3.4: Definition of a root square.

give two roots, one for *LSE* and the other for *LSM*. For example, in Fig. 3.3 we can identify the sequence of root squares where the hyperbola intercepts the *LSE/LSM* curves. The root sequence for this example is,

$$(1, 1) \longrightarrow (1, 2) \longrightarrow (2, 2) \longrightarrow \cdots$$

We have thus completed the first step of the root finding. That is, to move along the hyperbola from its apex and identify the root square sequence. The remaining two steps of the algorithm are now dealt with—finding good starting values and safe bounds, so that a root finding algorithm can start polishing a root.

3.3.3 Choosing a Starting Value

To find a good starting value in a root square, we proceed as follows. Since the *LSE/LSM* curves pass through A, B and C, the intersection between the diagonal $\overline{AC}$ and the hyperbola can be taken as a starting value. It is easy to find this point x_0, since it involves the solution of a quadratic. That is,

$$x_0 = \frac{\sqrt{(y_b + x_r)^2 + (r^2 - 1) \cdot \left[(y_b + x_r)^2 + (rc)^2 \right]} - (y_b + x_r)}{r^2 - 1} \quad (3.48)$$

There is yet another reason for opting for this starting value. We will show that the slope of the LSE curves at A, B and C tends to -1 in the limit. Therefore, in the limit, in a root square with the hyperbola, the LSE curves are close to the diagonal $\overline{AC}$.

To prove this, we estimate the slope of LSE curves at A, B and C using the following approximations of $\tan x$.

1. If x is around $m\pi$, then, $\tan x \sim x - m\pi$ for $m = 0, 1, \ldots$

2. If x is around $m\pi/2$, then, $\tan x \sim \pm 1 / \left[x - (m\pi/2) \right]$ for $m = 1, 3, \ldots$

Using these results in (3.45–3.46), we get

$$\left. \frac{dy}{dx} \right|_A = -r \bigg/ \left(\frac{y_b}{x_r} \right) \quad (3.49)$$

$$\left. \frac{dy}{dx} \right|_B = -\frac{1}{r} \left(\frac{y_c}{x_c} \right) \quad (3.50)$$

$$\left. \frac{dy}{dx} \right|_C = -r \bigg/ \left(\frac{y_t}{x_l} \right) \quad (3.51)$$

Note that y_b/x_r, y_c/x_c and y_t/x_l tend to r, since $y = rx$ is the asymptote of the hyperbola. Therefore, the slope at the three points tend to -1. These results do not hold good for LSM curves. However, experience with the solution has suggested that this is a good enough starting value.

Therefore LSE/LSM roots can be solved by applying Newton-Raphson method to (3.52–3.53) with x_0 as the starting value. That is,

$$f(x) = \frac{\tan x}{x} + r \frac{\tan y}{y} = 0 \quad \text{with } y = r \sqrt{x^2 - c^2} \quad (3.52)$$

$$f(x) = x \tan x + \frac{\epsilon_r}{r} y \tan y = 0 \quad \text{with } y = r \sqrt{x^2 - c^2} \quad (3.53)$$

It is also possible to solve an LSM root using an LSE root as the starting value.

3.3.4 Choosing a Root Bound
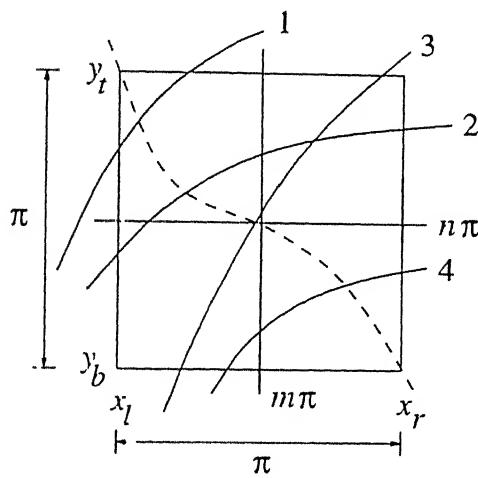
Figure 3.5: Passage of the hyperbola through a root square.

We define a root bound $[x_1, x_2]$ as an interval on the x axis such that the $f(x)$ has a simple zero within it. We shall soon see that the bounds which we are about to compute has the nice property that $f(x_1) < 0$ and $f(x_2) > 0$. This will be useful in bisection algorithm to decide how to update the root interval.

We introduce two functions $x(y)$ and $y(x)$ to facilitate the discussion of root bounds. Note that these functions give just the coordinates on the hyperbola.

$$y(x) = r\sqrt{x^2 - c^2}$$
$$x(y) = \sqrt{(y/r)^2 + c^2}$$

Fig. 3.5 shows the 4 possible cases by which a hyperbola can pass through a root square. In each case, it is easy to identify a root bound. For example, if it is case 1, we can choose the following root bound $[x_l, x(y_t)]$. For each case,

we can also identify the next[2] root square to which the hyperbola gets in. For example, in both case 2 and case 4 the next root square is $(m+1, n)$. Table 3.1 summarizes the essential information. Note that case 3 and case 4 do not occur in $(m, 0)$ root squares while case 1 and case 2 do not occur in $(0, n)$ root squares.

Table 3.1: Look up table for the root finding scheme

No	Case	Root Bound	Next root square
1	$y_b < y(x_l) < y_t$ & $x_l < x(y_t) < x_r$	$[x_l, x(y_t)]$	$(m, n+1)$
2	$y_b < y(x_l) < y_t$ & $y_b < y(x_r) < y_t$	$[x_l, x_r]$	$(m+1, n)$
3	$x_l < x(y_b) < x_r$ & $x_l < x(y_t) < x_r$	$[x(y_b), x(y_t)]$	$(m, n+1)$
4	$x_l < x(y_b) < x_r$ & $y_b < y(x_r) < y_t$	$[x(y_b), x_r]$	$(m+1, n)$

3.3.5   Modified Newton-Raphson-Bisection Algorithm

The root finding scheme is based on (3.52–3.53) with x_0 as the starting value. We also make use of Table 3.1 to decide the root bound and the next root square. Once we are in a root square, the following algorithm can be used to polish the root.

> **Algorithm rtsafe(x_1, x_2, x_0, f, x)**
> **parameter($NR = 10$, $BS = 50$, $err = 1.0d - 12$)**

c   **Solution of $f(x) = 0$ by combined Newton-Raphson and**

c   **Bisection. $[x_1, x_2]$ is the root bound, x_0 is the**

---

[2]It is assumed that we are currently at the (m, n)th root square

c   starting value. NR, BS are the maximum allowed number

c   of iterations for Newton-Raphson and Bisection respectively.

c err is the maximum allowable error in $|f(x)|$

$x = x_0$

do $i = 1, BS$

    $f = f(x)$

    if $(|f| \leq err)$ **return**

    $dif = f/f'$

    $x_{new} = x - dif$

    if $\Big((x_{new} > x_2) \textbf{ or } (x_{new} < x_1) \textbf{ or } (i > NR)\Big)$ **then**

       if $(f < 0)$ **then**

          $x_1 = x$

       else

          $x_2 = x$

       end if

       $x_{new} = (x_1 + x_2)/2$

    end if

    $x = x_{new}$

end do

stop

end

This discussion has not covered every exception that occurs while solving the *LSE/LSM* roots. However an implementation based on these ideas has been quite satisfactory.

3.4 $E_z(J_z)$ **Green's Function as a Distribution**

3.4.1 Introduction

Green's function is the solution of a Partial Differential Equation (PDE) with the right-hand-side replaced by a Dirac delta function [42]. The solution is to be interpreted in the sense of distributions. The rule for getting the solution for an arbitrary right-hand-side, involves the integral of the product of the Green's function with the right-hand-side, over the source domain. We shall refer to this as the *transformation rule*. Note that, a Green's function is a generalized function, whereas the solution obtained after the transformation rule is a function in the classical sense.[3] The dimension of the Dirac delta used in the derivation of Green's function implicitly dictates the number of quadratures to be performed in the transformation rule. Supposing, we deal with current sources and fields as in EM, a 3-D delta dictates a volume integral in the transformation rule.

If the source domain does not possess one of the linear dimensions, as an approximation to the actual geometry (or as an independent assumption by itself), it is possible to leave out the quadrature in that direction. However, the solution so obtained will continue to be a distribution since the legitimate number of quadratures have not been performed. In a boundary value problem (BVP), where we deal with incident and scattered fields together, the presence of a generalized function (scattered field) leads to awkward problems. A generalized function amidst classical functions demands sophisticated interpretations to make sense.

In the present section, this problem is illustrated considering the evaluation the E_z field from $E_z(J_z)$ Green's function. This problem is a part of the evaluation of the RSE$_{zz}$ submatrix in Chapter 2. Therefore, this section serves the

---

[3]The phrase "to make sense" will be used to mean "to make sense as a classical function".

dual purpose of an illustration as well as an elaboration of the MoM matrix evaluation of Chapter 2.

3.4.2   Problem Identification

Consider a slightly modified definition of the $E_z(J_z)$ Green's function based on (3.44).

$$
\begin{aligned}
E_z(J_z) \;=\;& \sum C_{TE} \underbrace{\sin u_1(a-x')\,\sin k_y y'\,\sin u_1(a-x)\,\sin k_y y}_{B_{TE}}\; e^{-\gamma_e|z-z'|} \\
+\;& \sum C_{TM} \underbrace{\sin v_1(a-x')\,\sin k_y y'\,\sin v_1(a-x)\,\sin k_y y}_{B_{TM}}\; e^{-\gamma_m|z-z'|} \\
+\;& \frac{-1}{j\omega\epsilon_0}\,\delta(\mathbf{r}-\mathbf{r}')
\end{aligned}
\tag{3.54}
$$

where

$$
C_{TE} \;=\; C^e_{E_z(J_z)} \;=\; \frac{1}{+2\,P_{LSE}}\left(\frac{k_y}{\epsilon_0}\right)^2
$$

$$
C_{TM} \;=\; C^m_{E_z(J_z)} \;=\; \frac{1}{+2\,P_{LSM}}\left(\frac{v_1\,\gamma_m}{j\omega\epsilon_0\mu}\right)^2
$$

The Green's function consists of two double series corresponding to LSE and LSM normal modes and an explicit Dirac delta term. The presence of the delta function definitely makes[4] (3.54) a distribution. Being a distribution, the Green's function need not make sense, so that both the series in (3.54) need not be convergent. However, we require the E_z field to make sense after the transformation rule between (3.54) and an arbitrary J_z current. Therefore, each of the summation in (3.54) should be convergent after performing the quadratures in the transformation rule. However, this does not happen if one

---

[4]An expression need not contain a Dirac delta to qualify as a distribution!

of the quadratures over the source domain are dropped.

For the printed strip problem of Chapter 2, we neglect the thickness of the strip and regard it as a domain,

$$S'_R = [-l_l, +l_l] \times [-w_l, +w_l] \quad \text{at } x' = t.$$

Therefore, we leave the quadrature in the x' direction while performing the transformation rule. The simplified transformation rule is given by,

$$
\begin{aligned}
E_z\big|_{J_z} &= \int_{S'} E_z(J_z)\, J_z\, dS' \\
&= \underbrace{\sum C_{TE} \int_{S'_R} B_{TE}\, e^{-\gamma_e |z - z'|}\, J_z\, dS'}_{\mathcal{S}_{LSE}} + \underbrace{\sum C_{TM} \int_{S'_R} B_{TM}\, e^{-\gamma_m |z - z'|}\, J_z\, dS'}_{\mathcal{S}_{LSM}} \\
&\quad + K\, \delta(x - x')
\end{aligned}
\tag{3.55}
$$

where

$$
\begin{aligned}
K &= \frac{-1}{\jmath \omega \epsilon_0} \int_{S'_R} \delta(u - u')\, \delta(v - v')\, J_z\, dS' \\
&= \frac{-1}{\jmath \omega \epsilon_0} J_z(u, v)
\end{aligned}
\tag{3.56}
$$

The following observations can be made regarding the terms of (3.55). .

1. $E_z\big|_{J_z}$ field contains a one dimensional delta since the quadrature in x' is left undone.

2. The series $\mathcal{S}_{LSE}$ is convergent.

3. The series $\mathcal{S}_{LSM}$ is divergent. Specifically, the partial sums of $\mathcal{S}_{LSM}$ in m diverges.

The term $\delta(x - x')$ makes the E_z field a distribution unlike its function counterparts E_y^{inc}, $E_z\big|_{J_y}$ etc. We cannot handle a situation where we treat

distributions and functions on the same category. The convergence or the divergence of the terms S_{LSE} or S_{LSM} are difficult to prove. We do not provide any rigorous convergence proofs in this regard, but outline the results to be used to prove such statements.

Each series in (3.55) is double indexed with respect to m and n. The convergence properties are primarily governed by the O dependence[5] of the coefficient part C_{TE} and the integral $\left(\int_{S'_R} B_{TE} \, e^{-\gamma_e |z-z'|} \, J_z \, dS' \right)$ on m and n. The function B_{TE} is bounded and is composed of four trigonometric functions. Of the four trigonometric functions, only $\mathrm{tr}(k_y y')$ participates in the integral. It is possible to get an approximate idea about the series by looking at the growth rates of the coefficient and the integral. At large values of m, there is also the result [33] that u_1, v_1, u_2 and v_2 tend to $k_x = m\pi/a$. Therefore, by using the results in page 69, we have

$$C_{TE} = \underbrace{\frac{1}{2} \, j\omega\mu \, \frac{\delta_n}{b \, S_{te}}}_{\text{bounded part}} \frac{k_y^2}{\gamma_e \, (u_1^2 - k_0^2)} \quad \sim \quad \frac{k_y^2}{\gamma \, k_x^2} \qquad (3.57)$$

$$C_{TM} = \underbrace{\frac{1}{2} \, \frac{1}{j\omega\epsilon_0} \, \frac{2}{b \, S_{tm}} \, \frac{v_1^2}{v_1^2 - k_0^2}}_{\text{bounded part}} \quad \gamma_m \quad \sim \quad \gamma \qquad (3.58)$$

The quadratures are bounded by the reciprocal of the coefficients so that,

$$\left| \int_{S'_R} e^{-\gamma |z-z'|} \, \mathrm{tr}(k_y y') \, J_z \, dS' \right| = O\left(\frac{1}{k_y \, \gamma} \right) \quad \text{for } z \in S'_R . \qquad (3.59)$$

Using the results in (3.57–3.59) in (3.55), we get

$$|S_{LSE}| \leq K' \sum_{m,n} \frac{|\sin k_y y|}{k_x^2 \, \gamma^2} \, k_y$$

---

[5]If $f = O(g)$, then, there exists suitable K such that, $|f(x)| \leq K \, g(x)$ for all sufficiently large values of x.

$$\leq K'' \sum_{m,n} \frac{|\sin k_y y|}{k_x^2 k_y}$$

$$\leq K'' \left(\sum_m \frac{1}{k_x^2} \right) \left(\sum_n \frac{|\sin k_y y|}{k_y} \right)$$

The series $\sum_n |\sin k_y y|/k_y$ is not absolutely convergent, so that this upper bound for $|\mathcal{S}_{LSE}|$ is divergent. We cannot therefore conclude that $\mathcal{S}_{LSE}$ is convergent. It is necessary to derive very tight upper bounds to prove the convergence of such series. However, for specific cases it is possible to prove the convergence of $\mathcal{S}_{LSE}$.
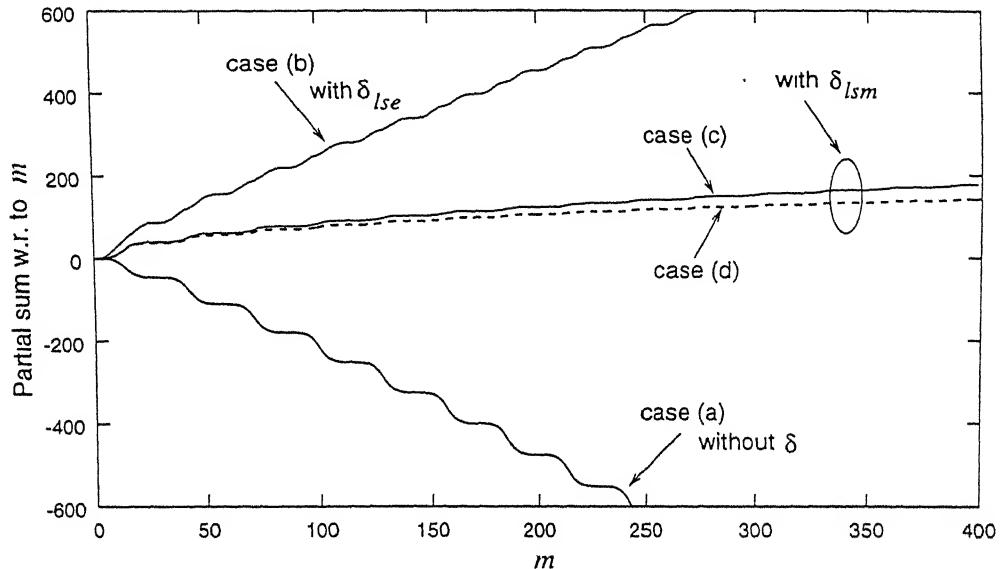

Figure 3.6: Partial sums of the LSM part of $RSE_{zz}(1,1)$ matrix entry under various conditions

The series $\mathcal{S}_{LSM}$ can be shown to be divergent without resorting to any elaborate convergence proofs. Note that C_{TM} grows as γ, whereas the integral in (3.59) is just $O(1/(k_y \gamma))$. Therefore, the series for $\mathcal{S}_{LSM}$ does not have any terms in the denominator which increase with m. We thus have a series in m whose mth term does not tend to zero. We can definitely make the statement that $\mathcal{S}_{LSM}$ is divergent in m. Fig. 3.6 shows the partial sum of the LSM part of RSE_{zz}

with respect to m. The curve in case(a) indicates an unbounded partial sum. We will be using this matrix entry for further illustrations, since S_{LSM} and this entry are identical insofar as the growth with respect to m is concerned.

We are thus faced with a problem of interpreting a diverging LSM series and an explicit Dirac delta in a supposedly classical expression (3.55). It is intuitively clear that the LSM series and the Dirac delta should be handled together to make the expression (3.55) meaningful. This is done by representing the delta function in terms of a valid complete orthonormal set.

3.4.3 Representation of Dirac Delta

We shall use the following result for representing Dirac Delta.

Theorem 3.1 *If* $\{\, e_m(x)\,\}$ *is a complete orthonormal set, then*

$$\delta(x - x') = \sum_m e_m(x)\, e_m(x')\,.$$

This result is known as the completeness expansion and is referred loosely as the *expansion of singularity*. The word *expansion* is misleading, since the right-hand-side of the above equality is not a series in the conventional sense. The series does not converge so that it is to be understood only in the context of doing a quadrature. That is, if $f(x)$ is any function then

$$f = \sum_m \langle f,\, e_m\rangle\, e_m$$

is a valid expression. We shall refer to this as the *representation of singularity* rather than the *expansion of singularity*.

We can choose between LSE or LSM eigenfunctions for representing $\delta(x - x')$. Incidentally, the LSE eigenfunctions are orthogonal to begin with, whereas LSM eigenfunctions are not. Therefore, we opt for the LSE eigenfunctions. The LSE eigenfunctions are defined by $\{\, f_m\,\}$, where

$$f_m = \begin{cases} \sin u_1 (a - x), & a \geq x > t \\ R_{te} \sin u_2 x, & t \geq x \geq 0 \end{cases} \tag{3.60}$$

Note that f_m satisfies all the boundary conditions to be satisfied by the E_z component in the x direction. That is,

1. $f_m(0) = f_m(a) = 0$

2. $f_m(x)$ is continuous at $x = t$

3. $f'_m(x)$ is continuous at $x = t$

The orthogonality of the set $\{ f_m \}$ can be derived from the general orthogonality statement in Equation 3.28. We can therefore use,

$$\delta(x - x') = \sum_m \frac{1}{\langle f_m, f_m \rangle} f_m(x) f_m(x') \tag{3.61}$$

in (3.55) and study the convergence of the partial sums in m. This is shown as case(b) in Fig. 3.6. It is to be noted that this series is divergent just as in the previous case where the series S_{LSM} was taken alone.

We explain the precise reason for this apparently strange result. If the expression (3.55) were to make sense, it is necessary that the series for S_{LSM} cancels the delta function. It then follows that the series for S_{LSM} *contains an LSM represented singularity.* Therefore, what we are attempting is to cancel the *LSM* represented singularity in S_{LSM} by combining it with an appropriately represented $\delta(x - x')$. If we do so by representing $\delta(x - x')$ as an *LSE* series, then we are trying to subtract two different representations of delta function. This however is a meaningless operation. We will clarify this point as follows.

Suppose $\{ e_m \}$ and $\{ h_m \}$ are two (different) complete orthonormal sets, then

$$\delta(x - x') = \sum_m e_m(x) e_m(x') \tag{3.62}$$

$$\delta(x - x') = \sum_m h_m(x) h_m(x') \tag{3.63}$$

$$\sum_m c_m(x) c_m(x') - \sum_m h_m(x) h_m(x') = 0 \tag{3.64}$$

are true statements in the sense of distributions. However, none of the statements makes sense if the summations are carried out literally. In fact, evaluating (3.64) and hoping to get zero is as meaningless as evaluating any of the expressions in (3.62–3.63).

It is therefore mandatory to represent the delta function as an orthonormalized LSM series so that a term wise subtraction takes place. The LSM eigenfunctions are however not orthogonal. Therefore, it is necessary to orthonormalize the system using the Gram-Schmidt procedure.

3.4.4 Gram-Schmidt Procedure

We begin with the LSM eigenfunctions suitable for representing the x variation of the E_z component. This set $\{ f_m \}$ is defined such that,

$$f_m = \begin{cases} a'_m(x), & a \geq x > t \\ \frac{1}{\epsilon_r} a'_m(x), & t \geq x \geq 0 \end{cases} \tag{3.65}$$

$$a_m = \begin{cases} \cos v_1(a - x), & a \geq x > t \\ R_{tm} \cos v_2 x, & t \geq x \geq 0 \end{cases} \tag{3.66}$$

This choice satisfies all the boundary and continuity conditions to be satisfied by the E_z component in the x direction. That is

1. $f_m(0) = f_m(a) = 0$

2. $f_m(x)$ is continuous at $x = t$

3. $a_m(x)$ is continuous at $x = t$

The set $\{\, a_m \,\}$ can be shown to be orthogonal in the following inner product

$$\langle f \,,\, g \rangle \;=\; \frac{1}{\epsilon_r} \int_0^t f \, g \, dx \;+\; \int_t^a f \, g \, dx \,. \tag{3.67}$$

We shall define the inner product in $\{\, f_m \,\}$ as

$$\langle f \,,\, g \rangle \;=\; \epsilon_r \int_0^t f \, g \, dx \;+\; \int_t^a f \, g \, dx \tag{3.68}$$

so that the orthogonality properties of $\{\, a_m \,\}$ can be used to simplify several steps while evaluating $\langle f_m \,,\, f_n \rangle$. Gram-Schmidt procedure requires $\langle f_m \,,\, f_n \rangle$ for all values of m and n. These can be computed by making use of (3.65–3.66), the orthogonality of $\{\, a_m \,\}$ and the 3 properties enumerated above. $\langle f_m \,,\, f_n \rangle$ for $m \neq n$ and $m = n$ is as follows.

$$
\begin{aligned}
\langle f_m \,,\, f_n \rangle \Big|_{m \neq n} &= \epsilon_r \int_0^t f_m \, f_n \, dx \;+\; \int_t^a f_m \, f_n \, dx \\[2mm]
&= k_0^2 \left(1 - \frac{1}{\epsilon_r} \right) \int_0^t a_m \, a_n \, dx \\[2mm]
&= \frac{v_{2,m}\, A \;-\; v_{2,n}\, B}{v_{2,m}^2 \;-\; v_{2,n}^2} \\[2mm]
A &= \sin v_{2,m} t \; \cos v_{2,n} t \\[2mm]
B &= \cos v_{2,m} t \; \sin v_{2,n} t
\end{aligned}
\tag{3.69}
$$

$$
\begin{aligned}
\langle f_m \,,\, f_m \rangle &= v_{2,m}^2 \, \frac{R_{tm}^2}{\epsilon_r} \, C \;+\; v_{1,m}^2 \, D \\[2mm]
C &= \frac{t}{2} \left(1 + \frac{\sin 2 v_{2,m}\, t}{2 v_{2,m} t} \right) \\[2mm]
D &= \frac{d}{2} \left(1 + \frac{\sin 2 v_{1,m}\, d}{2 v_{1,m} d} \right)
\end{aligned}
\tag{3.70}
$$

The parameters of $v_{2,m}$, $v_{1,n}$ etc. refers to v_2, v_1 etc. evaluated for the corresponding index. In the next subsection we shall construct the algorithm for

implementing the Gram-Schmidt procedure.

3.4.5 Algorithm Implementation

Given a finite or countably infinite sequence $\{f_i\}$ of linearly independent functions in an inner product space, Gram-Schmidt procedure generates both an orthogonal sequence $\{g_i\}$ and an orthonormalized sequence $\{e_i\}$. This can be represented symbolically as

$$\underbrace{\{f_i\}}_{\text{linearly independent}} \longrightarrow \underbrace{\{g_i\}}_{\text{orthogonal}} \longrightarrow \underbrace{\{e_i\}}_{\text{orthonormal}}$$

It is preferable to work with $\{g_i\}$ so that, we shall be using the latter of the following representations of the delta function.

$$\delta(x - x') = \sum_i e_i(x)\, e_i(x') \tag{3.71}$$

$$\delta(x - x') = \sum_i \frac{1}{\langle g_i,\, g_i \rangle}\, g_i(x)\, g_i(x') \tag{3.72}$$

Gram-Schmidt procedure [42] generates $\{g_i\}$ and $\{e_i\}$ in the following sequence

$$
\begin{aligned}
g_1 &= f_1 \\
g_2 &= f_2 - \langle f_2,\, e_1 \rangle\, e_1 \\
g_3 &= f_3 - \langle f_3,\, e_1 \rangle\, e_1 - \langle f_3,\, e_2 \rangle\, e_2 \\
&\;\vdots \\
g_k &= f_k - \sum_{p=1}^{k-1} \langle f_k,\, e_p \rangle\, e_p
\end{aligned}
\tag{3.73}
$$

Replacing e_p with $g_p/\|g_p\|$ in (3.73), we can rewrite the sequence as,

$$g_1 = f_1 \tag{3.74}$$

$$g_k = f_k + \sum_{p=1}^{k-1} \alpha_{kp}\, g_p\,, \quad k > 1 \tag{3.75}$$

$$\alpha_{kp} = -\frac{\langle f_k\,, g_p \rangle}{\langle g_p\,, g_p \rangle}\,, \quad k > p\,. \tag{3.76}$$

Despite being constructive in its very definition, Gram-Schmidt procedure is not convenient in the form presented in (3.74–3.76). In (3.75), the function g_k is defined recursively in terms of g_p's which is difficult to code. We need to define g_k directly as a linear combination of f_ks; that is,

$$g_k = f_k + \sum_{p=1}^{k-1} \beta_{kp}\, f_p\,. \tag{3.77}$$

We can state the objective of the algorithm as follows:

Objective 3.1 *Given* $\{ f_i \}$ *and* $\langle f_i\,, f_j \rangle$ *as in* (3.65), (3.69–3.70) *for* $i = 1, 2, \ldots, N$; *compute* β_{kp}, $N \geq k > p$ *and* $\langle g_k\,, g_k \rangle$, $k \leq N$ *so that,*

$$g_k = f_k + \sum_{p=1}^{k-1} \beta_{kp}\, f_p \tag{3.78}$$

$$\delta(x - x') = \sum_{i=1}^{N} \frac{1}{\langle g_i\,, g_i \rangle}\, g_i(x)\, g_i(x') \tag{3.79}$$

The algorithm is presented recursively. Assume that we have completed the sequence up to the $(k-1)$th stage. That is, α_{kp}, β_{kp} and $\langle g_k\,, g_k \rangle$ are known up to $k-1$. We shall indicate the operations for getting these for kth stage. With reference to (3.76), α_{kp} can be computed from $\langle f_k\,, g_p \rangle$ and $\langle g_p\,, g_p \rangle$. $\langle f_k\,, g_p \rangle$ is computed using,

$$\langle f_k\,, g_p \rangle = \langle f_k\,, f_p \rangle + \sum_{m=1}^{p-1} \beta_{pm} \langle f_k\,, f_m \rangle \tag{3.80}$$

whereas $\langle g_p\,, g_p \rangle$ for $p \leq k-1$ is already available. Having computed α_{kp}, the

term $\langle g_k, g_k \rangle$ can be computed using

$$\langle g_k, g_k \rangle = \langle f_k, f_k \rangle - \sum_{p=1}^{k-1} \alpha_{kp}^2 \langle g_p, g_p \rangle . \tag{3.81}$$

The evaluation of β_{kp} can be conveniently carried out once we adopt the matrix notation. Represent (3.75) and (3.77) in matrix form so that,

$$g_k = f_k + \begin{bmatrix} \alpha_{k1} & \alpha_{k2} & \alpha_{k3} & \cdots & \alpha_{k\,k-1} \end{bmatrix} \begin{bmatrix} g_1 \\ g_2 \\ g_3 \\ \vdots \\ g_{k-1} \end{bmatrix} \tag{3.82}$$

and

$$\begin{bmatrix} g_1 \\ g_2 \\ g_3 \\ \vdots \\ g_{k-1} \end{bmatrix} = \begin{bmatrix} 1 & 0 & 0 & \cdots & 0 \\ \beta_{21} & 1 & 0 & \cdots & 0 \\ \beta_{31} & \beta_{32} & 1 & \cdots & 0 \\ \vdots & \vdots & \vdots & \ddots & \vdots \\ \beta_{k-1\,1} & \beta_{k-1\,2} & \beta_{k-1\,3} & \cdots & 1 \end{bmatrix} \begin{bmatrix} f_1 \\ f_2 \\ f_3 \\ \vdots \\ f_{k-1} \end{bmatrix} \tag{3.83}$$

$$g_k = f_k + \begin{bmatrix} \beta_{k1} & \beta_{k2} & \beta_{k3} & \cdots & \beta_{k\,k-1} \end{bmatrix} \begin{bmatrix} f_1 \\ f_2 \\ f_3 \\ \vdots \\ f_{k-1} \end{bmatrix} \tag{3.84}$$

Substituting (3.83) in (3.82) and comparing it with (3.84) we get,

$$\beta_{k1} = \alpha_{k1} + \sum_{m=2}^{k-1} \alpha_{km}\, \beta_{m1}$$

$$\beta_{k2} = \alpha_{k2} + \sum_{m=3}^{k-1} \alpha_{km} \, \beta_{m2}$$

$$\vdots$$

$$\beta_{kp} = \alpha_{kp} + \sum_{m=p+1}^{k-1} \alpha_{km} \, \beta_{mp} \qquad (3.85)$$

The method of computing α_{kp}, β_{kp} and $\langle g_k, g_k \rangle$ for the kth stage from the $k-1$th stage has been illustrated. The following implementation is based on (3.76), (3.80–3.81) and (3.85).

	Algorithm gram_schmidt(N)
c	**The values $\langle f_\imath, f_\jmath \rangle$ is available for $\imath, \jmath \leq N$**
c	
c	**Algorithm start up**
	$\langle g_1, g_1 \rangle = \langle f_1, f_1 \rangle$
	$\alpha_{21} = -\langle f_2, f_1 \rangle / \langle g_1, g_1 \rangle$
	$\beta_{21} = \alpha_{21}$
	$\langle g_2, g_2 \rangle = \langle f_2, f_2 \rangle + 2\beta_{21} \langle f_2, f_1 \rangle + \beta_{21}^2 \langle g_1, g_1 \rangle$
c	**Algorithm main body**
	do $k = 3,\ N$
	do $p = 1,\ k-1$
	$sum = 0$
	do $m = 1,\ p-1$
	$sum = sum + \beta_{pm} \langle f_k, f_m \rangle$
	end do
	$sum = \langle f_k, f_p \rangle + sum$
	$\alpha_{kp} = -sum / \langle g_p, g_p \rangle$
	end do
	$sum = 0$

```
    do p = 1, k − 1
        sum = sum + α²_kp ⟨g_p, g_p⟩
    end do
⟨g_k, g_k⟩ = ⟨f_k, f_k⟩ − sum

    do p = 1, k − 1
    sum = 0
        do m = p + 1, k − 1
            sum = sum + α_km β_mp
        end do
    β_kp = α_kp + sum
    end do
end do
stop
end
```

In actual implementation it is necessary to use a 2-D array beta(N,N) for implementing β_{kp}. However, since $k > p$ both the diagonal and the upper triangular part of beta(k,p) remains unused. We can use this space for storing α_{kp} and $\langle g_k, g_k \rangle$. Therefore, in the code it is possible to replace α_{kp} by beta(p,k) and $\langle g_k, g_k \rangle$ by beta(k,k). Thus, the storage requirement of the code is exactly N^2.

3.4.6 Results and Discussion

Cases (c) and (d) of Fig. 3.6 illustrate the result of using the LSM representation of delta function. It can be seen that the partial sums are comparatively well behaved unlike the previous two cases. Cases (c) and (d) will be used to bring out the subtle issues involved in subtracting the Dirac delta numerically. Note

that, we are trying to subtract two series which by themselves are *divergent*. Therefore, even a small mismatch between the series will add up and starts showing up at large values of m. Therefore, subtracting two divergent sums is an intrinsically unstable operation. This can be observed on close observation of the curves (c) and (d) of Fig. 3.6. The partial sums starts growing *linearly* at large values of m. The linear growth of partial sums is an undesired result since it makes the partial sums divergent. However, we will be making the observation that the *linear growth arises from imperfect cancelation of Dirac delta*. Of the two cases case(d) exhibits lesser slope than case(c). These cases will be studied carefully to validate the above observation.

The two cases c and d arise from the different representation of Dirac delta $\delta(\mathbf{r} - \mathbf{r}')$ in (3.54). Note that, both

$$\delta(\mathbf{r} - \mathbf{r}') \; = \; \delta(x - x')\, \delta(u - u')\, \delta(v - v') \tag{3.86}$$

and

$$
\begin{aligned}
\delta(\mathbf{r} - \mathbf{r}') \; &= \; \delta(x - x')\, \delta(y - y')\, \delta(z - z') \\
&= \; \delta(x - x') \left(\frac{2}{b} \sum_{n=1}^{\infty} \sin k_y y \, \sin k_y y' \right) \delta(z - z')
\end{aligned}
\tag{3.87}
$$

are valid forms of $\delta(\mathbf{r} - \mathbf{r}')$. If we use (3.86) in (3.55), the term corresponding to the delta function is obtained as just $K^{\cdot}\, \delta(x - x')$. However, if (3.87) is used in (3.55), we get a series representation of $K^{\cdot}$. Thus, the last term corresponding to $\delta(\mathbf{r} - \mathbf{r}')$ in (3.55) can take two alternate forms, namely

$$E_z|_{J_z} \; = \; \mathcal{S}_{LSE} \; + \; \mathcal{S}_{LSM} \; + \; K^{\cdot}\, \delta(x - x') \tag{3.88}$$

$$K^{\cdot} \; = \; -\frac{1}{j\omega\epsilon_0}\, J_z(u, v) \tag{3.89}$$

or

$$E_z|_{J_z} \; = \; \mathcal{S}_{LSE} \; + \; \mathcal{S}_{LSM} \; + \; K_N\, \delta(x - x') \tag{3.90}$$

$$K_N = -\frac{1}{j\omega\epsilon_0}\frac{2}{b}\sum_{n=1}^{N}\left(\int_{S'_R}\sin k_y\, y'\,\delta(z-z')\,J_z\,dS'\right)\sin k_y\,y. \quad (3.91)$$

The series S_{LSM} is a double summation in both m and n. It is not possible to carry out either of the summation in closed form. Supposing we sum N number of terms along m, then the embedded singularity in S_{LSM} will be of the form,

$$S_{LSM} = S'_{LSM} - K_N\,\delta(x-x'). \quad (3.92)$$

In (3.92), we explicitly show S_{LSM} as containing an embedded Dirac delta. If this representation of S_{LSM} is used in (3.88) and (3.90), we get two alternate forms for $E_z|_{J_z}$. That is,

$$E_z\Big|_{J_z} = S_{LSE} + \underbrace{S'_{LSM} - K_N\,\delta(x-x')}_{S_{LSM}} + \begin{cases} \underbrace{K\,\delta(x-x')}_{\text{case (c)}} \\ \underbrace{K_N\,\delta(x-x')}_{\text{case (d)}} \end{cases} \quad (3.93)$$

In case(c) we use the closed form representation of $\delta(\mathbf{r}-\mathbf{r}')$, whereas in case(d) we use the truncated N term approximation. It can be seen that the Dirac delta cancels off completely in case(d), whereas a residual $(K-K_N)\,\delta(x-x')$ remains in case(c). Therefore, the difference between the curves c and d arises from the residual Dirac delta. This is illustrated in Fig. 3.7, where we have plotted the difference between curves c and d and the residual delta side by side. Note that, the presence of the Dirac delta causes a linear growth for the partial sums in m. Ideally speaking, we should have had no residual delta in case(d), and it should have been flat. In actual computations perfect cancelations do not occur, so that (3.92) may not be valid with K_N. Therefore, by the above reasoning, the small yet *definite* growth in case(d) can also be attributed to the presence of uncanceled Dirac delta. It is not easy to safeguard against such errors, except by limiting the number of modes summed to a reasonable number.
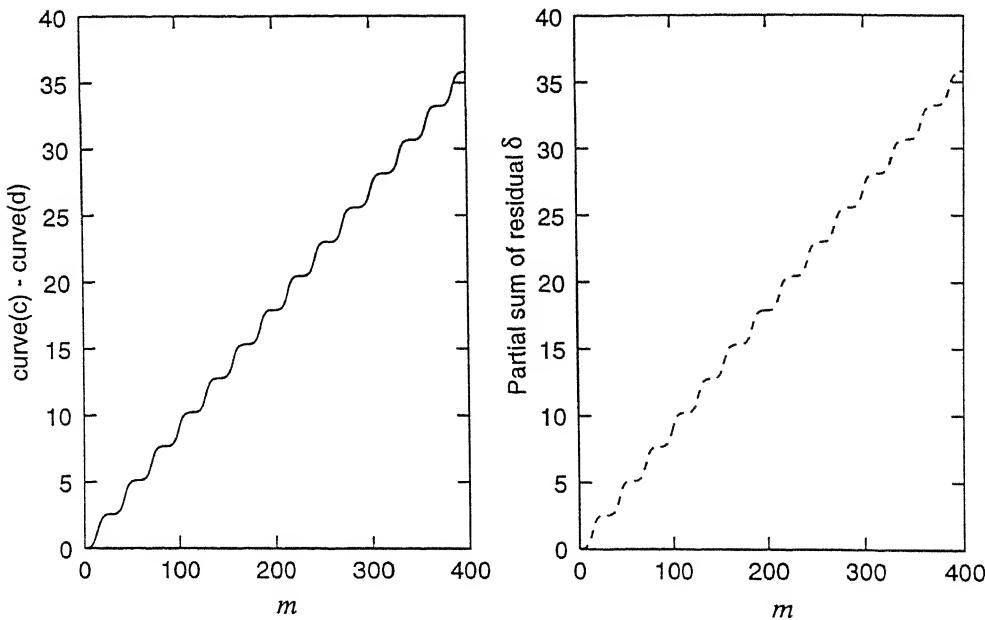
Figure 3.7: Explaining the linear growth of cases c and d as the presence of residual singularity. The partial sum on the right is due to the LSM represented $(K - K_N)\,\delta(x - x')$

3.5   Half Space Green's Function

The expressions for implementing the slot exterior matrix **SXT** is discussed. Fig. 3.8 shows the exterior view of the slot. A centered (y, z) coordinate system is used for analyzing this problem. The slot is assumed to be embedded in an infinite ground plane, so that we are interested in the magnetic field H_y at $x = 0^-$ in the external half space.

The half space problem is identical to free space if the ground plane is removed and the source strength is doubled. Consequently, the electric vector potential for the half space is given by, (**Note**: bold j denotes $\sqrt{-1}$).

$$
\begin{aligned}
F_y &= \frac{\epsilon}{4\pi} \int_{S'} \frac{e^{-jkr}}{r}\, 2\, M_y\, dS' \\
r &= \left[(y - y')^2 + (z - z')^2 \right]^{1/2} .
\end{aligned}
\tag{3.94}
$$
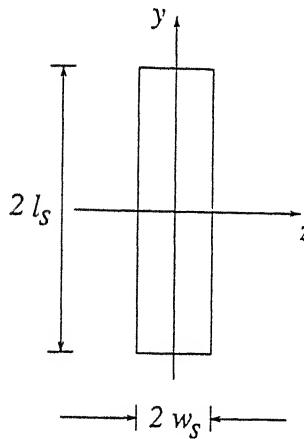
Figure 3.8: Slot exterior view

If $f_i\,\phi$ is the ith basis function on the slot, then we have $M_y = -f_i\,\phi$ and the ji-th matrix entry is given by,

$$H_y \;=\; \frac{1}{j\omega\epsilon\mu}\left(\frac{\partial^2}{\partial y^2} + k^2\right)F_y \tag{3.95}$$

$$SXT(j,i) \;=\; \int_S H_y\,f_j\,dS \tag{3.96}$$

Let G denote the canonical source point integral in (3.94) so that, $SXT(j,i)$ is given by,

$$G \;=\; G(y,z) = \int_{S'} \frac{e^{-jkr}}{r}\,f_i\,\phi\,dS' \tag{3.97}$$

$$SXT(j,i) \;=\; \underbrace{\frac{-1}{2\pi j\omega\mu}}_{\text{constant part}} \int_S f_j\left(G'' + k^2\,G\right)dS \tag{3.98}$$

where G'' denote $\frac{\partial^2 G}{\partial y^2}$. Note that $G(y,z)$ inherits the symmetry of $f_i\phi$. Therefore, $G(y,z)$ is even in z, whereas it is even or odd in y depending on whether f_i is even or odd. Consequently $SXT(j,i) = 0$ if $|j-i| = $ odd. We shall therefore

assume that j and i are both even or odd.

The fundamental problem in evaluating (3.98) is to get rid of the partial differentials within the integral sign. This can be done[6] by evaluating the y integral in (3.98) via. integration by parts. After doing the integration by parts and using the results $f_j(\pm l_s) = 0$ and $f_j'' = -k_j^2 f_j$, we get,

$$
\begin{aligned}
\int_{-l_s}^{+ls} f_j \, G'' \, dy &= \underbrace{f_j \, G' \Big|_{-l_s}^{+l_s}}_{0} - \int_{-l_s}^{+ls} f_j' \, G' \, dy \\
&= -f_j' \, G \Big|_{-l_s}^{+l_s} + \int_{-l_s}^{+ls} f_j'' \, G \, dy \\
&= -f_j' \, G \Big|_{-l_s}^{+l_s} - k_j^2 \int_{-l_s}^{+ls} f_j \, G \, dy
\end{aligned}
\tag{3.99}
$$

and

$$
SXT(j,i) = \frac{-1}{2\pi j\,\omega\mu} \left[(k^2 - k_j^2) \underbrace{\int_S f_j \, G \, dS}_{Z_{2d}} - \underbrace{\int_{-w_s}^{+w_s} f_j' \, G \Big|_{-l_s}^{+l_s} \, dz}_{Z_{1d}} \right]
\tag{3.100}
$$

where

$$
f_j' \, G \Big|_{-l_s}^{+l_s} = f_j'(+l_s) \, G(+l_s, z) - f_j'(-l_s) \, G(-l_s, z) .
\tag{3.101}
$$

(3.100) can be evaluated provided $G(y, z)$ is computable at any point. The evaluation of G cannot be carried out directly due to the presence of the $1/r$ singularity in the integrand. Though the $1/r$ singularity is integrable, it is necessary to reorganize the quadratures in (3.100) so that a standard algorithm can be used. To begin with, we separate e^{-jkr}/r into singular and nonsingular parts. That is,

$$
\frac{e^{-jkr}}{r} = \frac{(e^{-jkr} - 1)}{r} + \frac{1}{r}
\tag{3.102}
$$

---

[6]This idea is based on Elliott [7]

Let Z'_{2d} and Z'_{1d} denote the corresponding part of Z_{2d} and Z_{1d} arising from the $1/r$ term. Define,

$$Z'_{2d} = \int_S f_j \int_{S'} \frac{1}{r} f_i \, \phi \, dS' \, dS \qquad (3.103)$$

and

$$Z'_{1d} = 2 f'_j(+l_s) \int_z \int_{S'} \frac{1}{r} f_i \, \phi \, dS' \, dz \,. \qquad (3.104)$$

We will reorder the sequence of partial quadratures in (3.103–3.104) such that, both contain a term G_0 of identical structure. That is,

$$
\begin{aligned}
Z'_{2d} &= \int_S f_j \int_{S'} \frac{1}{r} f_i \, \phi \, dS' \, dS \\
&= \int_{S'} f_i \, \phi \, \underbrace{\int_y f_j \int_z \frac{1}{r} \, dz \, dy}_{G_0} \, dS'
\end{aligned}
\qquad (3.105)
$$

$$
\begin{aligned}
Z'_{1d} &= 2 f'_j(+l_s) \int_z \int_{S'} \frac{1}{r} f_i \, \phi \, dS' \, dz \\
&= 2 f'_j(+l_s) \int_{S'} f_i \, \phi \int_z \frac{1}{r} \, dz \, dS' \\
&= 2 f'_j(+l_s) \int_{z'} \phi \, \underbrace{\int_{y'} f_i \int_z \frac{1}{r} \, dz \, dy'}_{G_0} \, dz'
\end{aligned}
\qquad (3.106)
$$

Both Z'_{2d} and Z'_{1d} contains the generic integral G_0 which can be evaluated as follows. We carry out the z quadrature analytically using the identity

$$\int_z \frac{dz}{\sqrt{z^2 + a^2}} = \ln\left(z + \sqrt{z^2 + a^2}\right)$$

and combine the quadratures over $[-l_s, 0]$ and $[0, +l_s]$. That is,

$$\int_S \frac{1}{r} f_j \, dz \, dy = \begin{cases} \int\limits_{y=0}^{+l_s} f_j \, \ln\left[\dfrac{g(y-y')}{g(y+y')}\right] \, dy, & \text{for } j = 2, 4, \ldots \\[4ex] \int\limits_{y=0}^{+l_s} f_j \, \ln\left[g(y-y') \cdot g(y+y')\right] \, dy, & \text{for } j = 1, 3, \ldots \end{cases}$$

$$(3.107)$$

where

$$g(y) = \left[(w_s - z') + \sqrt{(w_s - z')^2 + y^2}\right] \cdot \left[(w_s + z') + \sqrt{(w_s + z')^2 + y^2}\right] \Big/ y^2$$

$$(3.108)$$

The quadrature in (3.107) can be evaluated using any standard routine which can take a logarithmic singularity at the end points. The routine *d01anf* (or *d01ajf*) from Nag [36] can be used.

3.6   Method of Moment

3.6.1   Introduction

Moment method is definitely the most widely used numerical technique in EM. Despite its widespread use, there has been few serious studies on it as a numerical method. MoM as a technique does not quite *qualify* as a numerical method, since it does not provide any error estimates nor any convergence rates. As a method, MoM does not have sound theory and it is based on the straight implementation of a very naive idea. In EM, MoM probably works because of the extremely well behaved right-hand-sides and the not so smooth nature of the kernels.

The absence of any error/convergence estimates is justified since the method is applied to complicated operators. However, the sequence of approximate solutions do not improve forever if the number of basis functions are increased. In fact, it can be shown that the solution of an integral equation via. MoM is an ill-conditioned problem, so that, the sequence of approximate solutions first improves and then becomes unstable. This aspect of MoM, which we think is the most serious of all has never been brought to the limelight.

The motivation for the present discussion is our experiences with MoM instabilities as well as the results from S. W. Lee [30], Raj Mittra [31] and M. Leroy [32]. This section is primarily devoted to certain problems, which illustrate the fact MoM is an intrinsically unstable method. In what follows, we discuss the theory and practice of MoM and interpret the instability of solutions from the point of view of regularization.

3.6.2 Theory of Method of Moments

Method of Moment solves a linear operator equation of the form $Tx = y$. Algorithmically, it gives a sequence of approximate solutions which converges to the actual solution. MoM can also solve coupled operator equations of the form,

$$T_{11}\, x_1 + T_{12}\, x_2 = y_1$$
$$T_{21}\, x_1 + T_{22}\, x_2 = y_2\,.$$

We define three spaces related to the operator T: Domain, Range and Null space. The domain of T is the set of all x for which Tx is defined. The problem $Tx = y$ also stipulates certain boundary condition on x which generally makes the domain a subspace. Therefore, any element of the domain is such that Tx is defined and x satisfies the boundary conditions of the problem. The set of all

elements of the form Tx constitute the range of T. The null space is defined as the set of all x such that $Tx = 0$.

Given $Tx = y$, it is necessary to worry about the existence and uniqueness of solutions. However, such discussions can be made only for concrete realizations of T such as a matrix or an integral operator. This topic will be postponed until we encounter an integral equation. The question of existence can be ignored on the argument that a solution exists on physical grounds. However, uniqueness is more serious since it enters indirectly while attempting to solve $Tx = y$. We therefore make the readers familiar with the four equivalent statements of uniqueness.

- $Tx = y$ has unique solution.
- $Tx = 0 \Leftrightarrow x = 0$.
- 0 is not an eigenvalue of T.
- The null space of T is empty.

We call a set $\{e_i\}$ *total* in a subspace V, if, given $\epsilon > 0$ and any $x \in V$, there exist $I_1, I_2 \dots, I_N$ such that $\|\sum_{i=1}^{N} I_i e_i - x\| \leq \epsilon$. Therefore, a total set can approximate any element of the space by a suitable finite linear combination.

The approximate solution of $Tx = y$ begins by identifying a set $\{e_i\}$ in the domain of T such that $\{Te_i\}$ is total in the range space of T. Therefore, given $\epsilon > 0$ and any y, there exist $I_1, I_2, \dots, I_N$ such that $\left\|\sum_{i=1}^{N} I_i Te_i - y\right\| \leq \epsilon$. That is,

$$\left\| T\left(\sum_{i=1}^{N} I_i e_i\right) - y \right\| \leq \epsilon.$$

Therefore $\sum_{i=1}^{N} I_i e_i$ is an approximate solution to $Tx = y$. We call it as the ϵ-approximate solution of $Tx = y$. Thus, we seek the ϵ-approximate solution of $Tx = y$ as ϵ tends to zero. The actual solution process differs from the above notion. Instead of fixing ϵ and demanding a solution, we fix N and ask for the best solution. That is, given N, we seek a solution $x_N = \sum_{i=1}^{N} I_i e_i$ such that, $\|\sum_{i=1}^{N} I_i Te_i - y\|$ is minimum. Therefore, we choose the coefficients $I_1, I_2, \dots, I_N$

appropriately such that the error in the range space is minimum. If we define ϵ_N as,

$$\epsilon_N = \min_{I_1, I_2, \dots, I_N} \left\| \sum_{i=1}^{N} I_i \, T e_i - y \right\|$$

then

$$\epsilon_N \geq \epsilon_{N+1} \geq \epsilon_{N+2} \geq \cdots \geq 0.$$

This inequality sequence is valid[7] such that ϵ_N tends to zero as N tends to infinity. Therefore, the sequence x_N converges to the solution of $Tx = y$. In its primitive form, the solution of $Tx = y$ thus involves a search for the right set of coefficients $I_1, I_2, \dots, I_N$. This is the idealized method for solving $Tx = y$.

By formulating the error $Tx_N - y$ appropriately, it is possible to reduce the search problem to a matrix equation. MoM *defines* the error in terms of the components of the term $Tx_N - y$. If $\{u_i\}$ is a total linearly independent set in the range space of T, then MoM enforces the first N projections of $Tx_N - y$ to be zero along $\{u_i\}$. That is,

$$\left\langle T \left(\sum_{i=1}^{N} I_i \, e_i \right) - y \; , \; u_j \right\rangle = 0 \text{ for } j = 1, 2, \dots, N \tag{3.109}$$

$$\sum_{i=1}^{N} I_i \left\langle T e_i, u_j \right\rangle = \left\langle y, u_j \right\rangle \text{ for } j = 1, 2, \dots, N \tag{3.110}$$

The sequence of approximate solutions obtained by solving (3.109–3.110) need not be *monotonically* improving. The method of point matching enforces the condition that $T x_N$ agrees with y on a set of N points in the range. The key idea of MoM is the use of matrix methods to solve the best approximation problem of y in the space spanned by $\{T e_i\}$.

We prefer to call this as the *naive approach* to MoM since no attention is

---

[7]except for few equality signs this is valid in the form $\cdots > \epsilon_N > \epsilon_{N+1} > \epsilon_{N+2} > \cdots$

payed to the performance of the algorithm in the presence of errors. We shall soon see that the errors in computing Te_i or $\langle T\,e_i\,,\,u_j\,\rangle$ lead to instabilities in the solution scheme.

3.6.3   Practice of Method of Moments

Introduction

EM boundary value problems are generally formulated as integral equations of the first kind. A Fredholm integral equation of first kind (in one dimension) is given by,

$$\int_a^b K(x,y)\,f(x)\,dx \;=\; g(y)\,,\;\; c \le y \le d \tag{3.111}$$

Despite the various possibilities in the kernel (such as finite rank, singular, higher dimensional etc.), the following result is valid for an integral equation of the above form. Since $g(y)$ is defined through a quadrature on $f(x)$, the right-hand-side of an integral equation is generally smoother than $f(x)$. Any numerical method which attempts to solve $f(x)$ from (3.111), in essence, is doing a differentiation[8] of the right-hand-side. Therefore (3.111) may not have any solution unless the right-hand-side possess a certain degree of smoothness. This is especially true if the right-hand-side is known with some error as in a measured data. Therefore, the existence of solutions is closely linked to the smoothness of the right-hand-side. In the context of EM, where we deal with incident fields on the right-hand-side, this problem does not arise. The incident

---

[8]See the following example from Tikhonov [43]: The nth derivative $z(t)$ of the function $u(t)$ is the solution of the integral equation,

$$\int_0^t \frac{(t-\tau)^{n-1}}{(n-1)!}\,z(\tau)\,d\tau \;=\; u(t)$$

field is infinitely differentiable and often analytic, so that it can be regarded as sufficiently smooth.

Even in cases where the right-hand-side is known to be smooth, and a solution exists, the direct solution of first kind integral equation is regarded as ill-conditioned. Note that ill-conditioning is intrinsic to the smoothing property of the quadrature process, and it does not depend on what appears on the right-hand-side. A right-hand-side with errors merely brings out the badness of the left side. The smoother is the kernel, the worse is the numerical evaluation of $f(x)$. The numerical solution of inverse Laplace transform and the problem of numerical differentiation etc. also fall into this category.

The purpose of the present discussion is to illustrate this problem via. a set of examples. We use our results as well as the results from the following sources [30, 31, 32, 44]. Despite its widespread use, the stability issues of MoM has not received any major attention in EM. The three works mentioned herein [30, 31, 32] and the pioneering work of R. Mittra on "Relative Convergence" remain the major EM investigations on stability.

This is in direct contrast with Mathematics where the stability issues of first type equations have received serious attention. In fact, the theory of regularization and inverse methods evolved based on the difficulties in solving first kind integral equations.

Literature on Stability Issues

S. W. Lee [30], Raj Mittra [31] and M. Leroy [32] studied the convergence of certain discontinuity problems in rectangular and parallel plate waveguides. Their investigations were on *transverse* discontinuities. Note that, this includes the iris, diaphragm and bifurcation problems. The numerical performance of both mode matching and the solution of integral equations via. MoM were studied. The first observation was that both the methods lead to the same set

of equations and are therefore identical.

We shall therefore assume that the transverse discontinuity problems are solved using integral equation MoM. The Green's function for *transverse* discontinuity problems does not have the $e^{-\gamma|z-z'|}$ factor. Therefore, the authors have used a waveguide Green's function of the form, (**Note:** tr stands for sin or cos).

$$K(x,y,x',y') \;=\; \sum_{m=1}^{\infty} \sum_{n=1}^{\infty} \operatorname{tr}(k_y y) \operatorname{tr}(k_x x) \operatorname{tr}(k_y y') \operatorname{tr}(k_x x') \qquad (3.112)$$

The computations were done using a truncated version of the kernel. Let P denote[9] the number of modes summed for the kernel, while N denote the number of basis functions used for the approximation of the unknown.

The authors used an iris in a parallel plate waveguide as the discontinuity. This problem was used as a benchmark for the study since it had an exact solution via. Wiener Hopf technique. Let s denote the ratio of the plate spacing[10] to the distance below the iris.

The authors make the following fundamental observation. For a given P, the computed results improves with increasing N and then starts deteriorating. By the word *deteriorating*, we understand that either the results becomes unstable and drifts off, or the result converges to the wrong value. Conversely, for a given N, increasing the number of modes P takes the solution from instability to inaccuracy. Therefore, for a given P, there exists an optimum value of N such that the results are not too bad either way. We can represent this symbolically as,

$$\text{Given } P: \qquad \text{inaccurate} \; \xrightarrow[\;\text{Optimum } N\;]{\;N\;} \; \text{unstable}.$$

It was proved via. rigorous arguments that the optimum value of N for a given

---

[9] A double summation can be regarded as a single summation via. a suitable ordering.
[10] If the iris does not exist then $s = 1$.

P is such that $P/N = s$. Therefore, the sequence of solutions do not indefinitely *improve*.

These observations contain sufficient pointers to all the aspects of stability. However, the conclusions are based on an integral equation with a finite rank kernel. A kernel is *finite rank* (also referred to as *separable, degenerate*) if it is of the following form,

$$K(x, y, x', y') = \sum_{k=1}^{P} A_k \, \psi_k(x, y) \, \phi_k(x', y').$$

Consequently an integral equation with a finite rank kernel takes the following form,

$$\sum_{k=1}^{P} A_k \, \psi_k(x, y) \int_a^b \int_c^d \phi_k(x', y') \, f(x', y') \, dx' \, dy' = g(x, y) \qquad (3.113)$$

A standard result on integral equations with finite rank kernels is that, they have infinitely many *zero eigenvalues*. That is, there exists a nonzero f such that the homogeneous equation has a solution. To prove this, all we need to do is to choose an f such that the P quadratures in (3.113) are zero. For example, we can orthonormalize the set $\{ \phi_k(x', y') \}$ in the rectangle $[a, b] \times [c, d]$, and then choose f from the orthonormalized family for $k > P$.

Since the (truncated) kernel for the transverse discontinuity problem is of finite rank, we have the result that the numerical solution of transverse discontinuity problem is not unique. Consequently, the ill-conditioning which the authors observe does not have a rigorous basis because the solution itself is not unique. In fact, there exists a suitable choice of basis such that the MoM matrix can always be made singular.

Except for this unfortunate choice of the problem, the results in these references have significant qualitative validity.

Our discussion will be based on the computation of scattering from a printed

vertical strip within a waveguide. This does not involve a separable kernel.

The reader may refer to Delves and Mohamed [44] or C. T. H. Baker [45] for further examples.

Illustration of Instabilities

Consider the scattering from a printed vertical strip within a waveguide. See Fig. 2.1 for the geometrical description of the problem. The integral equation is of the form,

$$\int_{y'=y_l-l_l}^{y_l+l_l} \int_{z'=-w_l}^{+w_l} E_y(J_y)\; J_y(y',z')\, dy'\, dz' \;=\; -1 \cdot e^{-j\gamma z} \qquad (3.114)$$

where

$$
\begin{aligned}
E_y(J_y) \;=\; & \sum C_{E_y(J_y)}^e \; \sin u_1(a-t)\; \cos k_y y' \; \sin u_1(a-x)\; \cos k_y y \; e^{-\gamma_e\,|z-z'|} \\
+ & \sum C_{E_y(J_y)}^m \; \sin v_1(a-t)\; \cos k_y y' \; \sin v_1(a-x)\; \cos k_y y \; e^{-\gamma_m\,|z-z'|}
\end{aligned}
$$

(3.114) is the statement that the scattered E_y component cancels the incident E_y component on the strip. This integral equation is valid on the strip domain S_R, namely

$$
\begin{aligned}
y_l - l_l \;\leq\; & y \;\leq\; y_l + l_l \\
S_R \;:\quad -w_l \;\leq\; & z \;\leq\; +w_l \\
x \;=\; & t
\end{aligned}
$$

(3.114) is solved using the same basis and testing functions as in Chapter 2. Let M_{max} (N_{max}) denote number of modes summed in the x (y) direction, whereas N_l denote the number of basis functions used for the strip current. We have measured two cases having different strip widths via. TRL standards. The fabrication and the measurements were done carefully so that the measured results can be regarded as reliable to check the computed results.

Fig. 3.9–3.10 show the measured S parameters along with computed results
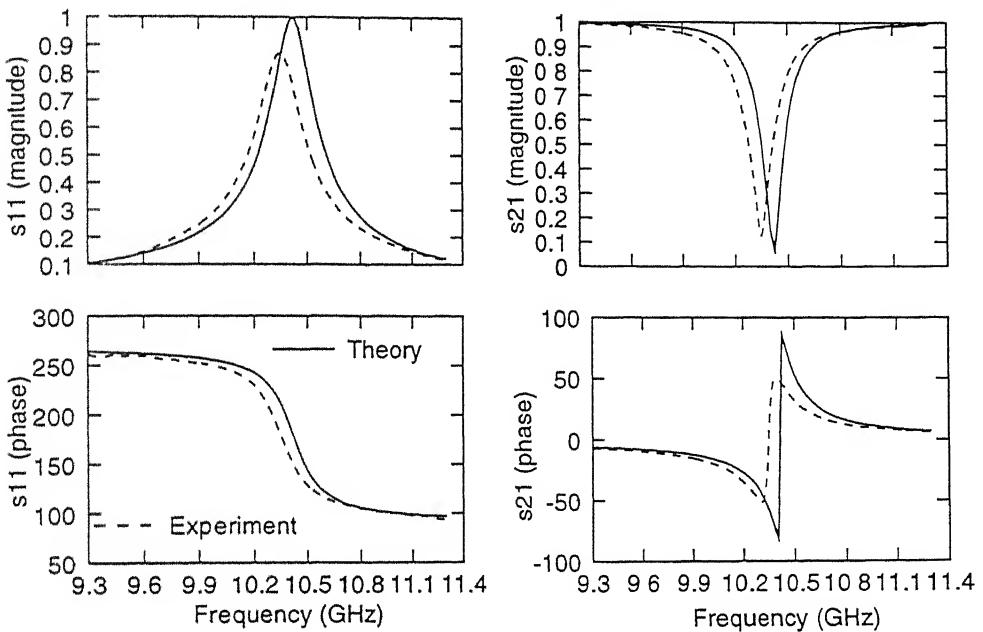
Figure 3.9: S parameters of strip scattering. $a = 22.86$ mm, $b = 10.16$ mm, $t = 1.57$ mm, $\epsilon_r = 2.5$, $2l_l = 9.0$ mm, $2w_l = 0\,8$ mm, $y_l = 5.08$ mm, $\theta = 90^0$, $M_{max} = 100$, $N_{max} = 100$, $N_l = 5$. Measurements were done using TRL standards

for a specific choice of M_{max}, N_{max} and N_l. Specifically, we have used 5 basis on the strip, whereas 100 modes were used in each direction. The results seem to suggest that the computations give accurate results and are stable. However, this is not quite the case.

The scattering behavior of the strip is as follows. The strip is a reactive element and it appears as a series L–C circuit in shunt. Consequently, there is complete reflection ($S_{11} = -1$) and no transmission ($S_{21} = 0$) at resonance. The measured results do not really reach these two values at resonance due to the losses in the structure. Fig. 3.10, which represents the wider strip, has a lower resonant frequency and has broader bandwidth.

We present two distinct cases of instability depending on whether the strip is offset on the narrow wall or not. An offset strip is one for which the center of
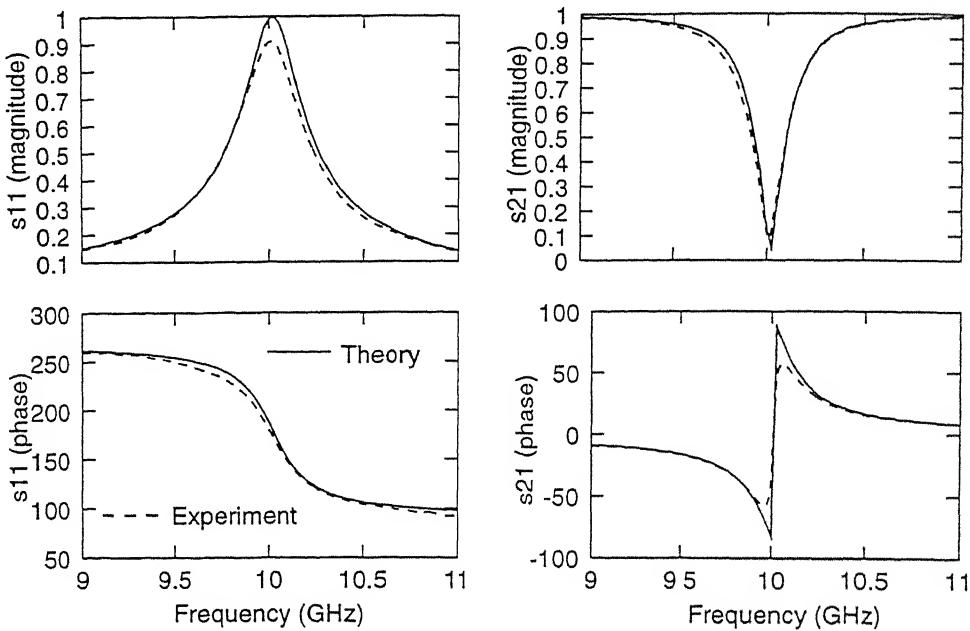
Figure 3.10: S parameters of strip scattering. $2w_l = 1.5$ mm. See Fig. 3.9 for other details.

the strip y_l is different from $b/2$.

Fig. 3.11 shows the S parameter of an offset strip with respect the number of basis functions. The results are computed sufficiently away from the resonance. The results are outright divergent for 50 modes[11] and it seems to improve on switching to 100 or 200 modes. Even for 100 or 200 modes the results exhibit a small yet definite linear growth which indicates instability. We do not have measured data for this case. However, the result seems acceptable at low values of N_l before the instability creeps in.

The computed results for the centered strip of Fig. 3.10 is more interesting. Fig. 3.12 and Fig. 3.13 shows the magnitude and phase of S_{11} with respect to the number of basis function. Since the strip is centered on the narrow wall, the even indexed basis functions do not contribute. This explains the stair like appearance of these curves. We have made these computations right at the

---

[11]"for N modes" mean "for N modes in each x and y direction"
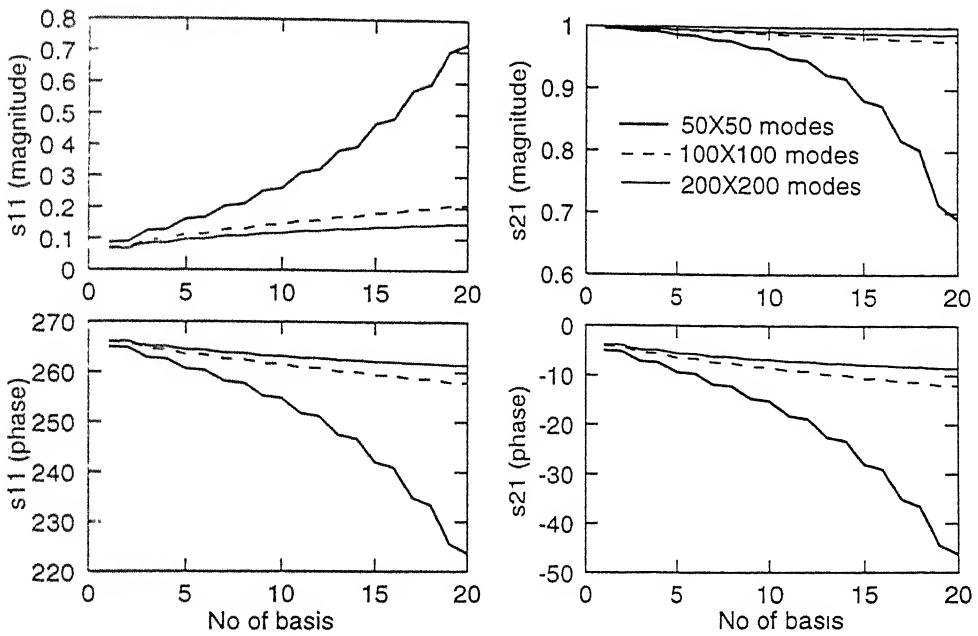
Figure 3.11: Illustration of instability with respect to the bases. $a = 22.86$ mm, $b = 10.16$ mm, $t = 1.57$ mm, $\epsilon_r = 2.5$, $2l_l = 8.0$ mm, $2w_l = 1.5$ mm, $y_l = 6.08$ mm, $\theta = 90^0$.

resonant point so that $S_{11} = -1$.

It can be seen that the computed result improves, reaches the true value and then starts deteriorating. For a given choice of M_{max} and N_{max} there exist and optimum value of N_l such that the results are accurate. An increase in the number of basis functions has to be compensated by a commensurate increase in the number of modes for maintaining the accuracy. But the relationship between modes and basis is not linear unlike the iris problem.

3.6.4 Conclusions

The numerical solution of integral equations of the first kind is an ill-conditioned problem. Algorithms based on the naive methods presented in Section 3.6 becomes unstable beyond a certain accuracy.
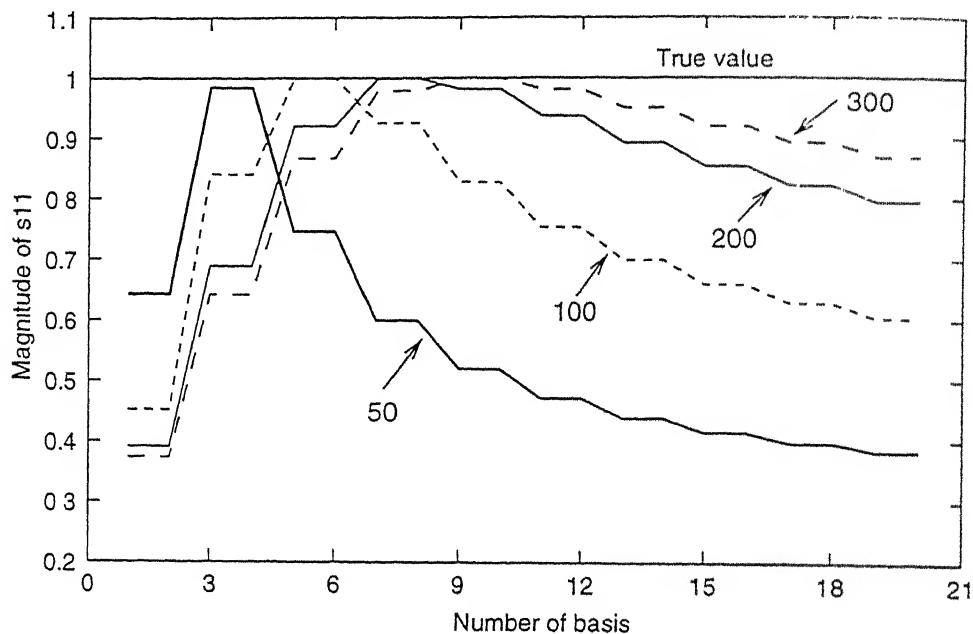
Figure 3.12: S_{11} magnitude versus number of basis functions at various values of number of modes. The number of modes used in each direction ($M_{max} = N_{max}$) is indicated on the curve. See Fig. 3.10 for details.

In EM, we encounter predominantly first kind integral equations with extremely well behaved right-hand sides. Consequently, it is necessary to pay attention to the quadrature/truncation errors of the left-hand-side, since there are no errors on the right-hand-side. Waveguide Green's function is an example of a kernel, where the quadratures can be done analytically, whereas the series can not be summed in closed form. In EM, we also have instances where there are quadrature errors and no truncation error.

The sequence of approximate solutions does not improve indefinitely as in theory. Instead, it first improves and then starts deteriorating. This behavior seems to depend on a parameter κ, such that, the results are best if the right value of κ is chosen. For example, the ratio P/N suggested by [30, 31, 32] serves this purpose. The optimum choice for P/N was found to be s for the iris problem in a parallel plate guide.
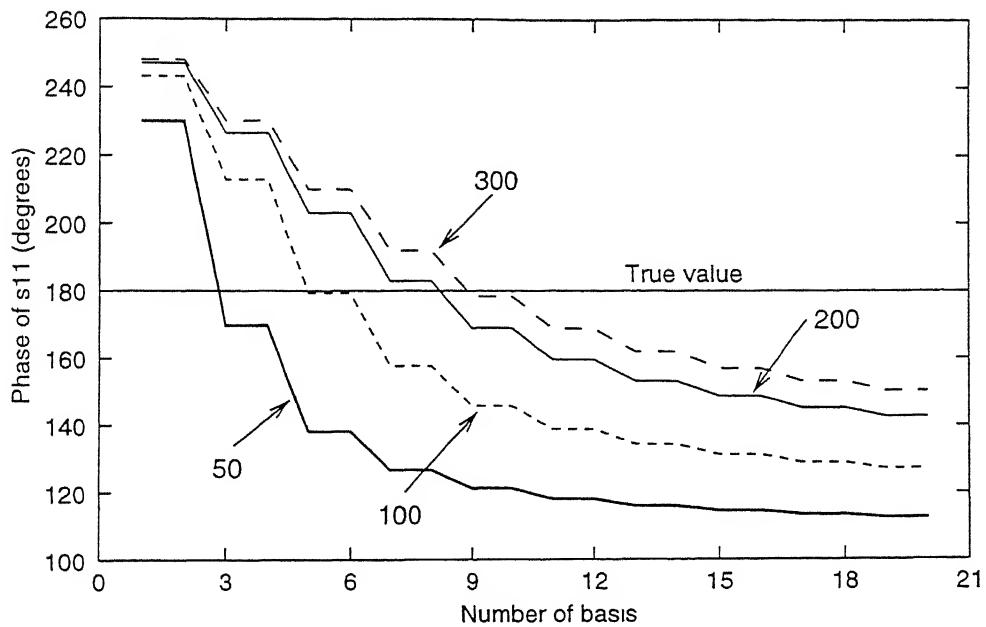
Figure 3.13· Phase of S_{11} versus number of basis functions at various values of number of modes. See Fig. 3.12 for details.

These observations can be viewed in the light of the theory of regularization proposed by Tikhonov [43]. Regularization belongs to one school of solving ill-conditioned problems. An elementary description of regularization is as follows.

Before we attempt to solve $Tx = y$, we expect the solution to belong to a specific smoothness class. For example, x can be assumed to be square integrable. Consequently, while generating the approximate solution x_N's, we also look whether the sequence ceases to belong to this class.

If the solutions $x_N = \sum_{i=1}^{N} I_i e_i$ has to be convergent, we expect the sequence $\{I_i\}$ to decrease fast enough. Consequently, instability is caused by an insufficient decay rate for the sequence $\{I_i\}$. For example, if x is square integrable and $\{e_i\}$ orthonormal, then $I_k = o(1/\sqrt{k})$.

If the sequence becomes unstable, it is to be understood that the higher order terms are not deceasing sufficiently fast. Therefore, smoothness and stability

are synonymous. Let L be a linear operator such that $\|Lx_N\|$ is a measure[12] of the smoothness of x_N. A regularized sequence of solutions is generated based on both the accuracy $\|Tx_N - y\|$ and the smoothness $\|Lx_N\|$. A parameter κ ties up the two such that, we minimize

$$\|Tx_N - y\|^2 + \kappa \|Lx_N\|^2.$$

The parameter κ is called the regularizer of the problem $Tx = y$.

Therefore, a regularized sequence of solutions is a tradeoff between accuracy and stability. For a given problem, there exists an optimum choice of κ. Too low a κ will lead to very unstable solutions, whereas too high a value will lead to inaccurate solutions.

The parameter P/N is a regularizer for the iris discontinuity. It is possible to identify regularizers for other type of problems. For example, If the MoM matrix has quadrature errors such that ε is the maximum absolute error for any MoM matrix entry, then εN may serve as a regularizer.

The numerical behavior of MoM solutions leads to certain significant afterthoughts. For an unstable problem, the practitioner of the method arrives at some intuitive criterion to stop at a good solution. This is very close to the choice of a regularizer and therefore justified. On the other hand, it also makes it difficult to *distinguish* between a formulation which is erroneously modeled and one that is unstable.

Because of these reasons, the computed results presented in Chapter 5 are generated for a suitable choice of basis and modes, which were found to give acceptable numbers in most of the computational experiments. The number of basis functions (N_l and N_s) and the number of modes (M_{max} and N_{max}) used for every computed result are indicated in the figure captions.

---

[12]A derivative can serve as a measure of the smoothness.

3.7 Summary and Conclusions

This chapter has discussed various issues of independent interest. Green's functions in inhomogeneously filled waveguides were derived, primarily to consolidate the notations and to understand the structure and properties in depth. The derivation made use of the method of normal mode expansion from "Field Theory of Guided Waves" by R. E. Collin. The normal modes being LSE and LSM, it became necessary to solve the LSE/LSM eigenvalues. The solution of eigenvalues were based on certain simple results, which made the salient properties of the curves analytically known. This led to the choice of good starting values and tight bounds for the roots.

A Green's function is a distribution so that it leads to various inconsistent results if we attempt to use it as a classical function. This theme was illustrated using the standard $E_z(J_z)$ Green's function, which is a distribution due to the presence of a Dirac delta. It was found necessary to represent this Dirac delta as an LSM series so that the E_z field was computable. This section also developed an algorithm for implementing the Gram-Schmidt procedure.

Section 3.6 dealt with an interesting topic, namely, the theory and practice of method of moment. MoM is a technique which attempts to solve a first kind integral equation directly. Since this problem is fundamentally illconditioned, instability creeps in approximately at the same time we tend to get acceptable solutions. The practitioners of MoM use various thumb rules to decide when to stop while solving a problem. This was interpreted as the choice of a regularizer based on regularization theory.

Chapter 4

Measurement Procedure

4.1   Introduction

In order to verify the computations of the previous two chapters, an experiment was designed to measure the equivalent network of the strip excited slot in a waveguide. Since impedances cannot be measured directly, it is obtained by measuring the S-parameters and then converting this to an equivalent two-port network. The strip excited slot in an inhomogeneously filled waveguide, is treated as a two-port network, with the ports defined at a large distance (few wavelengths) from the slot, so that only the propagating mode exists at the measurement planes. A vector network analyzer (VNA) is used for measuring the S-parameters. For accurate measurements it is necessary to calibrate the VNA. The standard waveguide calibration kit consists of short, shifted short, load and a standard length waveguide. These are precision fabricated, and can be used to establish measurement planes between which the waveguide two-port network can be inserted.

Since the computations give equivalent network impedances or the S-parameters referred to the center of the slot, it is required to shift the measured results to the center of the slot for comparison. This can be done theoretically, but in practice, this procedure was found to be unsatisfactory, for the reason that the shift is accurate only to the extent of accuracy with which the parameters of the waveguide section (inhomogeneously filled) are known. For improved accuracy of measurement, Thru-Reflect-Line (TRL) calibration was adopted in later measurements. In this procedure, the measurement planes are defined at the slot center itself, and the entire inhomogeneously filled waveguide section, along with the transition to normal waveguide is de-embedded automatically, to give the S-parameters of the strip excited slot at the slot center. Of course, for this the TRL standards have to be specially designed and fabricated. This chapter discusses the various aspects of experiment design, fabrication of standards, TRL calibration and some representative measurements.

4.2   Fabrication of Samples

The analysis of the strip excited waveguide slot assumes an infinite inhomogeneously filled waveguide. The strip and the slot are assumed to have no thickness whatsoever, and the conductor and dielectric losses are regarded as zero. The slot is assumed to be embedded in an infinite ground plane. Therefore, the test pieces should be fabricated in such a way that these idealizations are met at least approximately.

If the exciting strip and the slot are printed on either side of a low loss dielectric substrate, and the waveguide narrow wall is substituted with it, then the requirements of theoretical model are nearly met. A ground plane of certain size can be attached in flush with the narrow wall of the waveguide to simulate the effect of an infinite ground plane. The length of the dielectric substrate can

be chosen to be at least $2\lambda_g$, so that in the vicinity of the slot, the structure resembles a uniform inhomogeneously filled waveguide. For low filling factors (low ϵ_r and thin substrate), the length of the substrate used to simulate an inhomogeneously filled waveguide is not very critical.
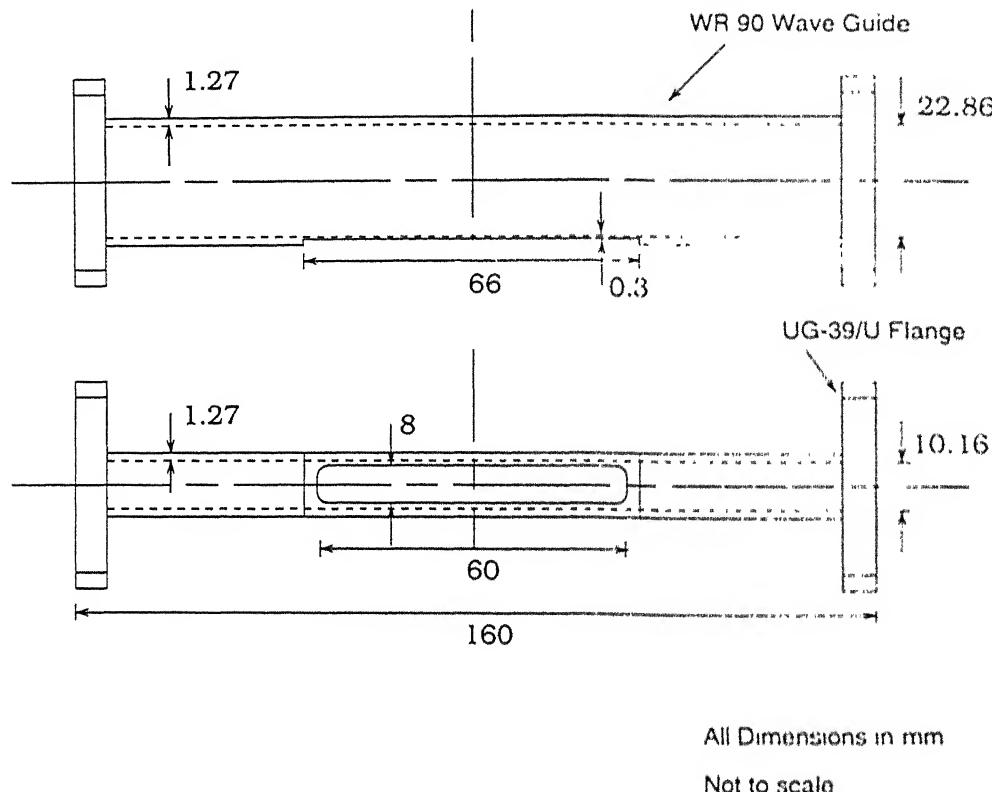
Figure 4.1: Details of waveguide test piece

In order to implement the above scheme of ideas, WR-90 Brass waveguides of length 160 mm are fabricated. [See Fig. 4.1]. The waveguides are fitted with X-Band brass flanges (UG-39/U). A portion of the narrow wall of size 66×8 mm is machined off and the narrow wall is thinned down to 0.3 mm. The waveguide pieces are silver plated after machining so as to keep the waveguide wall losses to a minimum. The test samples for measurements are made using this machined waveguide pieces. In order to fabricate the strip excited slot antenna, we proceed as follows. [See Fig. 4.2].
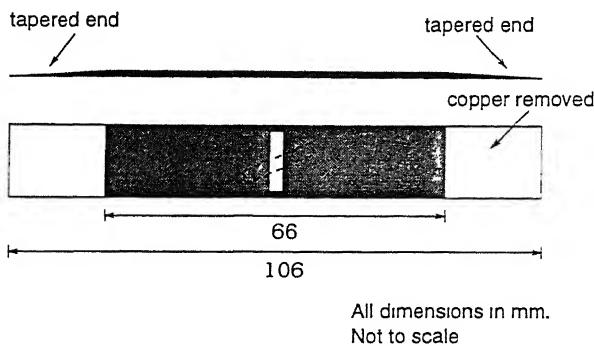
Figure 4.2: Substrate geometry for measurement using standard waveguide calibration

tion

A dielectric substrate is etched with the slot and the exciting line on either side. It is cut accurately to the dimensions indicated in the figure, so that the substrate fits snugly between the broad walls of the waveguide. The substrate is kept pressed from the waveguide interior to the machined narrow wall side, and the edge joining the substrate with the narrow wall is soldered around. [See Fig. 4.3]. The ends of the substrate for about 20 mm is kept free of copper, since this region is not involved while soldering to the narrow wall.
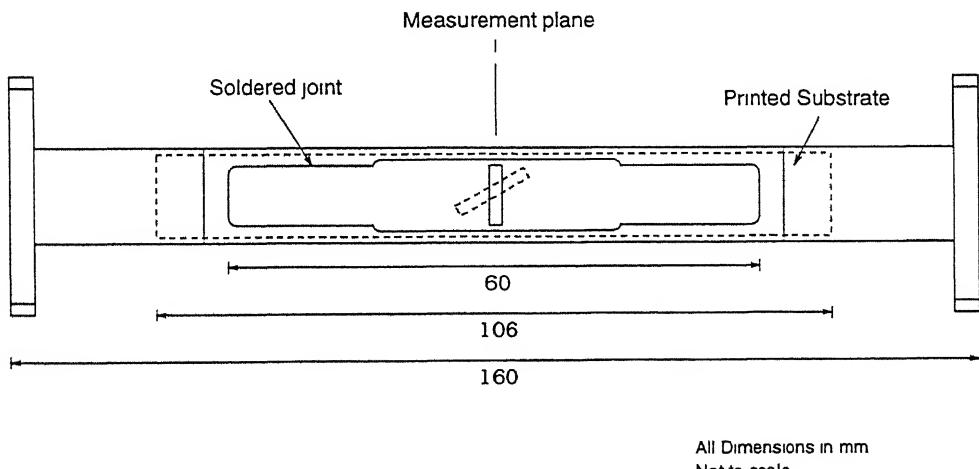
Figure 4.3: Details of the test antenna element

This procedure is carried out carefully, so that, the substrate is mounted

sufficiently close to the narrow wall of the waveguide to avoid any air gaps. It is necessary to align the slot with the center of the waveguide, so that measurement reference plane coincides with the slot center. This is done with aid of a traveling microscope. Since the width of machined off narrow wall is only 8 mm, it is necessary to leave more space around the slot ends, especially if the slot is more than 8 mm long. This is done by removing the remaining part of the narrow wall in the neighborhood of the slot, such that there is just sufficient narrow wall left for soldering. It is also necessary to remove any extra solder remaining on the substrate or the waveguide walls prior to making measurements.

A ground plane fixture is fabricated by attaching two L shaped Aluminum plates to a 1 inch ebonite spacer as shown in Fig. 4.4. The waveguide test piece can be lowered into the channel between the Aluminum plates and the spacer, so that the machined narrow wall plane becomes flush with the ground planes. Copper foil tape with a conducting acrylic adhesive is used to join the waveguide wall with the ground plane.

This method of fabrication, though unsuitable for a practical array, is found to be good enough for laboratory evaluation. If the calibration used is the standard waveguide cal-set, setting the reference plane at the flange planes, it is necessary to taper the substrate ends so as to minimize the reflections from the dielectric step discontinuity. The reflections from the dielectric step can be of the same order of magnitude as the reflections from the strip excited slot, especially if the latter is operated at lower conductance ranges. This is especially the case in an array of 30 or more elements, where each slot appears as a small discontinuity. If TRL calibration is used for measurements, it is not necessary to taper the substrate ends since the effect of the step discontinuity is automatically de-embedded in the calibration procedure.

The measurements are done on a *HP8510C Vector Network Analyzer*. The measurements are done on two types of substrates, namely, Taconic TLY-5-
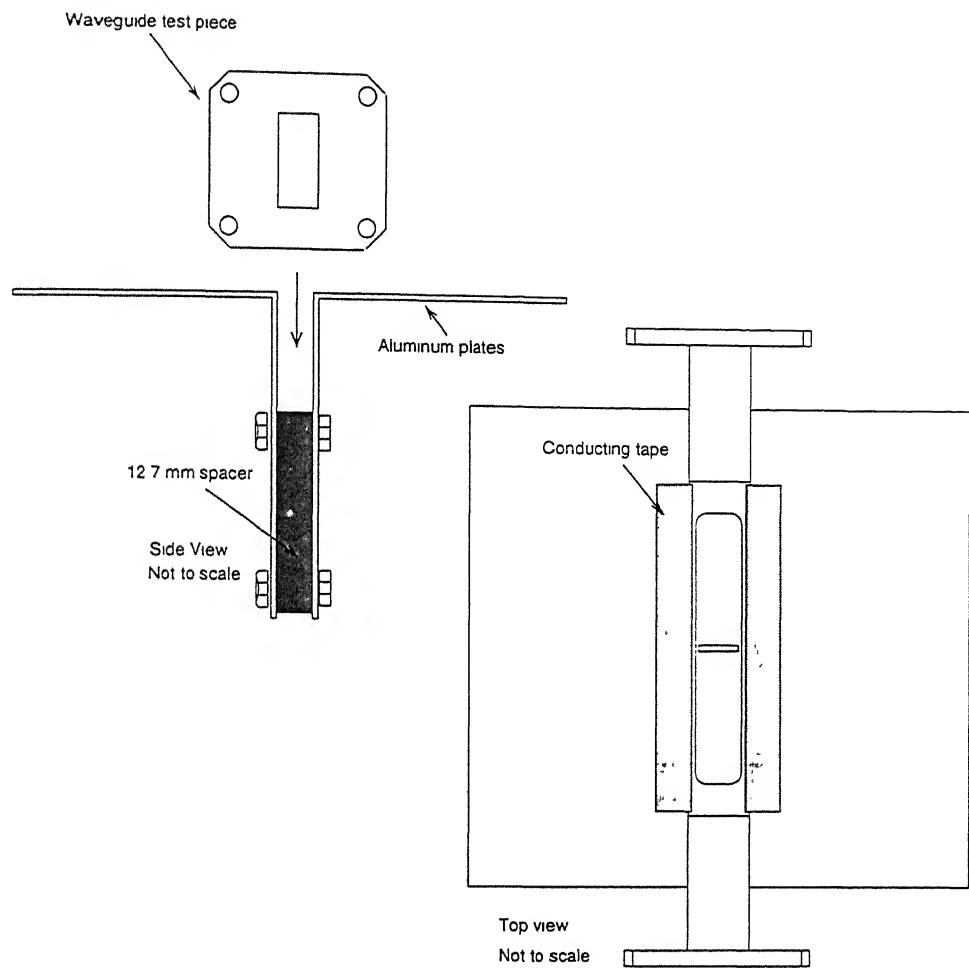
Figure 4.4: Ground plane fixture

0310-c1/c1 ($\epsilon_r = 2.18$, substrate thickness= 1/32 inch) and RT/duroid 5550 ($\epsilon_r = 2.5$, substrate thickness= 0.062 inch).

Fig. 4.5 illustrates the S-parameters measured using standard waveguide calibration. It can be seen that S_{21} phase does not pass through zero as required at resonance. This is due to the errors in shifting the reference plane from the flange to the slot center. The phase error is caused mainly by the errors in the distance involved as well as in the propagation constant. A distance error of 0.1 mm corresponds to approximately 1.8^0 in S_{21} at 10 GHz. The phase of S_{11} also contains shifting errors of the same order as in S_{21}. However, S_{11}
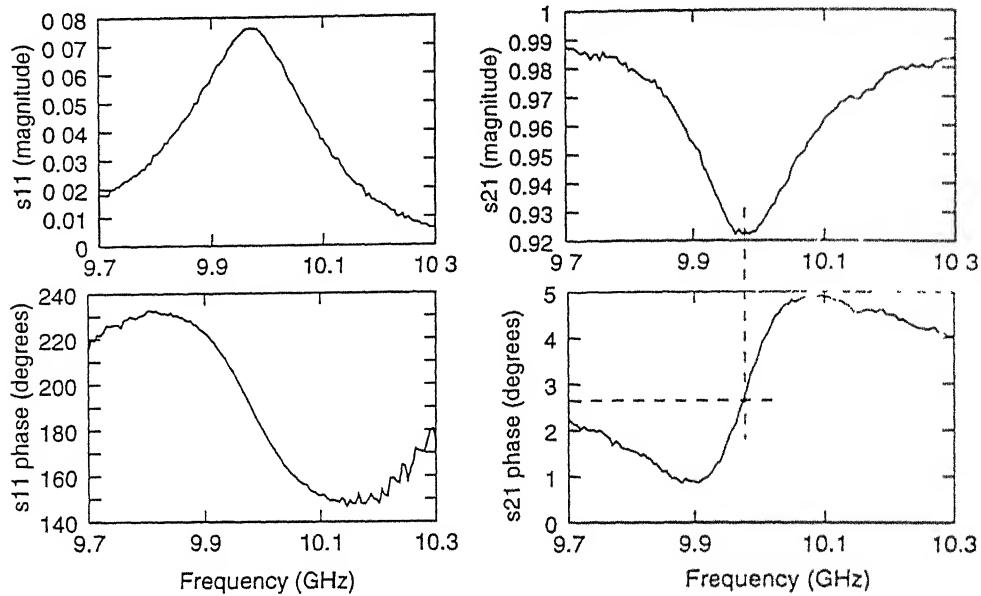
Figure 4.5· S-parameters measured using standard waveguide calibration. Note the 3 degree phase error in S_{21} due to the errors in shifting the reference plane from the flange plane to the slot center. No ground plane is used. $\theta = 50^0$, $2l_l = 8.0$ mm, $2w_l = 0.8$ mm, $y_l = 5.08$ mm, $z_l = 0$ mm, $2l_s = 8.5$ mm, $2w_s = 0.8$ mm, $\epsilon_r = 2.20$, $t = 0.8$ mm

phase error is not perceptible since it is in a scale of 180 degrees. Note that, while shifting the plane of reference, we encounter three regions starting from the flange plane to the slot center. There is a distance of 27 mm where the waveguide is unfilled, followed by a tapered region of 20 mm, and then a length of 33 mm where the substrate has full thickness. Since the propagation constant of the tapered region is not known exactly, either the value in the unfilled region or the value in the filled region has to be used in this section. This causes some error in the shifted S-parameters. Since, the reflections from the dielectric step are part of the measurement, the measured S-parameters will be slightly erroneous. The tapering of the substrate makes the substrate ends flexible and the chances of air gaps are increased.

4.3   Calibration Schemes for HP8510C VNA

A network measurement using VNA is reliable only if the errors in the measurement circuitry are identified and corrected for. The errors encountered in a typical measurement circuit are of varied types and affect the measurement to varying degrees. However, some class of errors are repeatable in a measurement session. The errors are modeled by introducing an error model which involves a certain number of error terms. In a calibration procedure, a set of devices (standards) with known characteristics are connected to the measurement ports of the VNA. The errors parameters are computed based on the measurements using the standards. The estimation of the error terms involve the solution of a set of complex, non-linear equations. A formal treatment of the theory of calibration schemes can be found in [46].

In the conventional waveguide calibration scheme, a set of three discrete impedance standards (namely, short, shifted short and load), and a transmission standard which is a standard length waveguide are used. These standards are precision fabricated and should have properties known to high degree of accuracy. This technique can be used to establish a reference plane at the center of an inhomogeneously filled waveguide. However, this requires high accuracy on the test pieces, in addition to having to fabricate and characterize a number of standards. The next two subsections illustrate the technique of establishing the reference plane at the center of slot using conventional as well as the Thru-Reflect-Line standards.

4.3.1   Standard Waveguide Calibration

Fig. 4.6 illustrates the necessary standards required to establish the reference plane at the center of the test waveguide. SHORT is a half length waveguide fitted with a dielectric substrate such that it is identical with one symmetric half
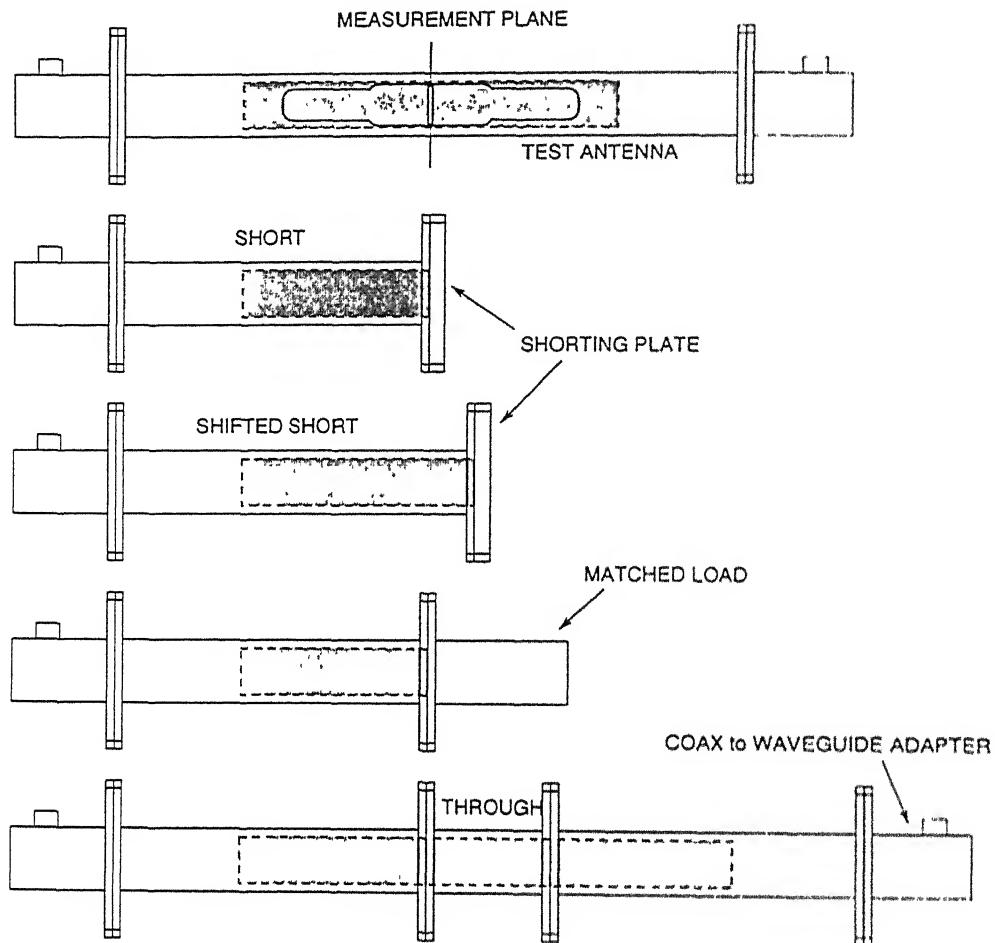
Figure 4.6: Standard waveguide calibration modified to establish the measurement plane at the center of an inhomogeneously filled waveguide

of the test waveguide piece. SHIFTED SHORT is identical with the SHORT, except that the former is slightly longer than the SHORT waveguide. MATCHED LOAD is implemented by connecting a matched termination at the end of the SHORT waveguide. THRU is a definite length of inhomogeneously filled waveguide which is introduced between the two half length waveguides. Note that, SHORT, SHIFTED SHORT and LOAD constitute three single port measurements (totaling to six), while THRU constitute a full two port measurement (totaling to four). It is necessary to have two half length waveguides since the THRU requires a half

length waveguide on either side. The shorting plate can be from a standard waveguide calibration set. However, the matched load is to be specifically fabricated such that it is a matched termination for an inhomogeneously filled waveguide. It is necessary to fabricate four standards namely SHORT (2 Nos.), SHIFTED SHORT (1 No.), MATCHED LOAD (1 No.) and THRU (1 No.). It is also necessary to characterize the length of the SHIFTED SHORT, THRU and the reflection coefficient of the LOAD very accurately to implement this calibration scheme.

4.3.2   The TRL Calibration for Waveguide

TRL calibration makes use of the properties of a short piece of transmission line and does not require a set of three precision impedance standards [47]. It assumes an 8 term error model for the measurement circuit. To do TRL calibration, it is necessary to carry out the following three steps, which amounts a total of ten measurements.

• THRU: connection of port 1 and port 2, directly or with a short length of transmission line. If directly connected, it is called *zero length* THRU

• REFLECT: connect identical one-port high reflection coefficient devices to each port

• LINE: insert a short length of transmission line between port 1 and port 2.

The lengths of THRU and LINE should be unequal. The difference in line length between LINE and THRU should preferably $\lambda_g/4$ at the center of the frequency range of calibration. For X-band waveguide $\lambda_g/4$ corresponds to about 10 mm at 10 GHz.

Since the TRL error model has only 8 terms and the number of measurements total to ten, it is possible to compute the two constants defining the REFLECT and the LINE standards. Therefore, the complex reflection coefficient of the REFLECT

and the propagation constant of the LINE need not be specified while specifying the calibration standards. It is only necessary to specify the characteristic impedance of the LINE, and this becomes the measurement reference. In the case of waveguide TRL, all the measurements are carried out with respect to a ·normalized characteristic impedance of unity, and the characteristic impedance entry is 1 Ohm.

4.3.3 TRL Calibration Standards
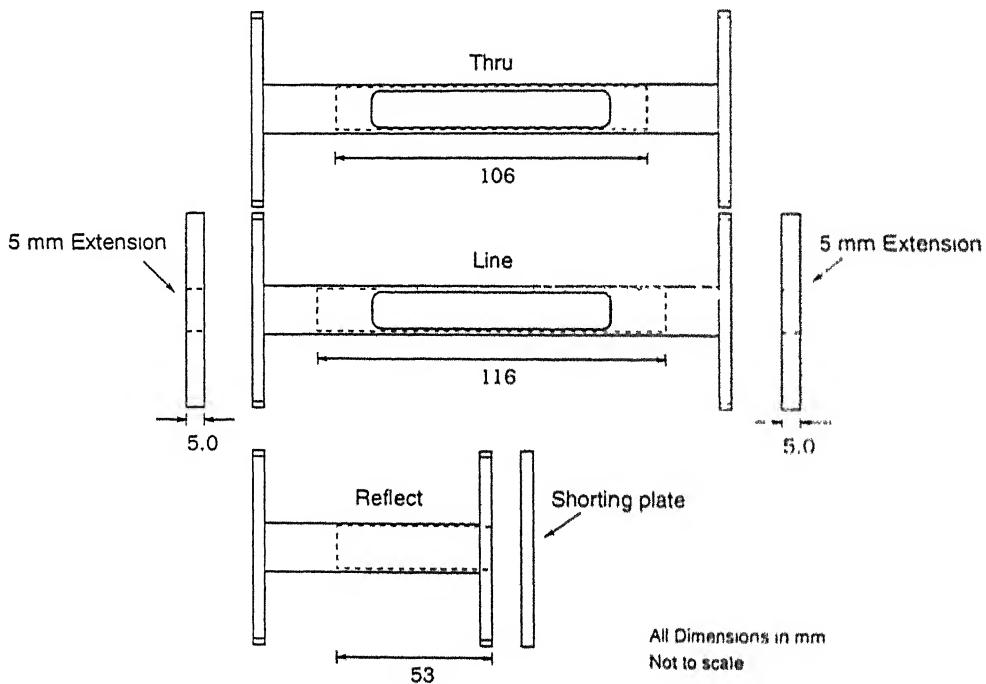
Figure 4.7: TRL calibration standards

Fig. 4.7 indicates the necessary calibration standards required for setting the measurement plane at the center of the slot [See also Fig. 4.3]. Two machined 160 mm waveguide pieces are used to make the THRU and the LINE. In order to fabricate the THRU, a dielectric substrate of dimensions 106×10.16 mm is fitted symmetrically inside the waveguide where the narrow wall is machined

off. The LINE is identical to the THRU except for the increase in substrate length by 10 mm. The substrate can be attached to the waveguide narrow wall by soldering from outside as in the case of the test pieces. Note that the facing side of the substrate should be copper clad.
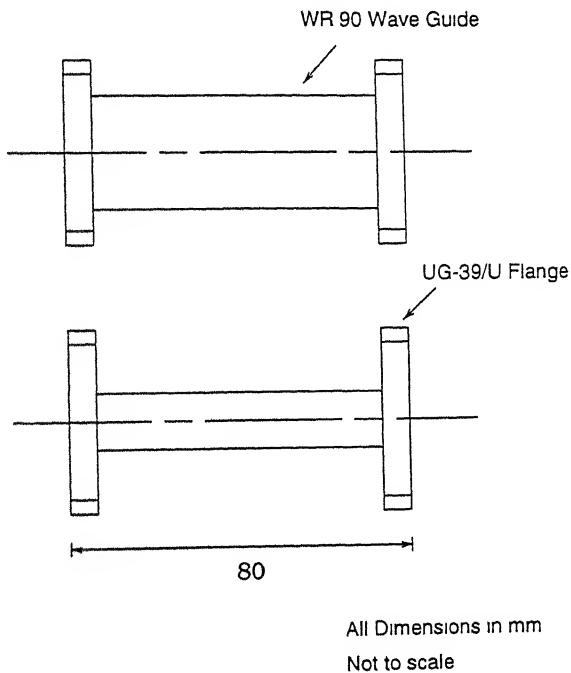
Figure 4.8: Half length waveguide with flanges

A half length waveguide of 80 mm is fabricated for use as a REFLECT. [See Fig. 4.8]. It is fitted with Brass X-Band flanges UG-39/U and is silver plated. A dielectric substrate of 53 mm is fitted inside this guide, such that the substrate end is in flush with the flange plane. This waveguide along with a shorting plate act as the REFLECT. Since the REFLECT simulates one symmetric half of the THRU, it can be used to establish a short at the measurement reference plane.

Two 5 mm waveguide extensions are also fabricated as indicated in Fig. 4.9. The choice of 5 mm corresponds approximately to $\lambda_g/8$ at 10 GHz. Therefore, attaching the 5 mm extensions to either sides of the line waveguide corresponds
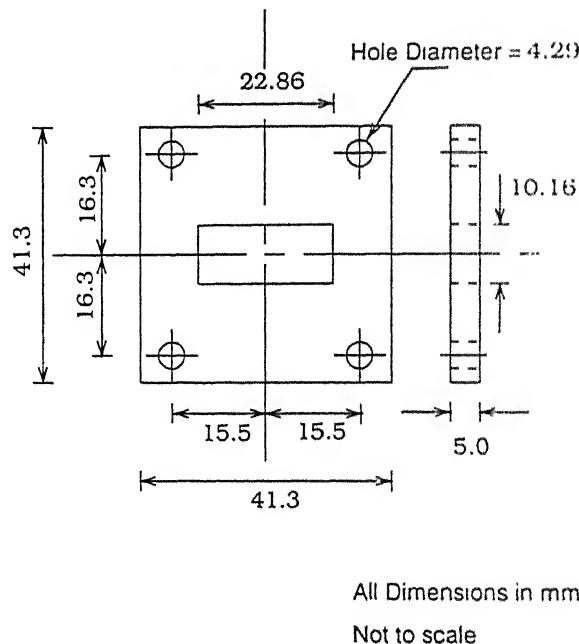
Figure 4.9: Details of the 5 mm waveguide extension

to a $\lambda_g/4$ extension at the measurement plane.

Fig. 4.10 indicates the connection schematics for TRL standards. The shorting plate for the REFLECT can be from the standard waveguide calibration set. Note that, this scheme corresponds to a zero length THRU and a $\lambda_g/4$ LINE implicitly. Since the waveguides used for THRU and test pieces are identical, the measurement reference at the THRU center corresponds to the slot center as well. The waveguides fabricated for making the test pieces are found to have an error of 160 ± 0.3 mm. Therefore, it is necessary to introduce small shifts in reference plane in TRL measurements as well. However, this is of the order of 1–2 degrees unlike the measurements using standard waveguide calibration.
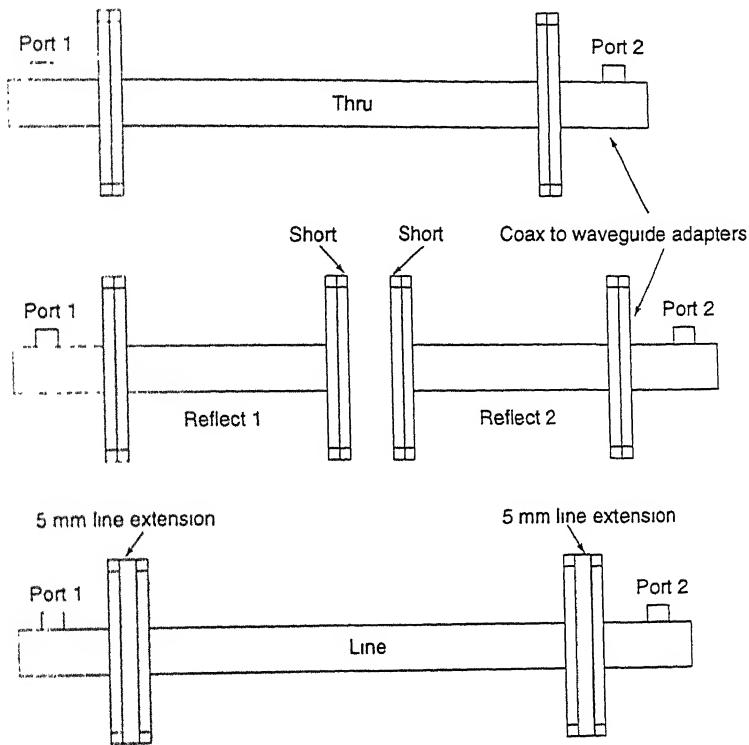
Figure 4.10: Connection schematic for TRL standards

4.4 Few Representative Measurements

This section contains few representative measurements which are used to illustrate certain aspects of the measurements. The examples also serve to illustrate the behavior of the strip excited slot.

Fig. 4.11 presents the S-parameters of a typical slot measured using the TRL calibration. The solid lines indicate measurement with the ground plane, and the dotted lines correspond to the measurement without the ground plane. It can be observed that S_{21} phase passes through zero at resonance, unlike the measurements using the standard waveguide calibration. The effect of the ground plane is a small shift in resonant frequency, approximately of the order of 0.5%.

The S-parameters can be converted to normalized Z-parameters using the
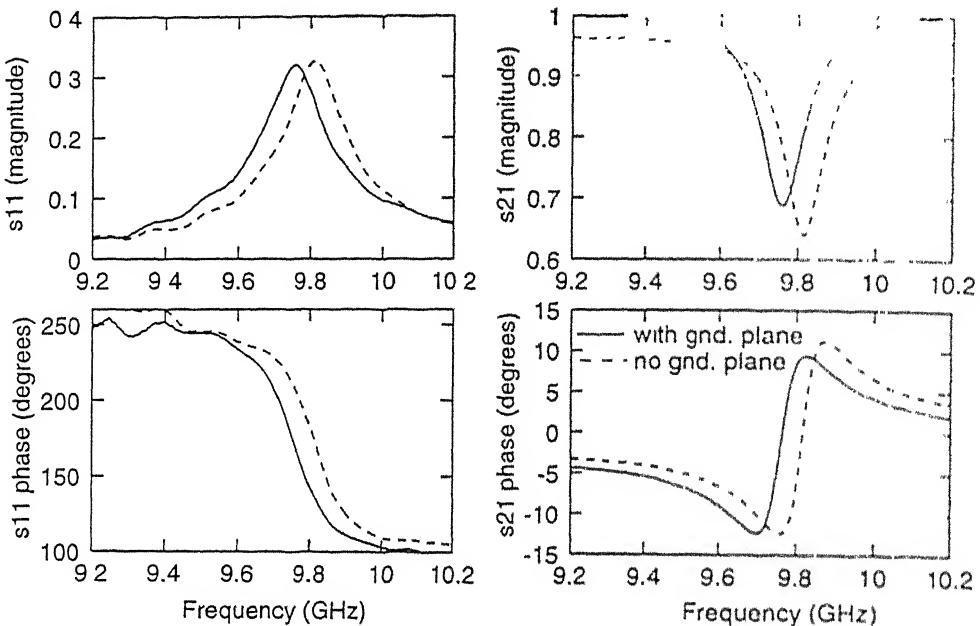
Figure 4.11: S-parameters measured by TRL standard with and without ground plane. $\theta = 70^0$, $2l_l = 9.4$ mm, $2w_l = 0.8$ mm, $y_l = 5.08$ mm, $z_l = 0$ mm, $2l_s = 8.0$ mm, $2w_s = 0.8$ mm, $\epsilon_r = 2.2$, $t = 0.8$ mm

transformation rule $Z = (I + S)(I - S)^{-1}$. The T-equivalent network gives a better insight into the behavior of the discontinuity than the S-Parameters. With respect to Fig. 4.12, the impedances z_1 and z_2 form the series arms, while the impedance z_t forms the shunt arm. Note that, all the impedances are normalized with respect to the characteristic impedance (wave impedance) of the waveguide for the propagating mode.

Fig. 4.13 gives a plot of the network parameters of the strip excited slot. The series arm impedances are seen to be small compared with the shunt arm impedance. Therefore, the strip excited slot is predominantly a shunt discontinuity. Note that, the real part of the shunt impedance is a constant while the imaginary part goes from negative to positive values. This is an example of a series resonance. It can therefore be stated that the strip excited slot is a shunt admittance, which goes through a series resonance.
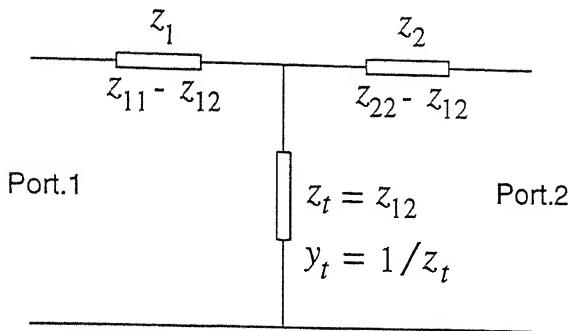
Figure 4.12: T-equivalent network
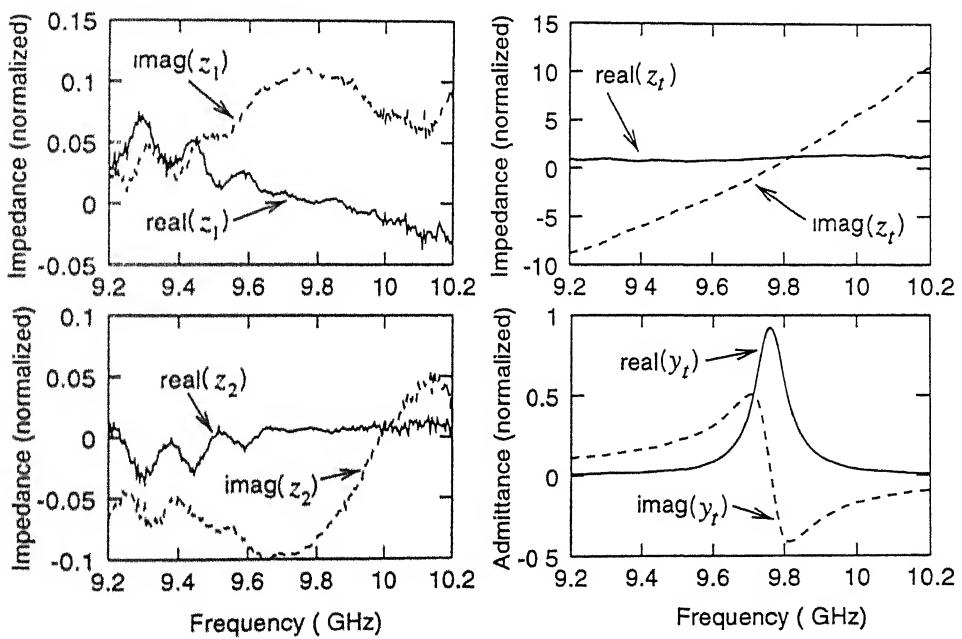
Figure 4.13: T-network parameters of the strip excited slot with ground plane. See Fig. 4.11 for further details.
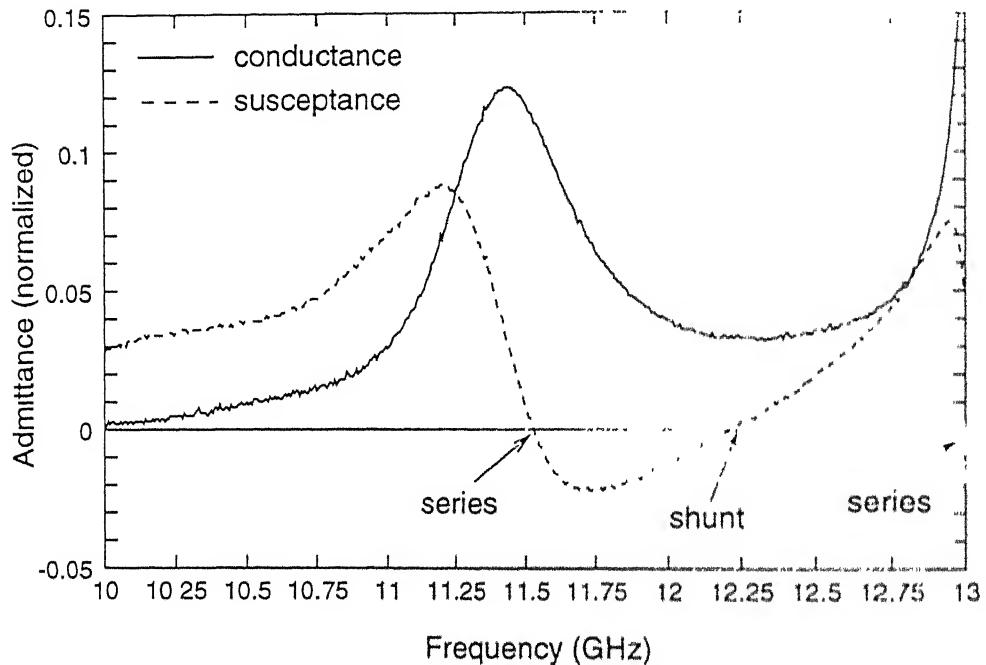
Figure 4.14: Multiple resonance exhibited by the strip excited slot. $\theta = 72^0$, $2l_l = 6.95$ mm, $2w_l = 0.6$ mm, $y_l = 5.08$ mm, $z_l = 0$ mm, $2l_s = 9.0$ mm, $2w_s = 1.5$ mm, $y_s = 5.08$ mm, $\epsilon_r = 2.5$, $t = 1.6$ mm
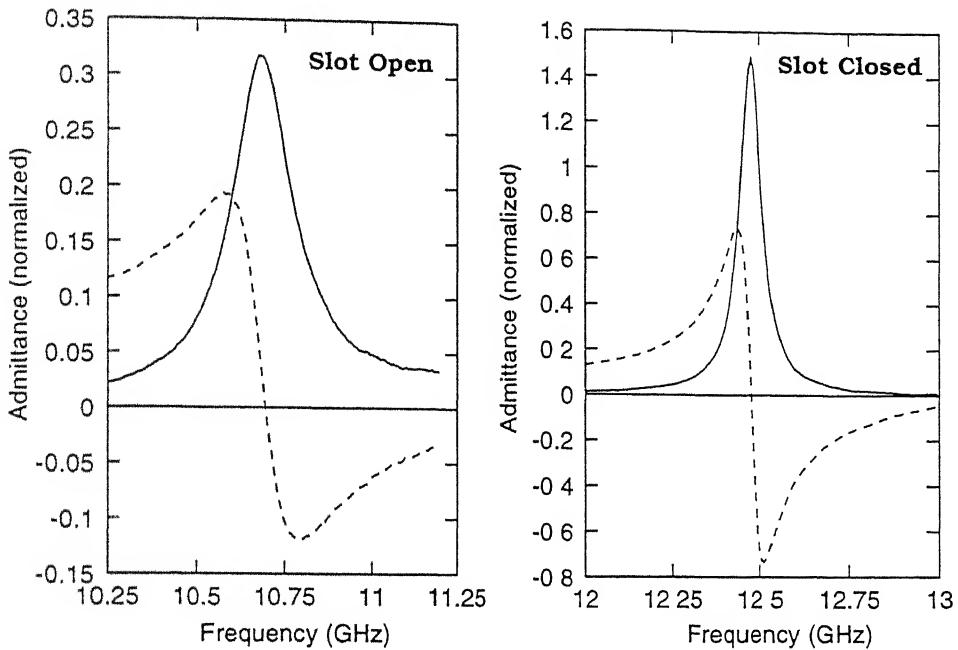
Figure 4.15: Normalized shunt admittance of the strip excited slot, illustrating the effect of closing the slot. $\theta = 40^0$, $2l_l = 7.37$ mm, $2w_l = 0.8$ mm, $y_l = 5.08$ mm, $z_l = 0$ mm, $2l_s = 8.0$ mm, $2w_s = 0.8$ mm, $\epsilon_r = 2.5$, $t = 1.6$ mm

The strip excited slot can exhibit multiple resonances for certain choice of parameters. This is illustrated in the following Fig. 4.14. There exists 3 resonances starting with the series resonance at 11.5 GHz, followed by a shunt resonance at 12.25 GHz, and a series resonance at 13 GHz. All resonances except the first are found to radiate very little. The bandwidth of the structure is considerably improved [compare Fig. 4.14 with Fig. 4.11], if the slot is made longer and made to resonate at the higher end of the frequency band. This amounts to the statement that the slot should be operated closer to its unloaded resonance for broader bandwidth. Both the conductance and the susceptance exhibit asymmetry around the first resonance. It can also be observed that the conductance peak does not coincide with the zero of the susceptance.

Measurements are carried out to study the behavior of the scattering from the strip in the absence of the slot. [See Fig. 4.15]. The slot can be covered

by a conducting tape while making these measurements. It is observed that
the strip resonance is narrow and it occurs at another frequency. Note that,
the strip admittance is not imaginary and has in fact a significant value for
the conductance, especially around the resonance. This conductance accounts
for the losses in the system and it is significant around the strip resonance.
The magnitude of the induced current on the strip is quite large if the strip is
resonant, and this leads to conductor losses. Since losses are directly related to
the magnitude of the strip current, it is not significant if the slot is radiating.

4.5   Summary and Conclusions

This chapter dealt with the topic of measurements. To validate the computa-
tions, it is found that the experimental model should meet the assumptions of
the analysis at least partially. A method of fabrication of the strip excited slot
was evolved which met this criterion. The technique was to attach a printed
dielectric substrate to the machined off narrow wall of a waveguide. A sim-
ple ground plane fixture was fabricated which could simulate the effect of an
infinite ground plane.

Measurements using the standard waveguide calibration were found to be
inaccurate due to the errors in shifting the measurement plane. The substrate
used for making the test pieces were tapered to reduce the reflections from
the dielectric step discontinuity. A calibration scheme such as TRL is found
to be excellent in setting up the measurement plane at the center of the slot.
The design and fabrication of the necessary TRL calibration accessories were
discussed.

A few representative measurements were presented which throw light on
the various facets of the strip excited slot. The set of measurements indicate
that TRL calibration gives accurate results. The ground plane is found to shift

the resonant frequency by a small amount. The strip excited slot is found to be a shunt discontinuity which exhibits a radiating series resonance. It can also exhibit multiple resonances in which case the admittance curves are skewed and asymmetric. The strip excited slot has a larger bandwidth if the strip loading on the slot is kept to a minimum. The conductor losses were found to be significant if the strip was made resonant in the absence of the slot.

Chapter 5

Characteristics of Strip Excited

Slot

5.1 Introduction

The strip excited narrow wall waveguide slot was conceived mainly for use as an array element. Details of the analysis procedure and experimental techniques have been discussed in the previous three chapters. The current/field distributions on the strip and the slot were obtained via. solution of a set of coupled integral equations, using MoM procedure. Experiments were designed and carried out to characterize the strip excited slot experimentally. However, experiments are expensive and time consuming to perform, for complete characterization. Therefore, few selected measurements were carried out to validate the theoretical computations and also to ascertain the errors involved in the computations. Knowledge of the accuracy and reliability of the theoreti-

cally computed characteristics enable one to evolve a mechanism of correcting these errors, so that, the computed results are useful in the design of high performance antenna arrays.

Precise control of the excitation coefficients is the key to a high performance antenna array. Practical realizations of this antenna is directly dependent on the ease with which these excitation coefficients can be realized and maintained over the bandwidth. Therefore, it is necessary to choose one or two of the parameters of the strip excited slot as variables of control and keep the rest of the parameters constant. Of course, appropriate choice of constant parameters is also important. Strip excited slot has several parameters, such as, slot length and width, strip length and width, strip inclination, strip offset, dielectric constant and thickness of the substrate, waveguide dimensions etc. Certain parameters such as the vertical offset do not significantly affect the behavior of the slot. On the other hand, there are others with respect to which the impedance characteristics is exceptionally sensitive. Therefore, it is necessary to identify the behavior of the strip excited slot with respect to each of the parameter, and single out those which are relevant in the context of array design. This calls for an enormous amount of data, representing the behavior of the slot with respect to various parameters. In order to generate this data, the analysis program is preferred to an extensive series of measurements. It then becomes essential to validate the program with select measurements.

The chapter therefore begins with a comparison of theoretical results with the measured results. Once the validity and limitations of the theoretical model are understood, it is possible to generate the parametric data through the program. The data sets generated are governed primarily by the requirements of an array design algorithm.

## 5.2   Comparing Theory with Experiment
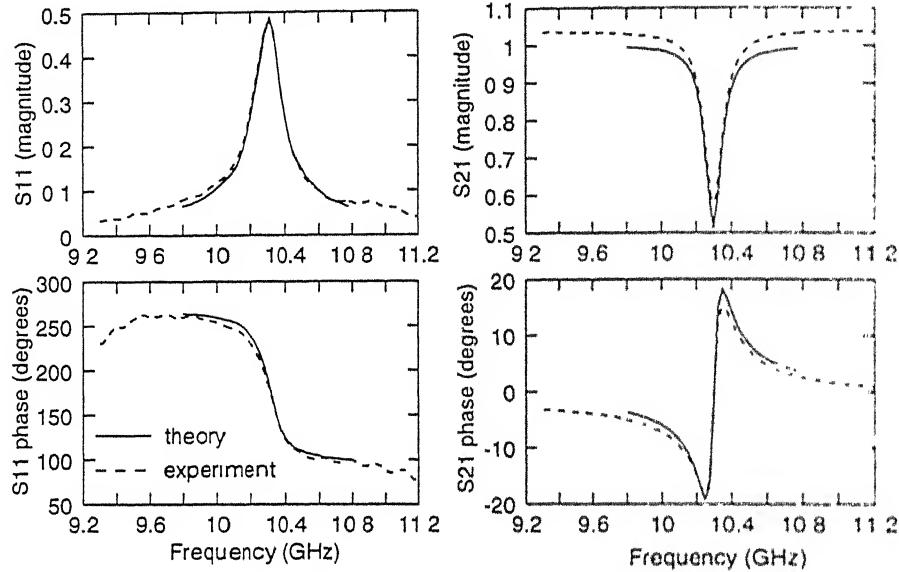
Figure 5.1: S-parameters of the strip excited slot. Measurements were done using TRL standards with ground plane. waveguide: $a = 22.86$ mm, $b = 10.16$ mm; strip: 9.4×0.8 mm, 80^0; slot: 8.0×0.8 mm, offsets: $y_l = 5.08$ mm, $z_l = 0$ mm; substrate: $\epsilon_r = 2.2$, $t = 0.8$ mm; modes, basis: $M_{max} = N_{max} = 100$, $N_l = N_s = 9$

Various sources of errors exist in the process of measurement as well as computation. It is therefore necessary to have an estimate of the agreement to be expected between theoretical and measured results before arriving at any definite conclusion. In practice, various parameters of the test antenna are known within a tolerance. For example, the substrate thickness as well as the permittivity are known within 2% of their actual values. The accuracy of the printed circuit fabrication in the laboratory is of the order of ±0.05 mm. This affects the linear dimensions and the inclination of the strip. The computed
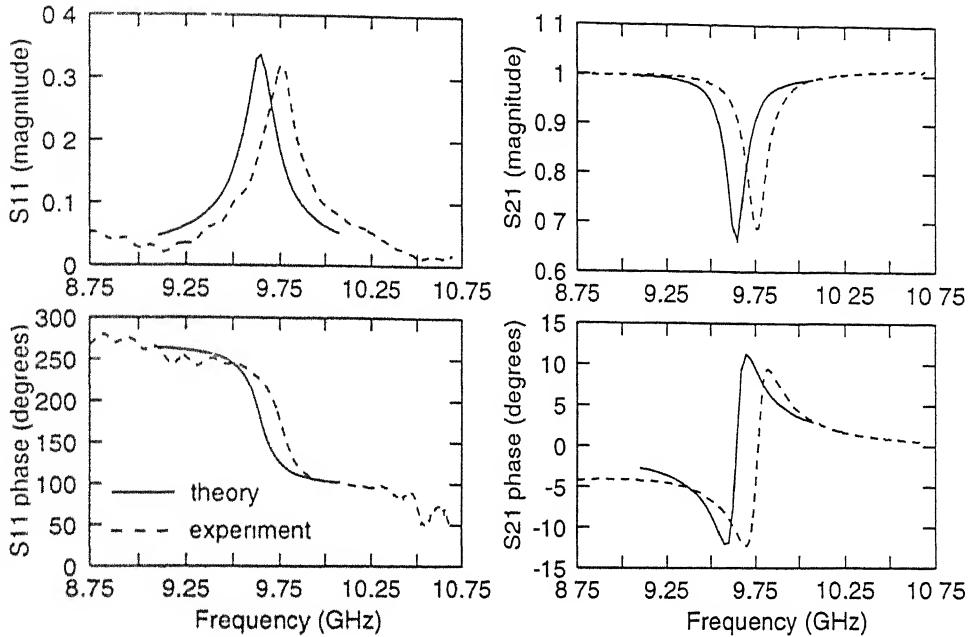
Figure 5.2: S-parameters of the strip excited slot. Measurements were done using TRL standards with ground plane. $a = 22.86$ mm, $b = 10.16$ mm; strip: 9.4×0.8 mm, 70^0; slot: 8.0×0.8 mm; offsets: $y_l = 5.08$ mm, $z_l = 0$ mm; substrate: $\epsilon_r = 2.2$, $t = 0.8$ mm; modes, basis: $M_{max} = N_{max} = 100$, $N_l = N_s = 9$

results depend on the assumptions made in the formulation. We have, for example, neglected the transverse current flow on the strip and assumed the longitudinal current to have a symmetric transverse variation. The extent to which these approximations affect the computed results will come to light in the comparison.

Fig. 5.1 to 5.6 will be used for comparing theory with measurement. First three figures give measured and computed S_{11} and S_{21}, and the other three present normalized admittance. All the parameters are shown as a function of frequency. The first three cases were measured using TRL standards with
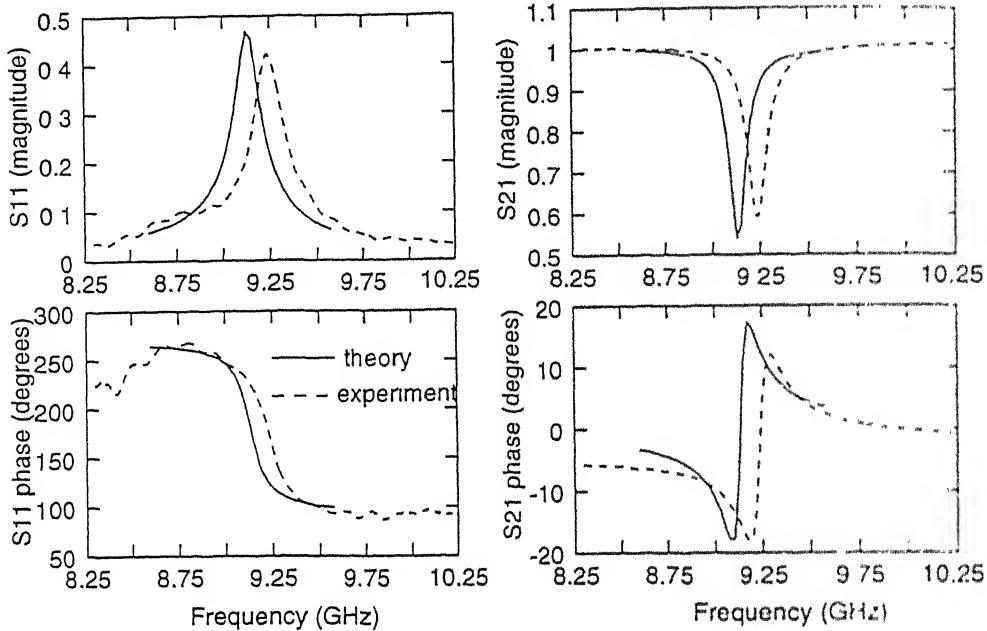
Figure 5.3: S-parameters of the strip excited slot. Measurements were done using TRL standards with ground plane. strip: 10.0×0.8 mm, 70^0; slot: 8.0×0.8 mm; offsets: $y_l = 5.08$ mm, $z_l = 0$ mm; substrate: $\epsilon_r = 2.2$, $t = 0.8$ mm; modes, basis: $M_{max} = N_{max} = 100$, $N_l = N_s = 9$

ground plane, whereas the latter three were measured using standard waveguide calibration without ground plane. Consequently, for the last three cases we choose to present the normalized admittance (*The admittance is normalized with respect to the* LSE_{10} *wave admittance*), rather than the S-parameters, since the latter contains appreciable errors due to shifting of the measurement plane. The susceptance curves of Fig. 5.4 to 5.6 have been shifted vertically to account for the errors in measurement plane shifting.

Referring to Fig. 5.1 it can be seen that the agreement between theory and experiment is excellent. This corresponds to the case when the strip angle θ is
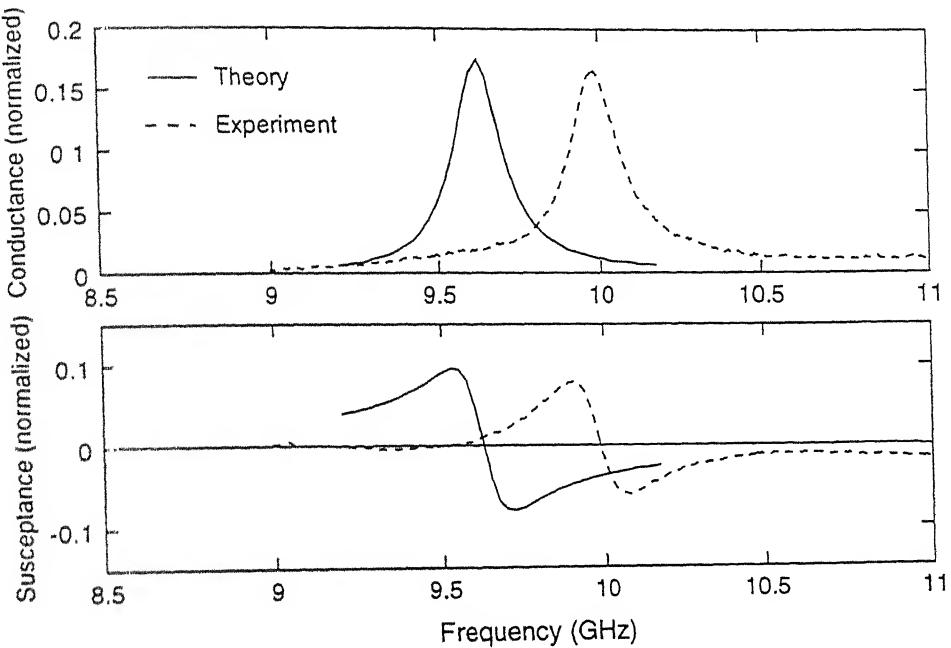
Figure 5.4: Normalized shunt admittance of the strip excited slot Measurements were done using standard wave guide calibration without ground plane. strip: 8.0×0.8 mm, 50^0; slot: 8.5×0.8 mm; offsets: $y_l = 5.08$ mm, $z_l = 0$ mm; substrate: $\epsilon_r = 2.2$, $t = 0.8$ mm; modes, basis: $M_{max} = N_{max} = 100$, $N_l = N_s = 9$

80^0 which is nearly vertical. Next two cases, namely Fig. 5.2 to 5.3 correspond to a strip angle of 70^0, but different strip lengths. It can be seen that the computed resonant frequency is lower than the measured by about 1% in these 2 cases. Referring to Fig. 5.4 to 5.6, with corresponding strip inclinations of 50^0, 30^0 and 20^0, the shift in resonant frequency is seen to be increasing. Note that, for these three cases, the computed values of resonant conductance as well as the bandwidth are considerably off compared with the measured results.

The following general observations can be made based on the 6 figures—the
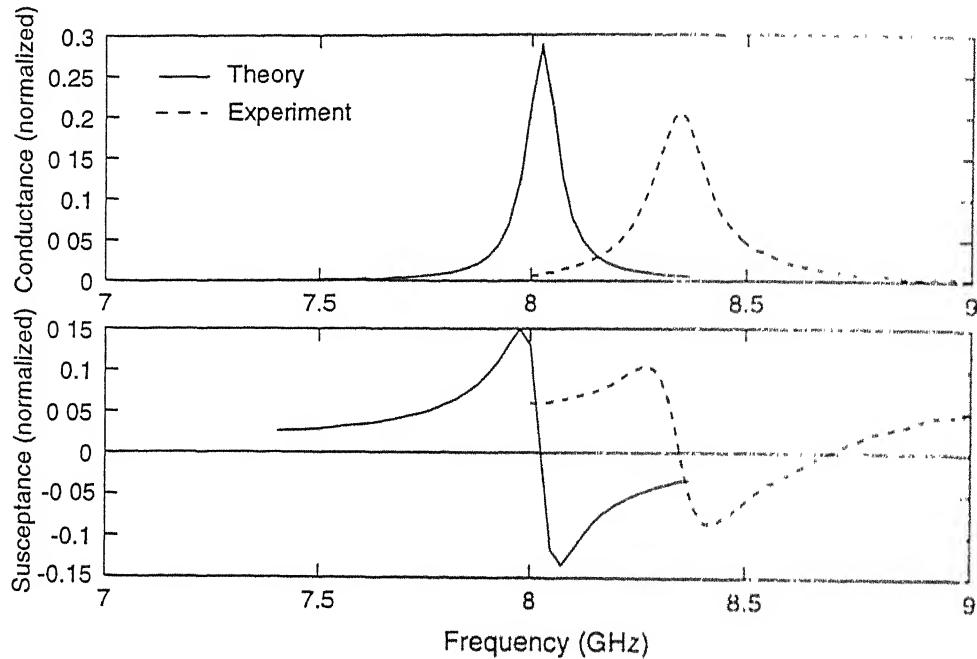
Figure 5.5: Normalized shunt admittance of the strip excited slot. Measurements were done using standard wave guide calibration without ground plane. strip: 10.0×0.8 mm, 30^0; slot: 9.0×0.8 mm; offsets: y_l ≈ 5.08 mm, z_l ≈ 0 mm; substrate: $\epsilon_r = 2.2$, $t = 0.8$ mm; modes, basis: $M_{max} = N_{max}$ ≈ 100, N_l ≈ N_s ≈ 9

computed resonant frequency is always lower than the measured; the error in resonant frequency appears directly related to the strip inclination and can be seen increasing progressively through the 6 cases; Fig. 5.7 shows the error in computed resonant frequency as a function of strip angle θ. The error is seen to be about 4% between $0 < \theta < 60^0$, and falls off to a small value at $\theta = 80^0$.

In order to identify the source of this error, a series of experiments were conducted to eliminate various possible factors. The substrate RT/duroid 5550 has the following material specifications provided by the manufacturer: $\epsilon_r =$
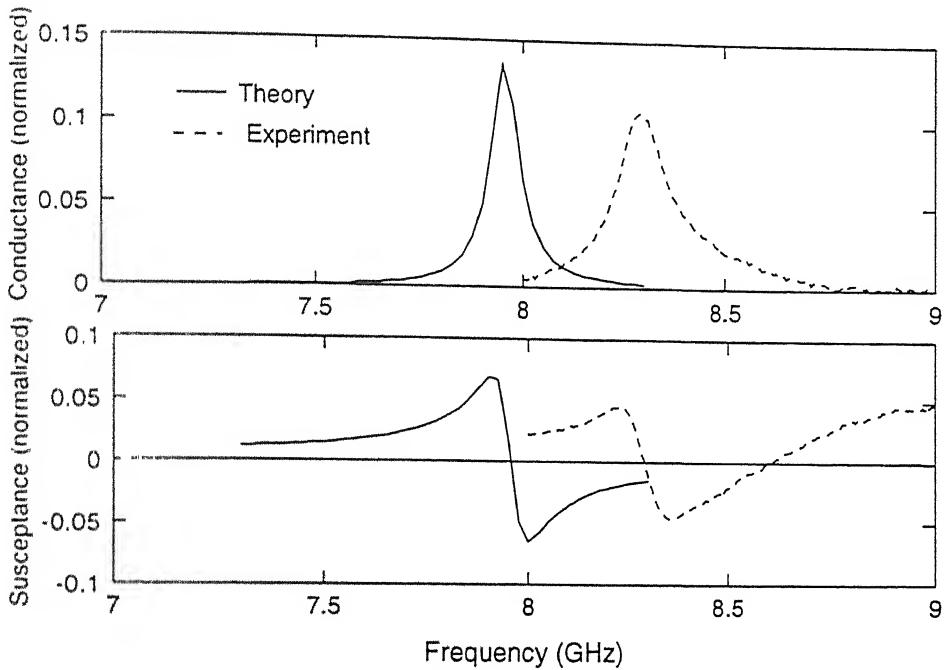
Figure 5.6: Normalized shunt admittance of the strip excited slot. Measurements were done using standard wave guide calibration without ground plane. $a = 22.86$ mm, $b = 10.16$ mm; strip: 10.0×0.8 mm, 20^0; slot: $9 0 \times 0.8$ mm; offsets: $y_l = 5.08$ mm, $z_l = 0$ mm; substrate: $\epsilon_r = 2.2$, $t = 0 8$ mm; modes, basis: $M_{max} = N_{max} = 100$, $N_l = N_s = 9$

2.5 ± 0.04, substrate thickness= 0.062 ± 0.002 inches. The accuracy to which the linear dimensions could be controlled are about ± 0.05 mm in the laboratory. This, incidentally, affects the dimensions and the inclination of both the strip and the slot. There also exist small alignment errors between the strip and the slot while making a double sided exposure of the substrate. This appears as a small strip offset. The program was run with slightly different parameters to check for the effect of parametric uncertainty. The computed results showed a maximum error of about 1% in the resonant frequency due the uncertainty of
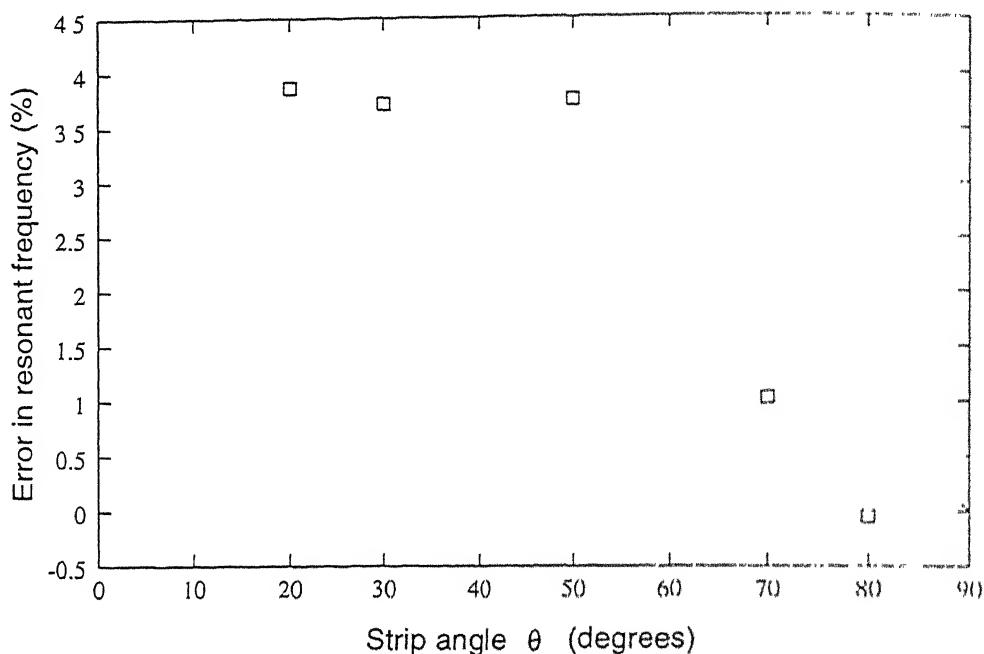
Figure 5.7: Percentage difference between measured and computed resonant frequency $(f_{meas} - f_{theory})/f_{meas}$ versus strip angle.

parameters. The error between theory and measurement below $\theta = 50^0$ is more than this, and hence it can be concluded that the uncertainty in the material parameters and fabrication tolerances are not the only cause of error.

There exists a 0.3 mm step in the region where the substrate is joined with the waveguide narrow wall. If this affects the slot as an end loading, then the measured resonant frequency could be different from the computed values. Measurements were repeated after thinning down the machined off narrow wall completely along with a ground plane. Measurements were also carried out on very narrow slots in order to reduce the effect the longitudinal component of the slot E-field. However, these additional set of experiments could not account for the order of magnitude errors appearing in Fig. 5.4 to 5.6. Therefore, it was concluded that the errors arise from the formulation rather than from the measurement.

It is possible to solve for the scattering from the inclined strip in the absence

of the slot. If we compare this result with the measurements on the strip excited slot in the absence of the slot (slot is closed with a conducting tape), then it is possible to check whether the problem arises from the modeling of the interaction of the strip with itself. This experiment, interestingly lead to identical observations as in the case when the slot was present. Thus there exist errors in the *inclined* strip scattering formulation itself.

We now accept the premise that the errors arise from the formulation and try to identify the reasons. An inclined strip inside a waveguide carries both longitudinal and transverse currents. Both the current components has variations in longitudinal and transverse direction. If the length to width ratio of the strip is large, the following assumptions are generally made.

- The transverse variation of the longitudinal current is assumed to be either a constant or an *even* edge current distribution. In the present case, an even edge current distribution is assumed.

- The transverse current is assumed to be zero. This is justified so long as its magnitude is much *smaller* than the longitudinal current.

Since these two approximations were made in the formulation, it is believed that the errors arise from these approximations. The incident E-field in an inhomogeneously filled waveguide has only the y component. This can be resolved into two components, namely along the strip and transverse to the strip. It is intuitively clear that the longitudinal E-field induces the longitudinal strip current, while the transverse E-field induces the transverse current. As the strip angle θ is reduced, the longitudinal E-field decreases as $\sin\theta$, whereas the transverse E-field increases as $\cos\theta$. Therefore, the longitudinal current decreases and transverse current increases with strip inclination. In fact, at small strip angles, the values of the transverse and longitudinal currents can become comparable.

The above reasoning is partly influenced by the following observation made by McNamara [20], and Espino [19], regarding the longitudinal offset broad wall slot—A longitudinal slot is excited primarily by the waveguide wall currents which flow transverse to it. This transverse current flow is odd about the broad wall center line. Therefore, increasing the slot offset from the center line increases the slot excitation. However, in practice (in an array environment) the excitation required for a longitudinal slot is quite small which results in small offset slots. Such slots often have offsets of the order of the slot width and are called *weakly excited*. The weakly excited slot is found to be different from its strongly excited counterpart in various aspects. Irrespective of the offset, every longitudinal slot is also excited by a longitudinal wall current causing a longitudinal E-field in the slot. This current is even about the centerline and therefore its effect on the slot scattering is negligible at large offsets. In a weakly excited slot, the magnitude of the longitudinal E-field is found to be comparable to that of the transverse E-field. This is true even in the case when the slot length to width ratio is large. It is also observed that the transverse variation of the transverse E-field is asymmetric about the slot center line. Thus the classical assumptions for the large offset slots are no longer valid in the case of a weakly excited slot—An analysis of the weakly excited slot (with the assumptions made in the case of a large offset slot) tends to give results which are off from the measured results.

The modeling of the strip excited slot, taking into account both the current distributions and allowing for variation in both the directions will be exceptionally difficult. The present analysis however predicts the trend in the behavior correctly. Consequently, it can be used to conduct a systematic preliminary set of experiments. It is perhaps worthwhile to characterize this error and correct for it, rather than attempting to solve the problem with complete rigor.

5.3   Behavior of the Strip Excited Slot

The next 8 sections describe various aspects of the strip excited slot. Since, the discussion is based on graphs, certain remarks are made to begin with. Standard waveguide calibration was used in the initial set of measurements, whereas TRL calibration was used for subsequent measurements. The measured susceptance curves using standard waveguide calibration are shifted appropriately to account for the errors in shifting the measurement plane. It is also indicated, whether a ground plane was used while making the measurements.

For the computed results, M_{max} (N_{max}) is the number of modes summed in the x (y) direction; N_l (N_s) denote the number of basis functions used on the strip (slot). The measured and computed results are presented together (if possible) to indicate the trends. This however should not be taken as an indication of the agreement between theory and experiment. This aspect has been discussed in the previous section.

5.3.1   S-parameters, Equivalent Circuit

The strip excited slot is a resonant structure and is relatively narrow band. Off resonance, the structure scatters very little, with the result that the S-parameters resemble that of a waveguide section: $S_{11} \approx 0$ and $S_{21} \approx 1$, indicating very little reflection and almost complete transmission. However, around the resonance, there is appreciable scattering, and both S_{11} and S_{21} attain non-trivial values. The resonant point is defined as the frequency at which the S-parameters are real at center of the slot. The phase of S_{11} and S_{21} are 180^0 and 0^0 respectively at resonance. The peak values of $|S_{11}|$ and $|S_{21}|$, however occurs at slightly lower frequency. In fact, $|S_{11}|$ and $|S_{21}|$ are not exactly symmetrical about their peak values and are slightly skewed. The strip excited slot
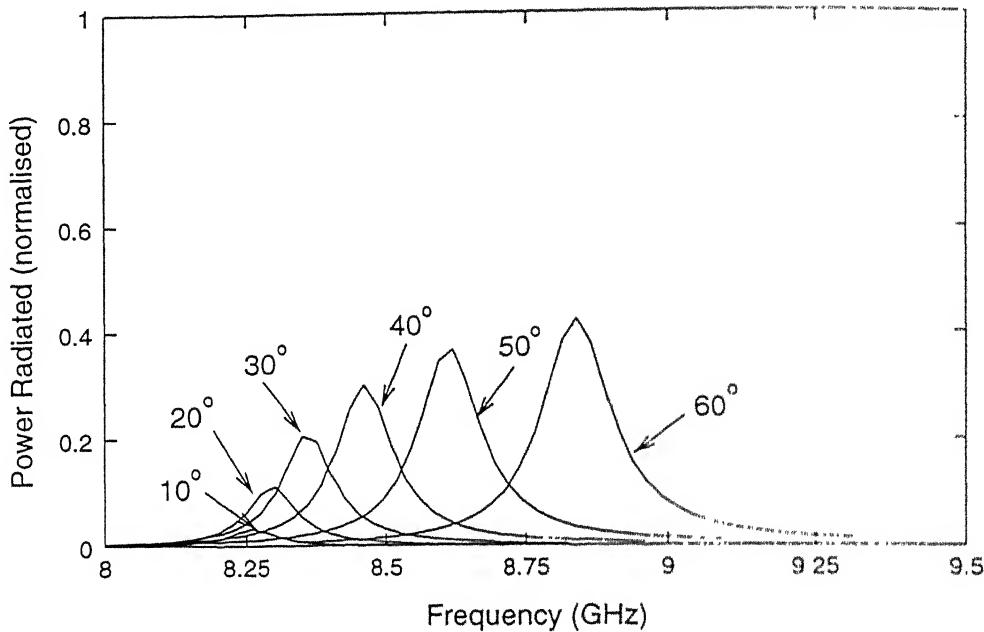
Figure 5 8: Normalized radiated power ($1 - |S_{11}|^2 - |S_{21}|^2$) vs. frequency at various strip angles. waveguide: $a = 22.86$ mm, $b = 10.16$ mm; strip: 10.0×0.8 mm; slot: 9.0×0.8 mm, offsets: $y_l = 5.08$ mm, $z_l = 0$ mm; substrate: $\epsilon_r = 2.2$, $t = 0.8$ mm; modes, basis: $M_{max} = N_{max} = 50$, $N_l = 5$, $N_s = 3$

is also a symmetric passive structure so that $S_{22} = S_{11}$ and $S_{12} = S_{21}$.

The value of $1 - |S_{11}|^2 - |S_{21}|^2$ gives the ratio of the power lost inside the two-port to the incident power. If the losses in the structure are small compared with the radiated power, then this represents the normalized radiated power. [See Fig. 5.8]. If the structure is loss less (as in the case of scattering from the strip in the absence of the slot), then the identity $|S_{11}|^2 + |S_{21}|^2 = 1$ can be used to check whether the formulation is erroneous. However, this is a necessary condition and is not sufficient to comment on anything else. Therefore, if a scattering formulation does not satisfy this identity, we can conclude that the results are incorrect.

The T-equivalent network gives better physical insight into the behavior than S-parameters. The T-network is drawn with respect to the propagating

LSE_{10} mode in an inhomogeneously filled waveguide. Referring to Fig. 4.12 and Fig. 4.13 (See Chapter 4), it can be seen that the series arm impedances are about 1/10 that of the shunt arm. The variation of the shunt impedance with respect to frequency, suggests that it is a series resonance. Thus the strip excited slot is predominantly a shunt admittance which goes through a series resonance. Off resonance, the admittance is very small indicating the absence of any scattering.
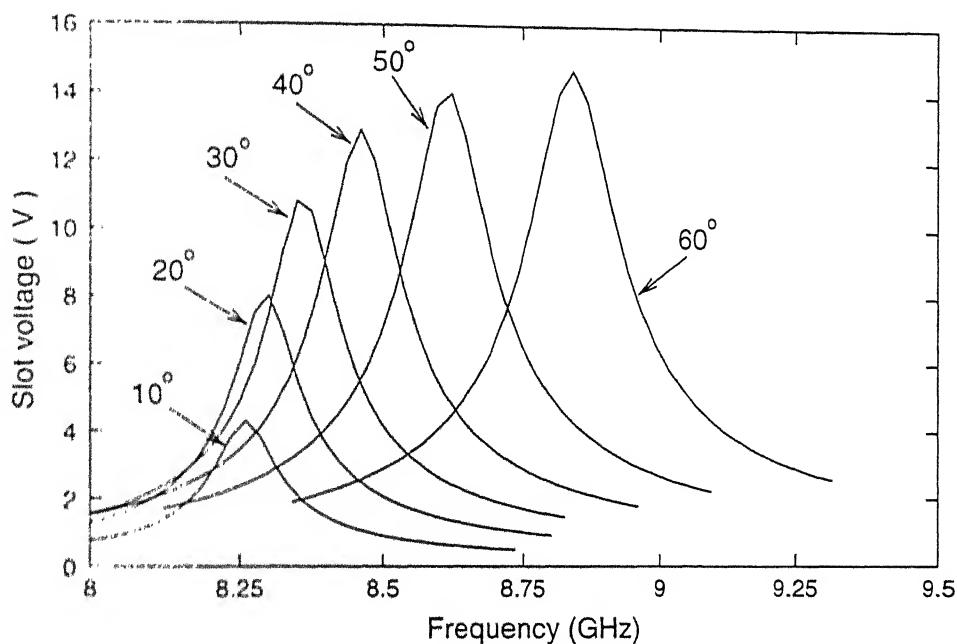

Figure 5.9: Slot voltage magnitude vs. frequency at various strip angles. See Fig. 5.8 for other details.

If a discontinuity is a shunt admittance, it can be shown that the maximum power transfer takes place when the normalized admittance is $2 + \jmath 0$. Thus a normalized shunt admittance of 2 corresponds to maximum radiation from the slot. It is also obvious that this corresponds to the case when half the incident power gets radiated, while the other half gets distributed as reflected and transmitted power. It can be concluded that, for a given incident field, the maximum slot voltage occurs at this value of admittance. With respect to
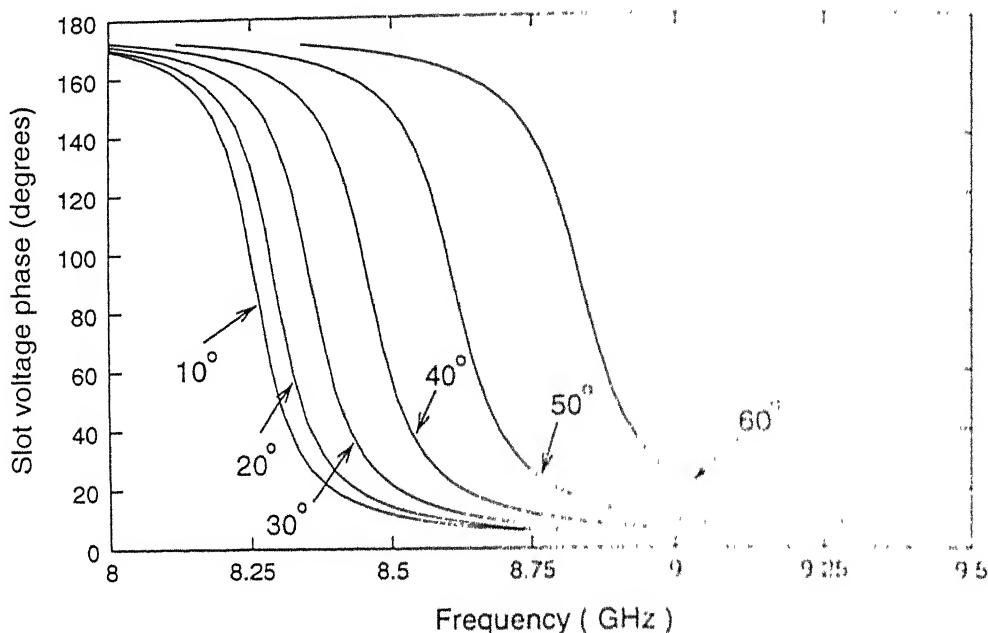
Figure 5.10: Slot voltage phase vs. frequency at various strip angles. See Fig. 5.8 for other details.

Fig. 5.9 to 5.10, the magnitude of the slot voltage is seen to be maximum, while the phase of the slot voltage is 90^0 at resonance. The slot voltage is specified with the assumption that the incident E_y component is $1 \cdot j \cdot$ at the center of the slot at $x = t$.

The strip excited slot exhibits multiple resonances due to the various interactions between the strip and the slot. Fig. 4.14 indicates a sequence of three resonances series-shunt-series starting from the lower end of the band. Experiments indicate that only the first series resonance corresponds to appreciable radiation from the slot. This suggests the following approximate equivalent circuit for the shunt admittance. With respect to Fig. 5.11, one can identify two series R-L-C circuits connected in parallel. The first R-L-C circuit corresponds to the slot, whereas the second corresponds to the strip. The resistance R_{loss} is introduced to account for the losses in the strip. Each R-L-C circuit has its own series resonance and the combined admittance behavior is identical to that
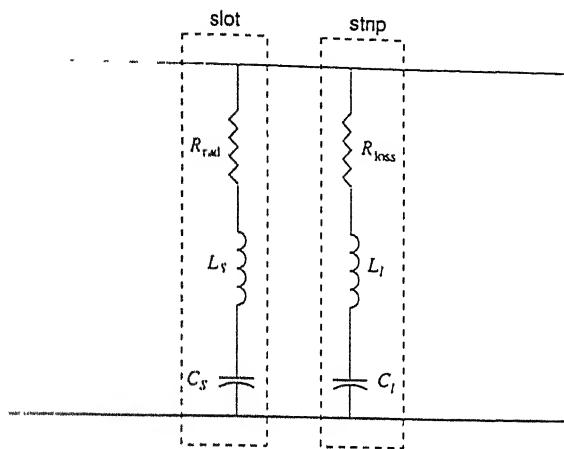
Figure 5.11: Approximate equivalent circuit of the strip excited slot

shown in Fig. 4.14. This equivalent circuit is approximate since the two circuits interact to some extent.

In the absence of the slot, the strip scatters on its own without any radiation. The strip appears as a shunt susceptance which goes through a series resonance. The measurements, however indicate that the strip admittance has an appreciable real part. This is due to the losses in the structure. In the absence of the slot, the resonant strip current reaches much larger values than what is induced in the presence of the slot at the combined resonant frequency, which is away from the strip resonance. This leads to increased conductor losses in the strip.

5.3.2 Strip Angle

The incident wave does not couple directly to the slot and cause radiation. The inclined strip acts as the intermediary between the vertical slot and the incident propagating mode. Specifically, this involves two coupling stages, namely the incident wave to the strip, followed by the strip to slot coupling. The strip scattering is maximum when it is kept vertical and it is zero when the strip
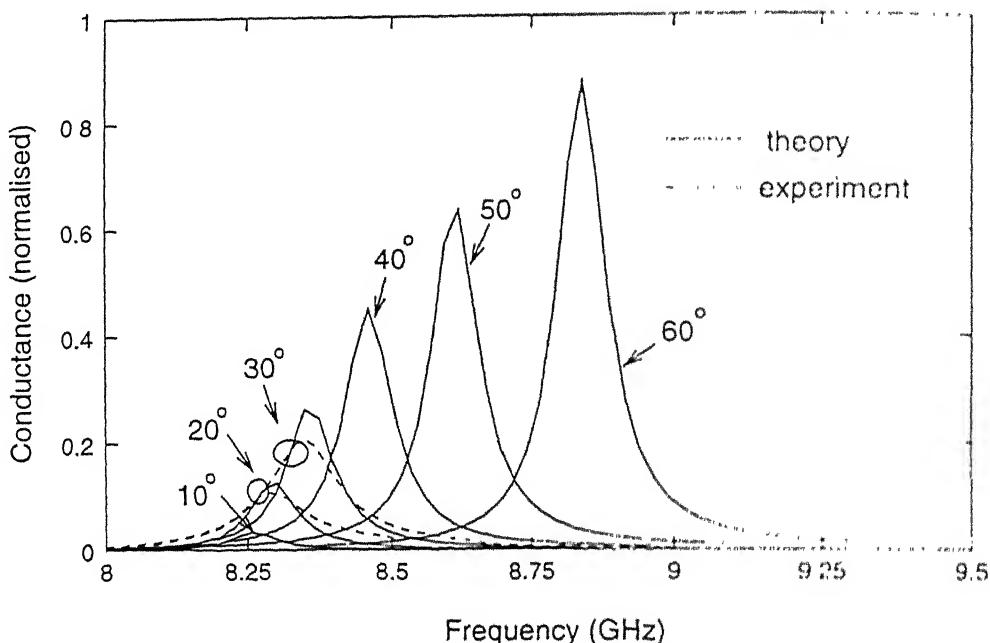
Figure 5.12: Normalized shunt conductance vs. frequency at various strip angles. Measurements were done using standard waveguide calibration and no ground plane. See Fig. 5.8 for other details.

is made horizontal. However, the strip to slot coupling is maximum when the two are orthogonal (i. e. when the strip is horizontal) and zero when the two are made parallel. Therefore, the strip excited slot ceases to radiate at both $\theta = 0$ and $\theta = 90$. The reduction in coupling around $\theta = 90$ is extremely fast, and it happens in a very small angular sector. The analysis program has a restriction and cannot be used to generate data for nearly vertical strips. Therefore, no theoretical data is provided to substantiate this claim. However there are measured data in this region and it confirms this observation. Since this data does not contain any other information it is not present here. The S-parameters of the strip excited slot is identical to that of the strip inside the waveguide when the strip is made vertical.

Fig. 5.12 to 5.14 illustrate the effect of strip angle at lower angles, whereas Fig. 5.15 to 5.17 illustrate the effect of the strip inclination at higher angles. The
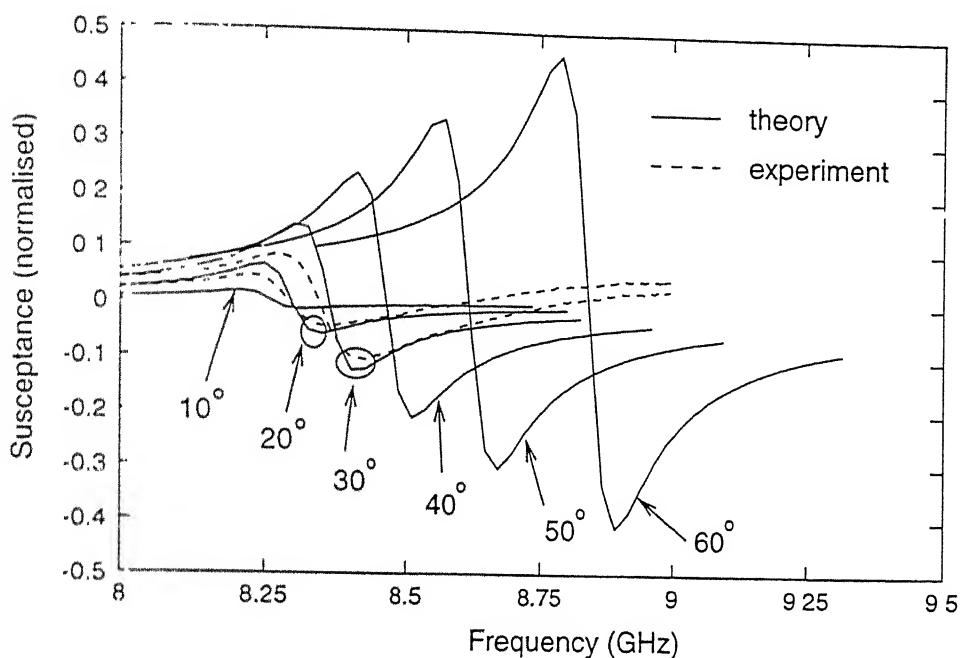
Figure 5.13: Normalized shunt susceptance vs. frequency at various strip angles. See Fig. 5.8 for other details.
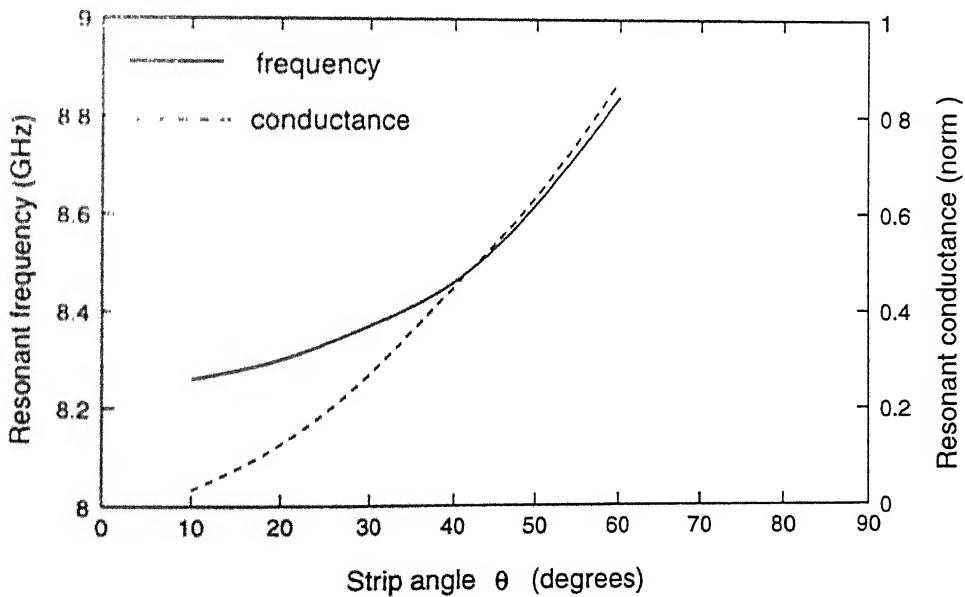

Figure 5.14: Variation of resonant frequency and resonant conductance with respect to strip angle. See Fig. 5.8 for other details.
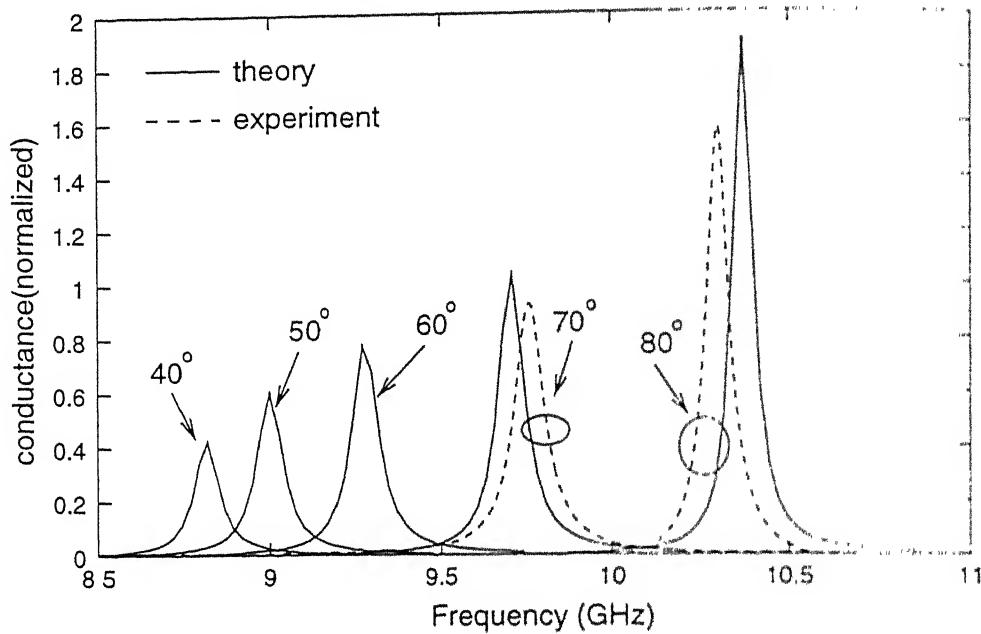
Figure 5.15· Normalized shunt conductance vs. frequency at various strip angles. Measurements were done using TRL calibration with ground plane. waveguide, $a =$ 22.86 mm, $b = 10.16$ mm; strip: 9.4×0.8 mm; slot: 8.0×0.8 mm, offsets: $y_l =$ 5.08 mm, $z_l = 0$ mm; substrate: $\epsilon_r = 2.2$, $t = 0.8$ mm; modes, basis, $M_{max} =$ $N_{max} = 100$, $N_l = 5$, $N_s = 3$

following observations can be made regarding the effect of the strip angle. A very wide range of conductances can be realized within 0^0 to 80^0. The resonant frequency increases with increase in the strip inclination. It can be seen that the change in resonant frequency with respect to strip inclination is faster in the higher angle ranges.

Altering the strip angle from θ to $-\theta$ changes the sign of the slot voltage. This is analogous to flipping the offset in a longitudinal slot or altering the tilt in an inclined narrow wall slot. It is required the flip the strip angle to cancel the propagation phase shift of 180^0 between two adjacent slots, so that the slot fields are in the same direction.
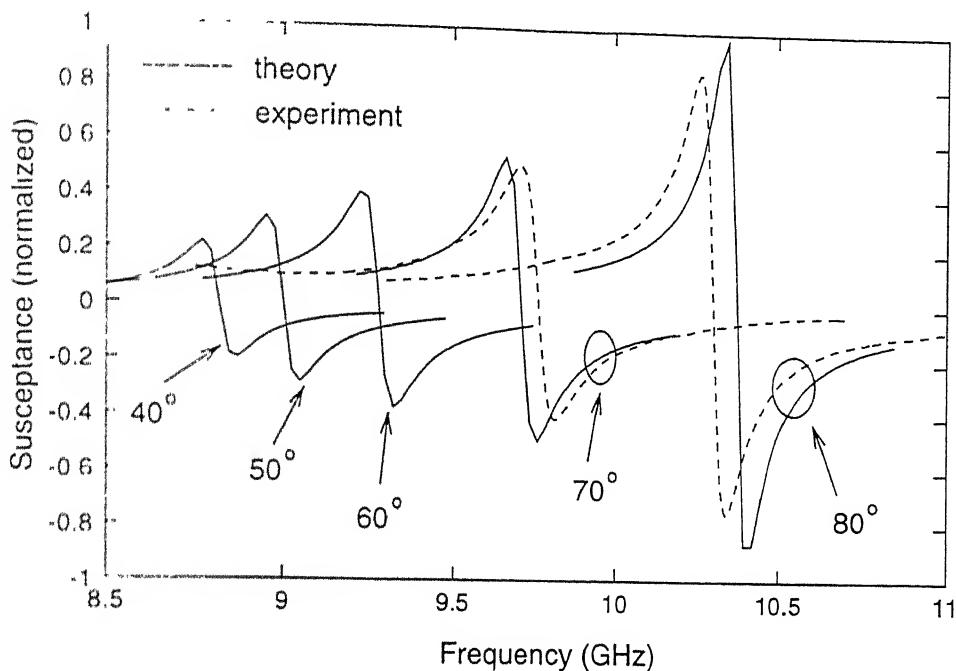
Figure 5.16: Normalized shunt susceptance vs. frequency at various strip angles. See Fig. 5.15 for other details.
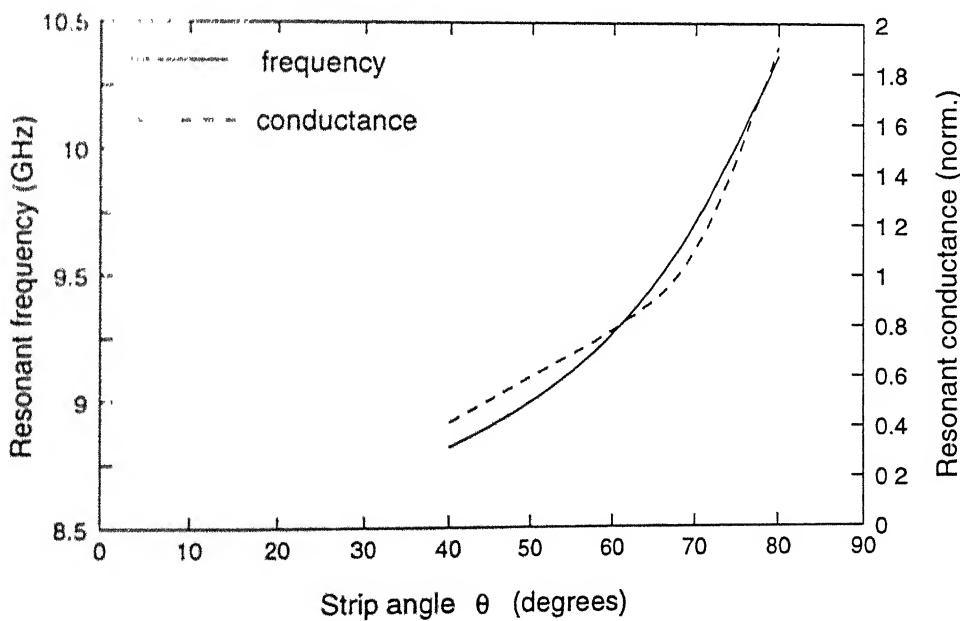
Figure 5.17: Variation of resonant frequency and resonant conductance with respect to strip angle. See Fig. 5.15 for other details.

5.3.3 Strip Length
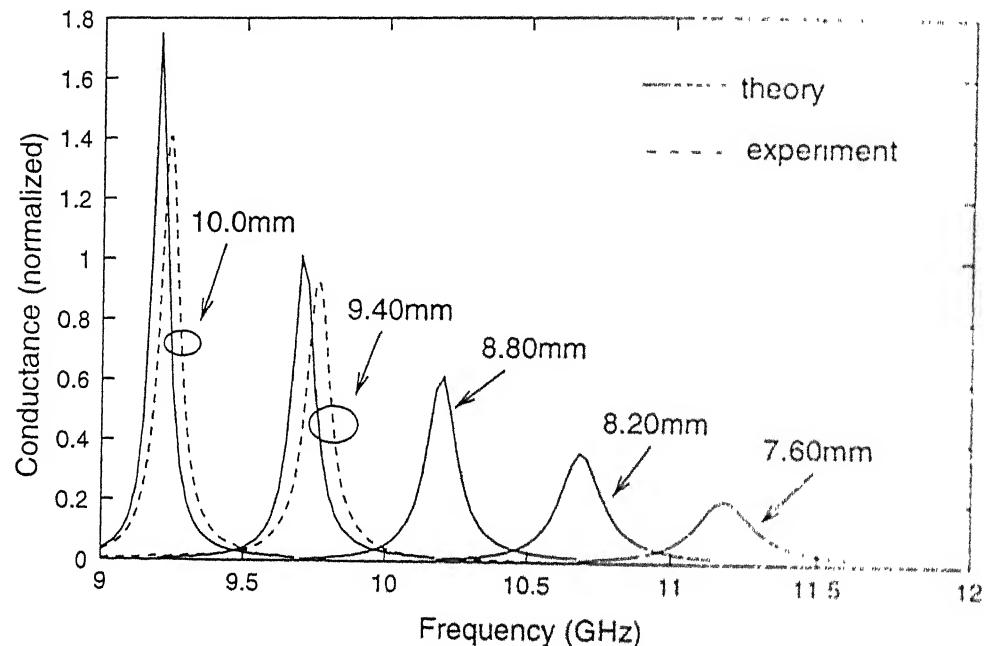
Figure 5.18: Normalized shunt conductance vs. frequency at various strip lengths. Measurements were done using TRL calibration with ground plane. waveguide, a = 22.86 mm, b = 10.16 mm; strip: $2w_l$ = 0.8 mm, 70°; slot: $8.0 \cdot 0.8$ mm; offsets: y_l = 5.08 mm, z_l = 0 mm; substrate: ϵ_r = 2.2, t = 0.8 mm; modes, basis: $M_{max} = N_{max} = 100$, $N_l = 5$, $N_s = 3$

As shown in Fig. 5.18 to 5.19 the strip length affects both the resonant frequency and the conductance of the element. A longer strip interacts more with the incident field and leads to increased radiation from the slot. The resonant frequency, on the other hand, decreases *linearly* with the strip length as shown in Fig. 5.20. By adjusting the strip length along with strip inclination, it is possible to operate the strip excited slot at any given frequency at a specific admittance level.
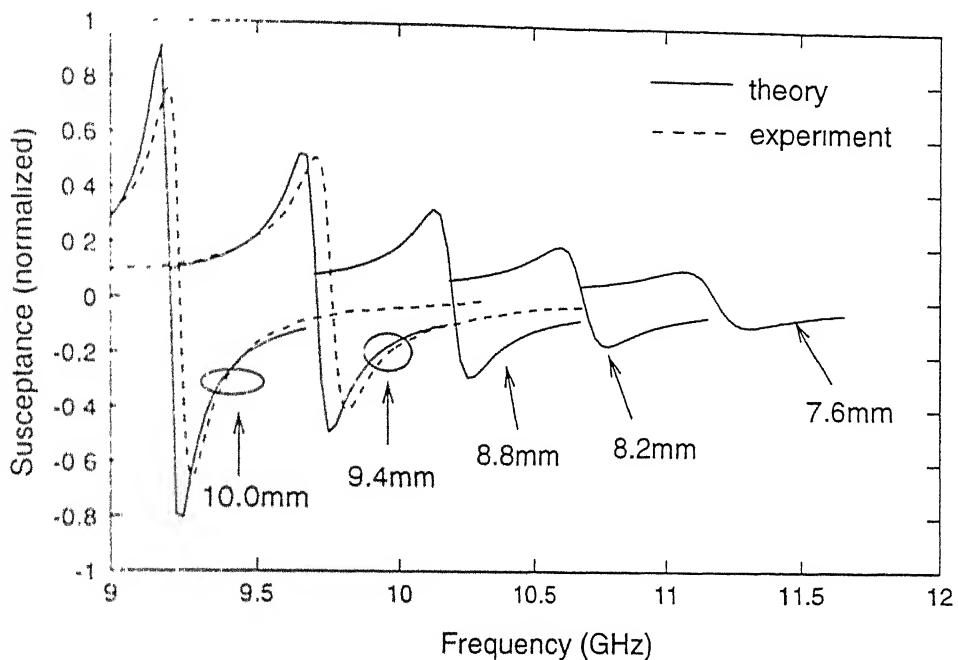
Figure 5 19: Normalized shunt susceptance vs. frequency at various strip lengths See Fig 5.18 for other details.
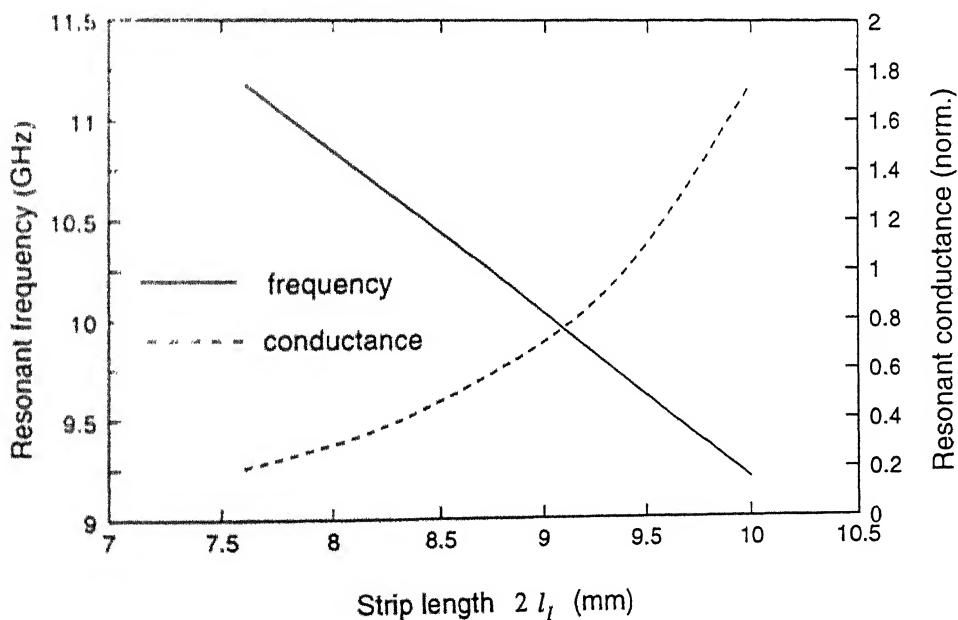
Figure 5.20: Variation of resonant frequency and resonant conductance with respect to strip length. See Fig. 5.18 for other details.

## 5.3.4 Slot Length and its Effect on Bandwidth
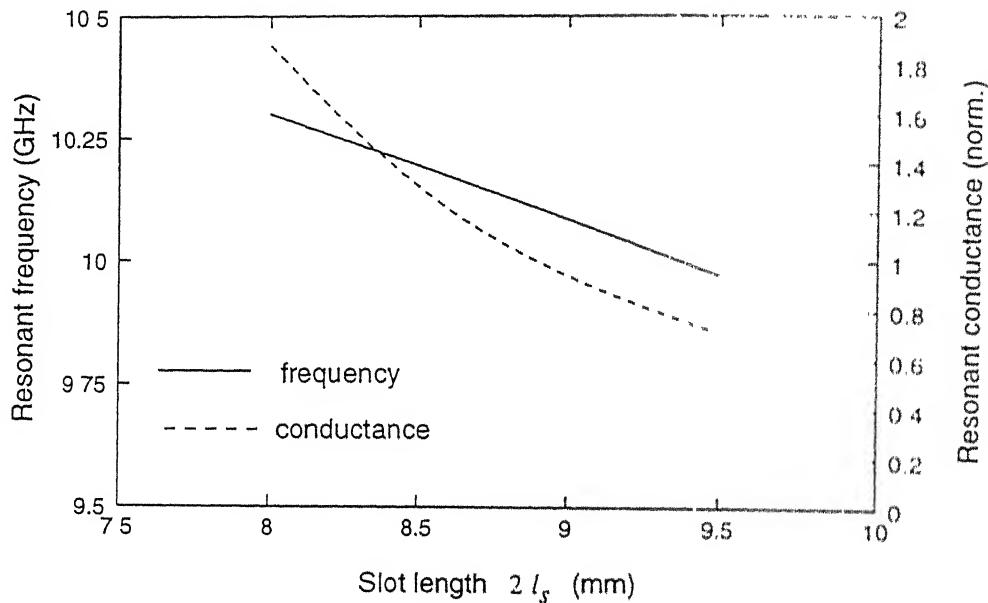
Figure 5.21: Variation of resonant frequency and resonant conductance with respect to slot length. $\theta = 80^0$, $2l_l = 9.4$ mm, $2w_l = 0.8$ mm, $y_l = 5.08$ mm, $s_l = 0$ mm, $2w_s = 0.8$ mm, $\epsilon_r = 2.2$, $t = 0.8$ mm, $M_{max} = N_{max} = 100$, $N_l = N_s = 9$

The slot length does not affect the admittance behavior as much as the strip length. With respect to Fig. 5.21 it can be seen that the resonant conductance decreases with slot length. The resonant frequency also decreases *linearly* with slot length. The effect of slot length on resonant frequency is much less than that of the strip length. The slot length however affects the bandwidth of the strip excited slot.

Fig. 5.22 to 5.23 shows the effect of slot length on the bandwidth of the strip excited slot. The bandwidth of the strip excited slot depends on how close the element is being operated to the slot's unloaded resonant frequency. It is to be noted that a narrow wall slot in a WR 90 waveguide is much smaller than its resonant length. Fig. 5.22 illustrates the conductance behavior of 4 slots A, B, C and D made to operate at 8.0, 9.0, 10.0 and 11.5 GHz respectively.
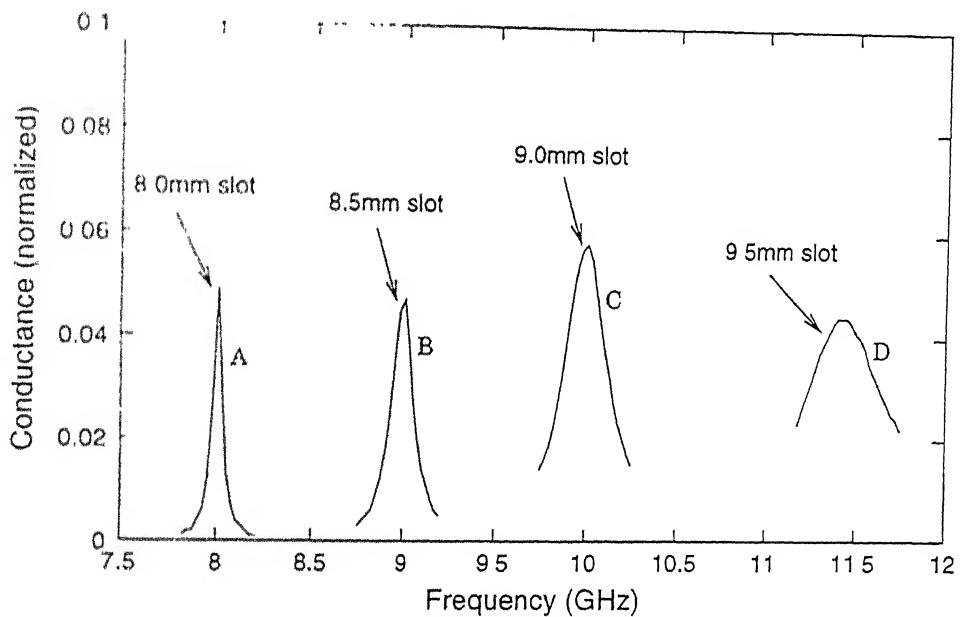
Figure 5.22: Illustrating the bandwidth improvement with respect to the slot length. slot: $2w_s = 0.8$ mm; offsets. $y_l = 5.08$ mm, $z_l = 0$ mm; substrate: $\epsilon_r = 2.2$, $t = 0.8$ mm; basis, modes: $M_{max} = N_{max} = 100$, $N_l = N_s = 9$ (A) strip: 10.38×0.8 mm, 9^0; (B) strip: 8.30×0.8 mm, 20^0; (C) strip: 6.91×0.8 mm, 47^0; (D) strip: 7.24×0.6 mm, 78^0.

The strip length and strip angle are adjusted appropriately for this. Note that even a 9.5 mm slot at 11.5 GHz is only about $0.36\lambda_0$ which is shorter than the unloaded resonant length (approximately $0.5\lambda_0$). The bandwidth achievable for any narrow wall vertical slot is limited by the narrow wall dimension of the waveguide. This can be improved by opting for a nonstandard waveguide such that the narrow wall is wider than the standard waveguide dimension.

5.3.5 Strip and Slot Width

The effect of strip width is similar to that of strip length. Fig. 5.24 to 5.25 illustrate 2 cases where the effect of the strip width is presented. It can be observed that the resonant frequency decreases and the resonant conductance
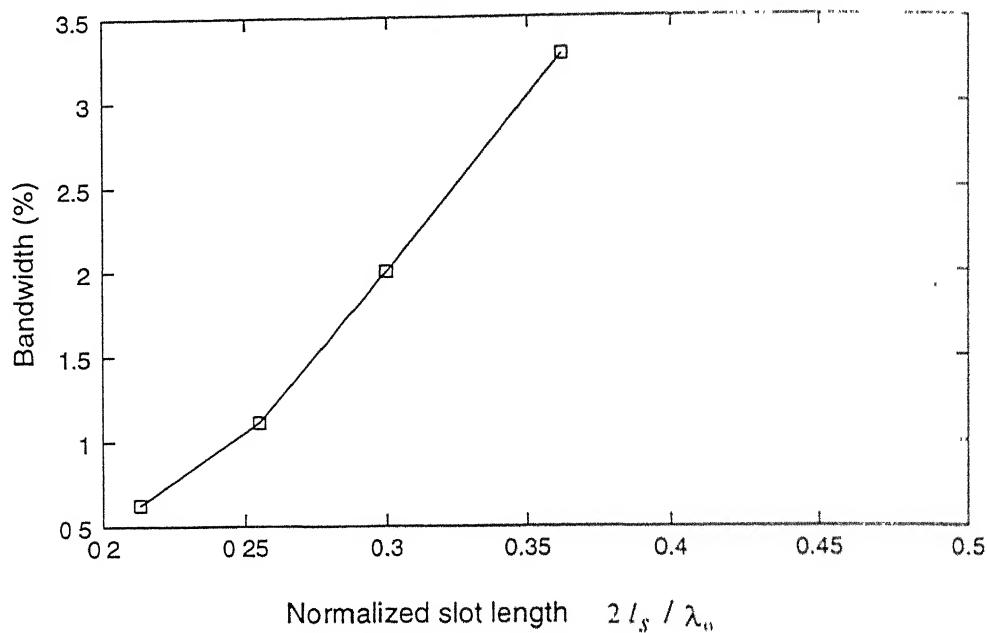
Figure 5.23: Variation of 3dB bandwidth with respect to normalized slot length
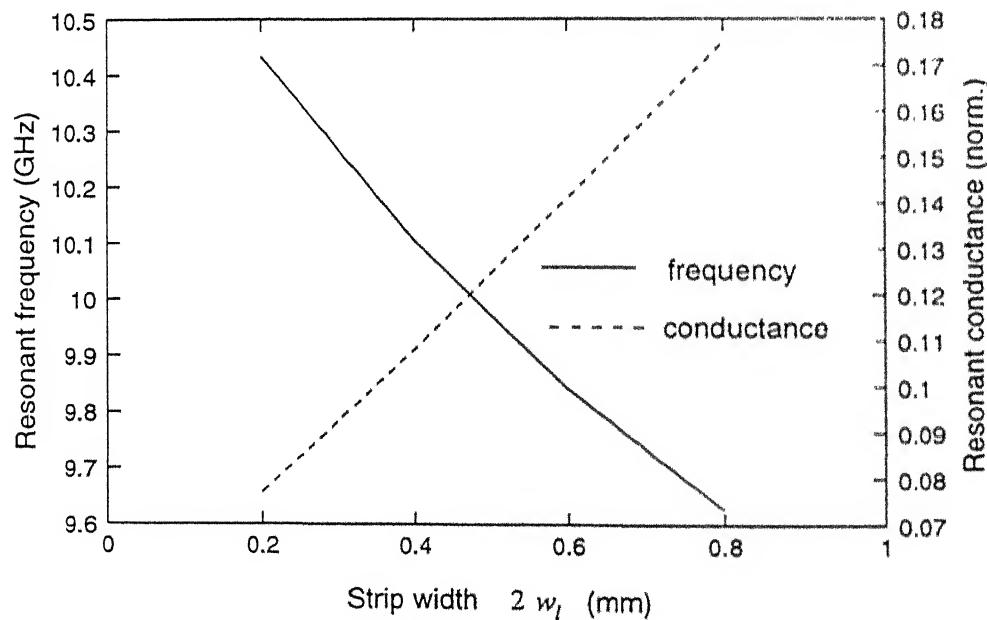

Figure 5.24: Variation of resonant frequency and resonant conductance with respect to strip width. See Fig. 5.4 for other details.
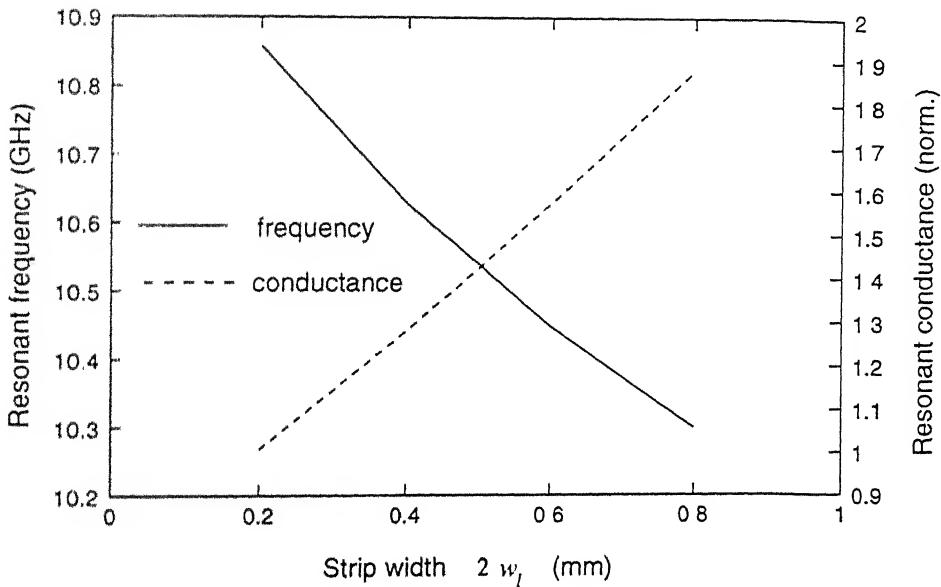
Figure 5.25: Variation of resonant frequency and resonant conductance with respect to strip width. See Fig. 5.1 for other details.

increases with strip width. The change in resonant frequency is not linear with respect to the strip width but the conductance variation is noticeably linear. Though the effect of strip width can be achieved by adjusting the strip length, it is possible to use strip width as a controlling parameter in a strip excited slot element. Strip widths of the order of 0.4 mm can be fabricated easily in the laboratory. We have for example reduced the strip width from 0.8 mm to 0.6 mm while generating case D of Fig. 5.22.

Fig. 5.26 shows the effect of slot width on the admittance behavior of the strip excited slot. There is a reduction in resonant frequency with increasing slot
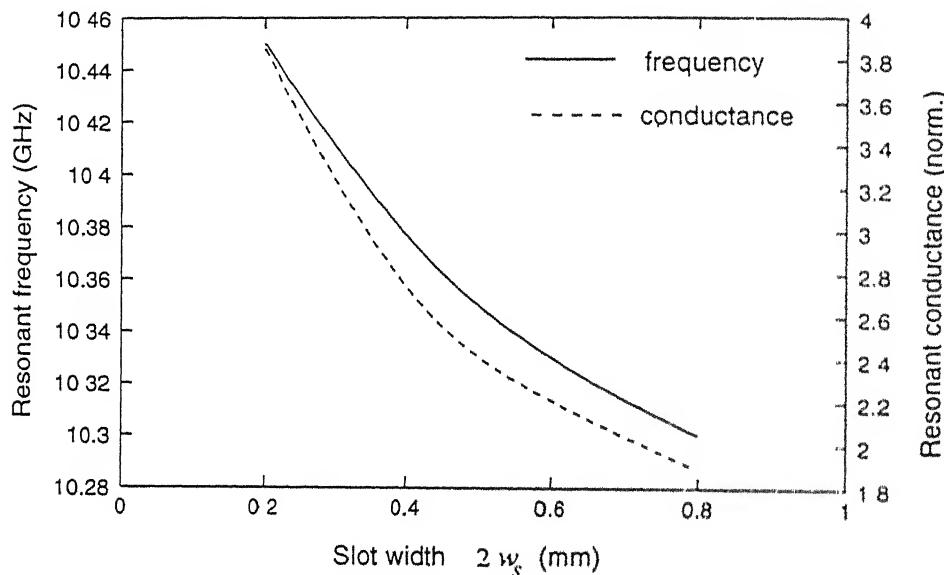
Figure 5 26: Variation of resonant frequency and resonant conductance with respect to slot width. See Fig. 5.1 for other details.

width. This is nonlinear and less prominent than due to the strip width. The normalized conductance of the slot is above 2.0 in the graph and it decreases to 2.0 with slot width. If the slot width were to be increased beyond 0.8 mm, we can expect the conductance to fall sufficiently below 2.0, which implies a reduction in the radiated power. However, for an array design, it is not necessary to change the slot dimensions at all since the required resonant point and admittance can be synthesized with the strip parameters.

5.3.6   Strip Offsets
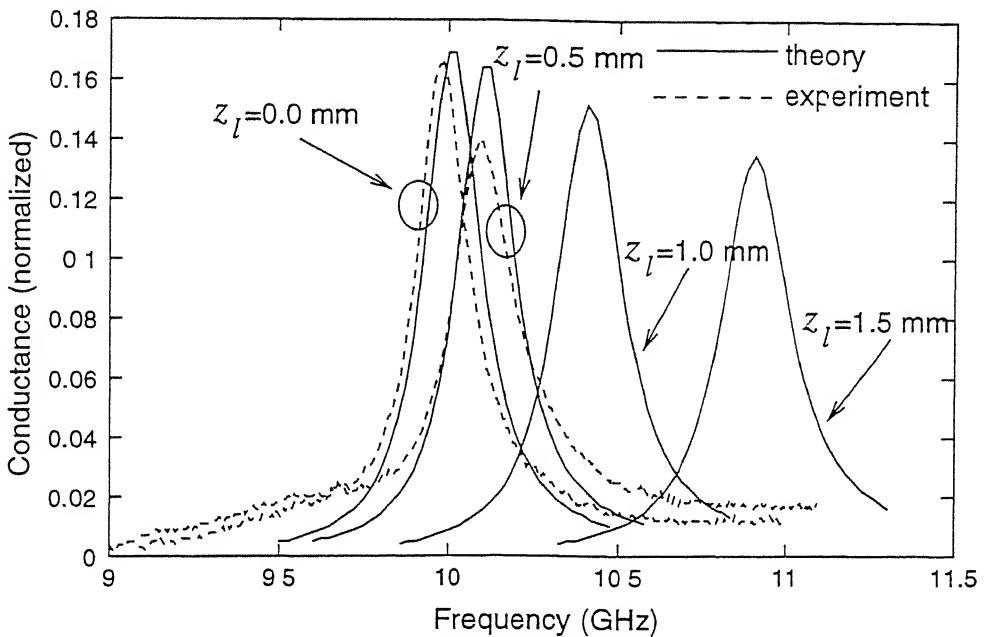
Figure 5.27· Normalized shunt conductance vs. frequency at various strip offsets z_l. Measurements were done using standard waveguide calibration and no ground plane. strip: 8.0×0.8 mm, 50^0; slot: 8 5×0.8 mm; offsets: $y_l = 5.08$ mm; substrate: $\epsilon_r = 2.2$, $t = 0.8$ mm; basis, modes: $M_{max} = N_{max} = 50$, $N_l = 5$, $N_s = 3$

The cross-over point of the strip with respect to the slot can be altered by offsetting the strip. The strip can be moved vertically, horizontally or both ways. We shall call z_l as the horizontal offset and y_l as the vertical offset. Fig 5.27 to 5.29 show the effect of horizontal offset on the radiation characteristics. The resonant frequency increases and resonant conductance decreases with horizontal offset. The change in resonant frequency is faster at larger offset values.

Fig. 5.30 presents the variation of resonant frequency and resonant conductance with respect to vertical strip offset. Note that the effect of vertical offset is very small. Therefore, it can be assumed that the effect of a compound offset will be governed by the horizontal offset rather than the vertical offset. For
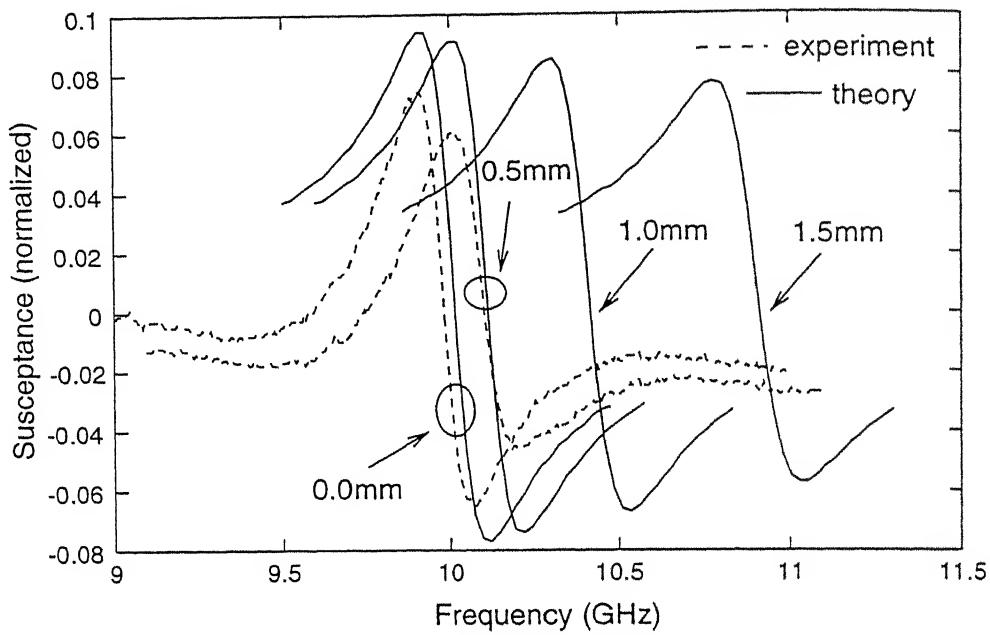
Figure 5.28: Normalized shunt susceptance vs. frequency at various strip offsets z_l.
See Fig. 5.27 for details.
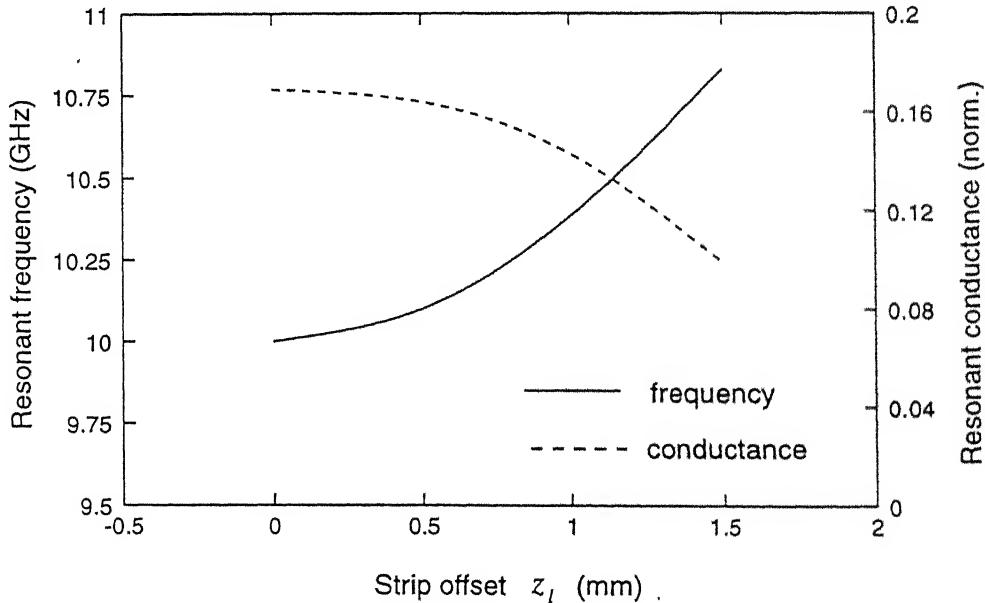
Figure 5.29: Variation of resonant frequency and resonant conductance with respect
to the strip offset z_l. See Fig. 5.27 for details.
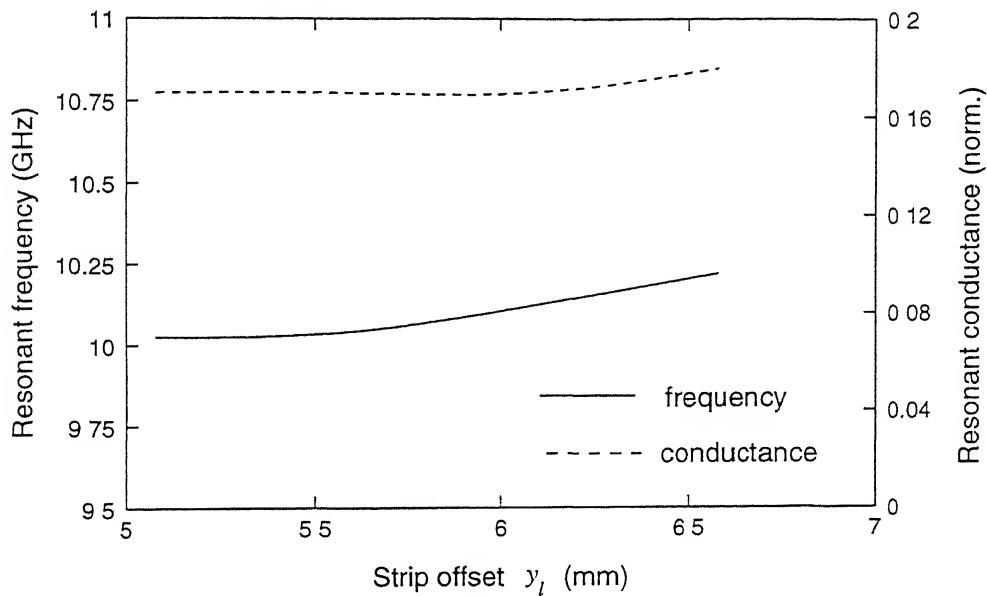
Figure 5.30· Variation of resonant frequency and resonant conductance with respect to the strip offset y_l. offset: $z_l = 0$ mm, See Fig. 5.27 for other details

a test antenna with a centered strip, we can expect the measured resonant frequency to be slightly higher due to alignment errors.

5.3.7 Substrate Thickness

Changing the substrate thickness alters the propagation constant and the mode patterns of an inhomogeneously filled waveguide. However, for the strip excited slot, a change in substrate thickness also amounts to changing the distance between the strip and the slot. We can expect an increase in coupling between the incident field and the strip with increasing substrate thickness, since the strip is now moving into stronger incident field region. However, the strip to slot coupling might be decreasing with substrate thickness leading to an overall reduction in slot radiation. It can therefore be expected that the radiated power first increases and then decreases with substrate thickness. Fig. 5.31 confirms that this is indeed true. It is to be noted that the normalized conductance first
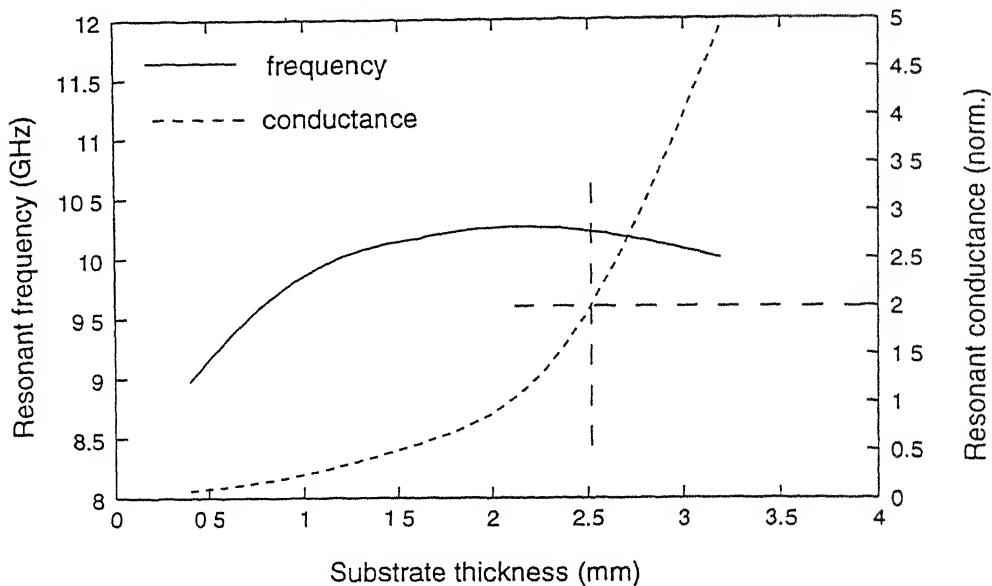
Figure 5.31. Variation of resonant frequency and resonant conductance with respect to substrate thickness. strip: 8.0×0.8 mm, 50^0; slot: 8.5×0.8 mm; offsets: $y_l =$ 5.08 mm, $z_l = $ 0mm, substrate: $\epsilon_r = 2.2$; basis, modes: $M_{max} = N_{max} = 100$, $N_l = N_s = 9$

increases up to 2.0 and then increases beyond it. Note that, an increase in conductance beyond 2.0 is actually a reduction in radiated power. The resonant frequency also increases with substrate thickness and then starts decreasing approximately around the same point where the radiation starts dropping.

5.3.8   Substrate Permittivity

Fig. 5.32 shows the effect of changing the substrate permittivity. The permittivity affects both the resonant frequency as well as the conductance considerably. Note that, a change of ϵ_r from 1.5 to 3.5 takes the resonant frequency all the way from 11.75 GHz to 8.5 GHz. The variation of the conductance with respect to ϵ_r is similar to that of substrate thickness. The radiation first increases and then decreases with ϵ_r. The relative permittivity also changes the equivalent
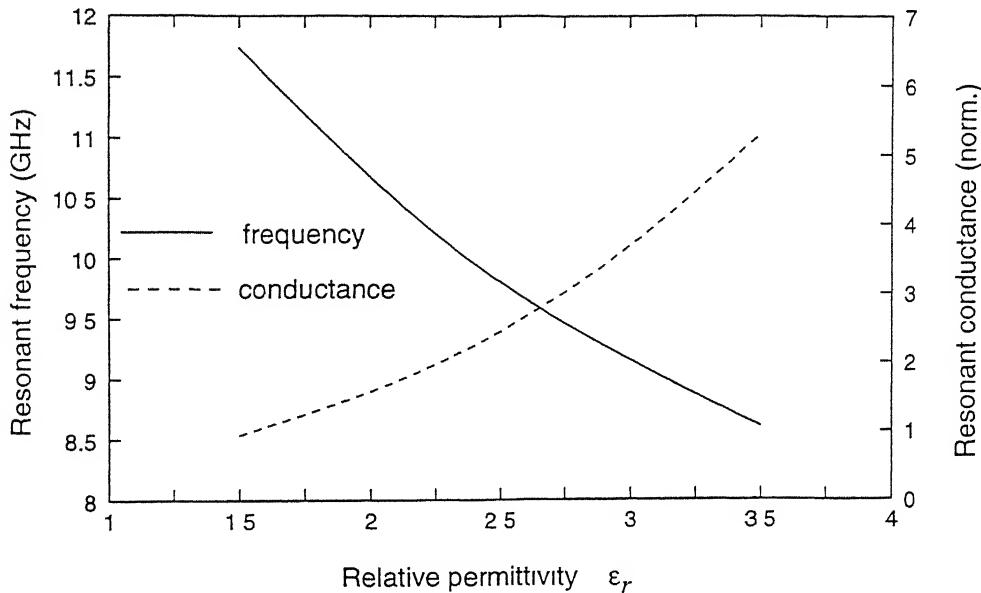
Figure 5.32: Variation of resonant frequency and resonant conductance with respect to the relative permittivity of the dielectric substrate. strip 9.4×0.8 mm, 80^0; slot: 8.0×0.8 mm, offsets: $y_l =, 5.08$mm, $z_l = 0$ mm, substrate: $t = 0.8$ mm; modes, basis: $M_{max} = N_{max} = 100$, $N_l = N_s = 9$

slot length.

5.4   Array Design Aspects

The principles of waveguide fed slot array design is exhaustively discussed in [48, 17, 16, 18]. A qualitative introduction of array design using the strip excited slot will be taken up based on these references. A linear array of equispaced slots is considered to make the discussion simple.

A waveguide fed slot array consists of a waveguide with a series of equally spaced slot elements excited from one end. Each slot radiator is a strip excited slot. The array is termed *standing wave fed* or *traveling wave fed* depending on the load end termination. A traveling wave array is terminated in a matched

load, while a standing wave array is terminated in a short circuit $\lambda_g/4$ away from the last slot. In addition, the slots are spaced $\lambda_g/2$ apart in a standing wave array, whereas the slot spacing is different in a traveling wave array. Irrespective of these differences, the following results are true for any type of serially fed array of radiators.

When an array of slots is fed from one end, each slot radiates a fraction of the incident power with the result that a set of slot voltages gets established on the slots. In an array, the slot radiators are designed such that the required set of slot voltages are established (and maintained) over a designated frequency band. When a propagating mode interacts with a slot, the slot radiates as well as scatters the incident power to either side inside the waveguide. The scattered wave in turn propagates to either end of the array, thereby influencing every other slot. This can be regarded as an internal excitation regardless of whether the mode is due to the scattering from a slot or due to the array driving source. The first few evanescent modes also affect the slot to some extent, and it is necessary to take their effect into account if the array is to meet specific design goals. Each slot also interacts with every other slot through the exterior of the array and this is termed *external mutual coupling* .

The situation can be summarized as follows. A slot is excited by three distinct mechanisms—the two waves incident from either side internally, and the wave incident externally due to the mutual coupling via. other slots. Internal interaction is predominantly through the propagating mode, but it is necessary to take into account the effect of at least the nearest evanescent mode namely LSE_{20}, in addition to the propagating mode.

If the strip excited slot is represented as a shunt admittance, then the array can be represented to a first approximation as an array of shunt admittances in an equivalent transmission line. This presumes that we are neglecting both the external mutual coupling and higher order internal mutual coupling. Elliott's procedure [18] introduces the concept of active admittances to account for mu-

tual coupling. Instead of regarding the array as an array of shunt admittances, it regards it as an array of active admittances. The active admittance is the sum of self admittance along with a term which linearly depends on all the slot voltages. This is termed mutual coupling term and it includes the effect of both internal and external mutual coupling. What is required of an array element is the ability to achieve any specified shunt admittance by a suitable choice of parameters. The shunt admittance is to be adjusted such that the active admittance of each slot is made real. Note that, if we were to ignore mutual coupling, the resonant *conductance* variation as a function of the parameters of the strip excited slot would have been sufficient for the design.

In an array design, one starts with a pattern and chooses an appropriate number of elements and excitation coefficients to meet this. It is also necessary to have an input match and a specified efficiency for the array. The array coefficients are identical to the set of slot voltages within a scale factor. The array design scheme comes out with the specification of each slot radiator iteratively, such that the set of slot voltages are approximately realized. In the case of strip excited slot, it is possible to achieve any shunt admittance by adjusting the strip length and strip inclination alone. All other parameters can be fixed once for all. Therefore, the external mutual coupling effects are not changed while iterating to get the appropriate strip length-angle combination. The following results are required for designing an array.

- The shunt admittance variation as a function of strip angle and strip length.

- The voltage induced across the slot, if the slot were excited by LSE_{10} or LSE_{20} mode from either side.

- The scattered wave amplitudes of both LSE_{10} and LSE_{20} modes, had the slot been excited by LSE_{10} or LSE_{20} mode from either side.

- The scattered wave amplitudes of both LSE_{10} and LSE_{20} modes, if the slot were to be excited by another slot having a specified voltage across it at an arbitrary location in the array plane.

The above data set can be generated based on the methods developed in Chapter 2.

5.5 Design Data Generation

The behavior of the strip excited slot with respect to each of the parameter suggests numerous ways of tailoring the excitation level and resonant point. It appears sufficient to use only the strip length and inclination in adjusting the admittance level of the slot. In order to get better bandwidth, it is necessary to choose the slot length close to its unloaded resonant length. In general, this cannot be achieved on the narrow wall of a standard waveguide. It appears necessary to use waveguides with increased narrow wall dimensions such that the LSE_{20} cut off is still sufficiently far.

It is necessary to realize any shunt admittance if the strip excited slot were to be used as an array element. However, if the mutual coupling is moderate, it is not necessary to realize admittances which are far from resonance. It is generally sufficient to generate the admittance values around the resonant point. This implies that a slot radiator in an array environment is operated off from the resonant point, but not too far from it.

Fig. 5.33 shows the normalized admittance variation with respect to strip length and strip inclination. This data is generated at 11.0 GHz, and the normalized conductance range from 0.015 to 0.10 was selected, for the design of a 21 element traveling wave array. The strip inclination is varied from 52^0 to 76^0 in steps of 4^0 while the strip length is varied from 4.0 mm to 10.0 mm in
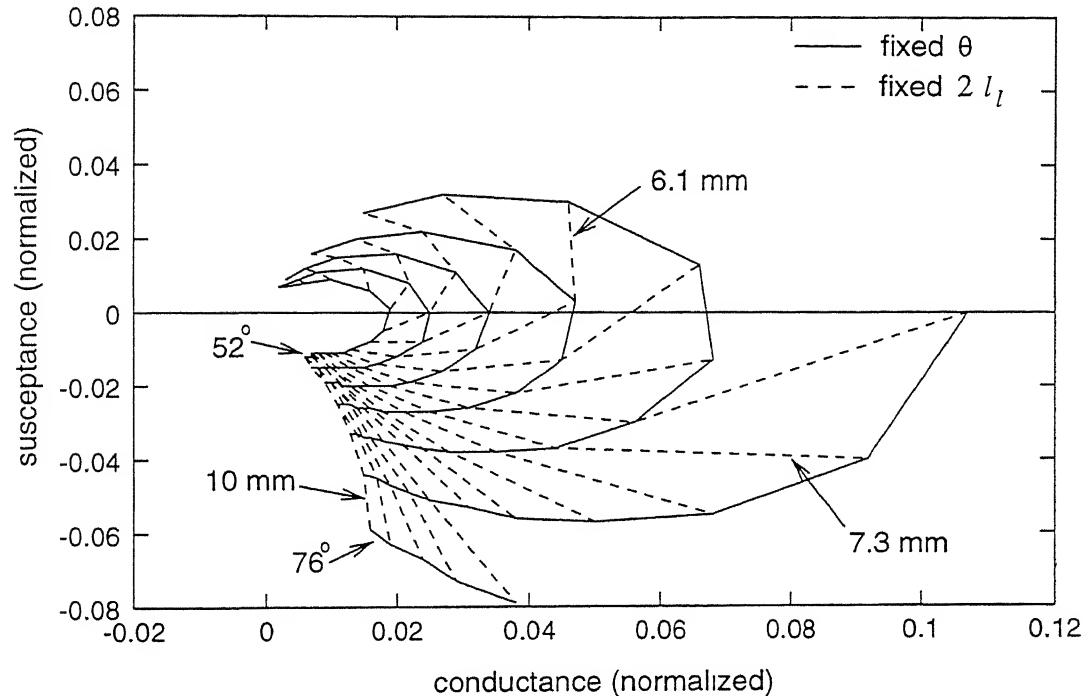
Figure 5.33: Admittance design curve: Shunt admittance variation with respect to strip angle θ and strip length $2l_l$ at 11.0 GHz. θ is varied from 52^0 to 76^0 in steps of 4^0, while $2l_l$ is varied from 4 mm to 10 mm in steps of 0.30 mm. strip: $2w_l = 0.6$ mm; slot: 9 0×1.5 mm; offsets: $y_l = 5.08$ mm, $z_l = 0$ mm, substrate: $\epsilon_r = 2.5$, $t = 1.6$ mm; modes, basis: $M_{max} = N_{max} = 100$, $N_l = N_s = 9$

steps of 0.3 mm. The following points are worth amplifying: for a given strip length, it is possible to adjust the inclination to make it resonant; conversely, for a given strip inclination, resonance can be achieved by adjusting the strip length.

Five points are identified from Fig. 5.34, such that they correspond to strip inclinations 56^0, 60^0, 64^0, 68.8^0 and 72^0. The strip lengths are chosen such that all of them are resonant at 11.0 GHz. This corresponds to the case when all the points lie on the zero susceptance line of Fig. 5.33. The corresponding strip lengths are found to be 5.49 mm, 5.80 mm, 6.14 mm, 6.62 mm and 6.95 mm from Fig. 5.34. Note that it is necessary to increase the strip length along with
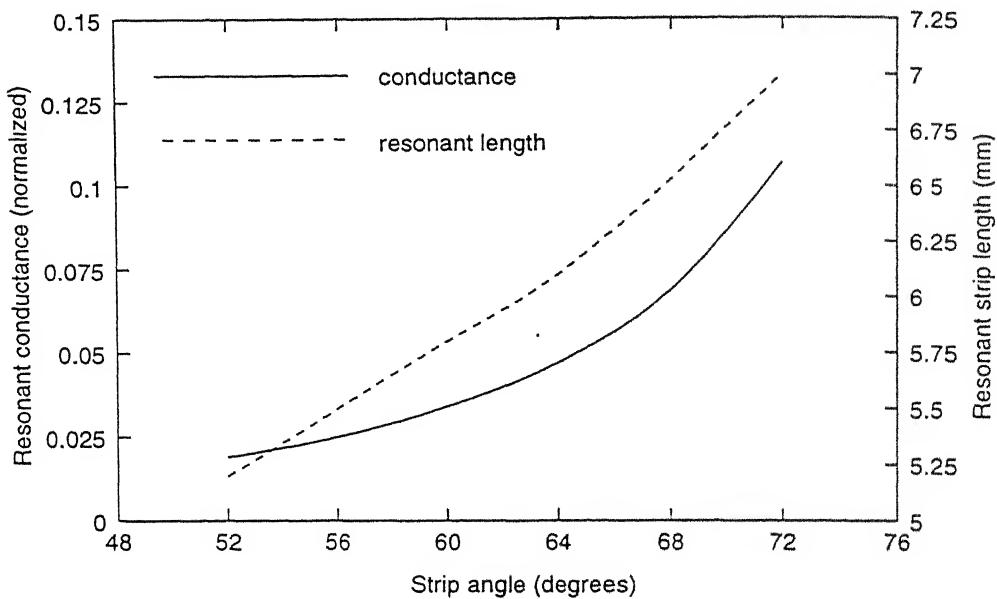
Figure 5.34: Variation of resonant conductance and resonant strip length with respect to strip angle, from the Admittance Design curve of Fig. 5.33
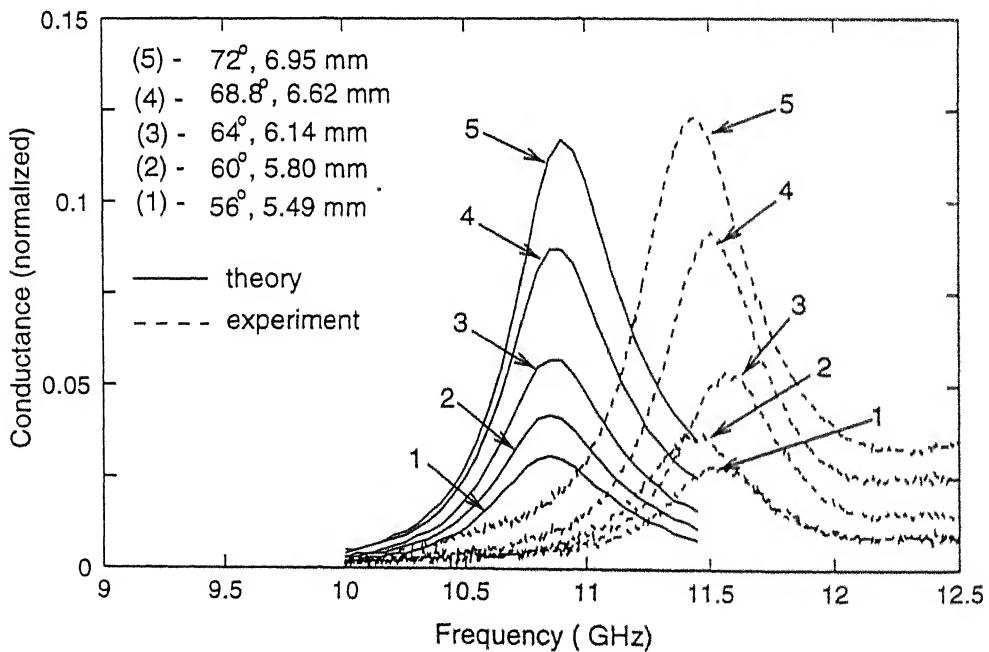

Figure 5.35: Comparison of computed and measured conductance values based on Fig. 5.33. Measurements were done using TRL standards and no ground plane.

strip inclination to maintain the resonant frequency.

Fig. 5.35 shows the computed and measured conductance for these 5 cases of length-angle combinations. It can be seen that the measured resonant frequency is about 4.5% higher than the computed value. Interestingly, the resonant frequencies for the last 3 cases is progressively decreasing. This seems to support the conclusion that the error in resonant frequency is directly related to the strip inclination. The conductance values are in moderate agreement in all the 5 cases. The measured conductances are slightly larger than the computed ones. This can be attributed to the losses in the antenna. Note that, the peak conductance values in Fig. 5.35 are larger than the resonant conductances from Fig. 5.33. This is because the resonant point does not coincide with the peak of the conductance value.

This experiment suggests the relevance of the present analysis in conducting a systematic preliminary set of experiments.

5.6 Summary and conclusions

A comprehensive discussion of the properties of the strip excited slot was made in this chapter. The strip excited slot has numerous parameters which affect its behavior. Therefore a proper understanding of the nature of this antenna required extensive parameter-wise characterization. The analysis program was preferred for generating this data to an extensive series of measurements. This required validating the theoretical analysis by comparing it with a select set of measurements. The computed results were found to be inaccurate as the strip inclination was reduced. A series of experiments were conducted to identify the reasons for this behavior. It was found that the approximations used in the formulation was not quite true at lower strip inclinations, and this lead to the errors.

Computed results with respect to 8 parameters of the strip excited slot were made. Certain observations are as follows. The strip angle could change the conductance of the element over a very wide range. By changing the strip inclination from θ to $-\theta$ the slot voltage can be flipped. It is found that the slot ceases to radiate at both 0^0 and 90^0 strip angle. The strip length could be adjusted to change the resonant frequency of the element. The variation of resonant frequency with respect to strip length was found to be nearly linear. The substrate permittivity changes the resonant frequency and conductance considerably. The radiated power first increases and then decreases with the substrate thickness. Similar effect was found for the slot width. Any relative offset between strip and the slot was found to increase the resonant frequency. The bandwidth of the element increases as the slot was made to approach its unloaded resonant length.

Array design aspects using the strip excited slot were discussed based on Elliott's work on longitudinal slot arrays. An array element should possess the ability to achieve any shunt admittance, if an array is to designed in the presence of mutual coupling. For the strip excited slot, a suitable combination of strip length and strip angle exist such that any admittance could be realized. A design curve was generated from which the required strip parameters could be read for a given admittance. An experiment was conducted to verify the validity of the design curve at a set of 5 points. The theoretical results shows moderate agreement in conductance values, however the resonant frequency was considerably off. This experiment confirms the observation that the computed results are inaccurate at lower strip angles. This experiment also suggests the significance of theoretically generated results in conducting systematic initial trials.

Chapter 6

Summary and Conclusions

A method of exciting the narrow wall vertical non-wrap around slot was presented in this thesis. The method makes use of an inclined or an L shaped strip for exciting the slot. The strip and the slot can be etched together on either sides of a dielectric substrate and can be substituted for the narrow wall. It is possible to get good accuracy and square ended slots, since this method makes use of printed circuit technology.

This thesis has presented a complete investigation of the strip excited slot as a prospective array element. Both computations and measurements were used for an in-depth parameter wise study. The measured results were used primarily for illustrating certain effects—that of ground plane, losses etc.—for which computations could not be carried out.

6.1 Strip Excited Slot—Major Characteristics

• The strip excited slot is predominantly a shunt discontinuity which goes through a radiating series resonance. It also exhibits multiple resonances for certain choice of parameters, in which case it has broader bandwidth.

• An L shaped strip can also be used to couple the slot to an incident LSE_{10} mode. The slot was found to get excited (for both inclined strip and L-strip) even in the extreme, when the strip does not overlap with the slot.

• In the absence of the slot, the strip scatters on its own and appears as a series L–C circuit in shunt. The measurement, however indicated a significant real part which is indicative of the losses in the antenna. This happens, since the resonant strip current is much larger than its value at the combined resonant frequency when the strip and the slot are present simultaneously.

• The strip length and the strip angle affect the resonant frequency and admittance of the element considerably. The resonant conductance increases with strip angle. The resonant frequency also goes up with strip angle. Therefore, the coupling and resonant point are tied up. However, the resonant frequency is found to scale linearly with strip length, so that, a given admittance can be realized by a suitable choice of strip length and angle.

• The length of the slot decides the bandwidth of the element. Bandwidth increases (approximately) linearly with the normalized slot length, and for practical applications it is necessary to choose the slot length as close to its unloaded resonant length. This necessitates the use of a non-standard waveguide with an increased narrow wall dimension.

• The effect of offsetting the strip horizontally was to increase the resonant frequency and to reduce the resonant conductance. The vertical offset of the

strip, however did not show any noticeable effects. The radiated power was found to go through a maximum with respect to the substrate thickness.

6.2   Quadrature Methods for MoM Matrix Entries

The analysis of the strip excited slot via. integral equation (solved using MoM), was exceptionally involved. The inclination of the strip along the z direction and the presence of the $e^{-\gamma|z-z'|}$ factor in the waveguide Green's function, complicates the MoM matrix quadratures. This problem was identified as one which calls for an elaborate symbolism and an algorithm was developed for implementing the same. The algorithm was based on two ideas: the recognition of a multiple integral as a binary tree, and the representation of trigonometric function in exponential form. These two results were used to decouple the source and field points such that the quadrature could be expressed algorithmically.

6.3 $E_z(J_z)$ Green's Function as a Distribution

Green's functions are distributions, whereas the scattered field derived using them are classical functions. The subtle issues involved, in using a Green's function, if one of the source domain quadratures are dropped has been explained. It was shown that, in the event of neglecting the x' quadrature, the E_z field remains a distribution due to the presence of $\delta(x - x')$. The major result of this study is that, for the E_z component to make sense, it is necessary to use an *LSM* represented Dirac Delta. An algorithm for implementing the Gram-Schmidt orthonormalization has been developed in this connection. The numerical subtraction of Dirac delta is also shown to be unstable in the limit of summing large number of modes.

6.4   Solution of LSE and LSM Eigenvalues

The *LSE* and *LSM* eigenvalues are used extensively in the computations, since the waveguide Green's function involves a series of *LSE* and *LSM* normal modes. A robust algorithm for solving these values, for an inhomogeneously filled waveguide has been presented. The algorithm makes use of a modified Newton-Raphson-Bisection root finding. The procedure is based on set of simple results for the *LSE* and *LSM* curves based on the properties of tan functions. These provided good starting values and tight bounds for the root finding scheme.

6.5   Theory and Practice of Method of Moments

Method of Moment attempts to solve a first kind integral equation with complete disregard for the essential ill-posedness of the problem. The method does not give progressively better solutions as it claims to be, but the sequence of solutions initially improves and then goes unstable: a behavior typical of direct methods for first kind integral equations. A set of examples were used to illustrate this point. Tikhonov Regularization forms the right basis for explaining the instability issues and for developing stable MoM algorithms.

6.6   Measurement Techniques

TRL calibration has been used for measuring the S parameters of the strip excited slot, since conventional waveguide standards could not conveniently set the measurement plane at the slot center. The design and implementation of the TRL calibration standards were dealt with. The test antenna was fabricated on

a machined waveguide, to which a printed substrate was attached via. soldering. The effect of the ground plane was a shift in the resonant frequency by 0.5%. The losses in the structure were found to be substantial if the strip is made resonant in the absence of the slot.

6.7 Scope for Further Work

The study carried out in this thesis could be repeated for an L shaped strip, since the L-strip is simpler to analyze. It is necessary to generate accurate design data, and develop an algorithm for implementing an array of strip excited slots. The practical issues of making a planar array are to be sorted out. Since the analysis can be used to compute (to a first order), both the external and internal LSE_{20} mode mutual coupling, this data also should be generated and validated.

The study on $E_z(J_z)$ Green's function as a distribution gave a nearly acceptable solution to the problem of subtracting a Dirac Delta numerically. Since this problem is of interest in inhomogeneously filled waveguides with an axial source, the method is to be improved, if the errors due to residual delta is to be removed completely.

A *numerically* acceptable implementation of MoM should be developed on the lines of Tikhonov Regularization. Such an attempt will help the EM community consolidate the thumb rules used to get optimum solutions in a numerical implementation. It improves the authenticity of the computed results, which otherwise is difficult to accept, in the absence of specifying how the author reaches at the correct value.

References

[1] A. F. Stevenson, "Theory of slots in rectangular wave-guides," *J. Appl. Phys.*, vol. 19, pp. 24–38, January 1948.

[2] A. A. Oliner, "The impedance properties of narrow radiating slots in the broad face of rectangular waveguide: pt.1- theory, part 2-comparison with measurement," *IRE Trans. Antennas Propagat.*, vol. 5, pp. 4–20, January 1957.

[3] T. Vu Khac and C. T. Carson, "Impedance properties of a longitudinal slot antenna in the broad face of a rectangular waveguide," *IEEE Trans. Antennas Propagat.*, vol. 21, pp. 708–710, September 1973.

[4] H. Y. Yee, "Impedance of a narrow longitudinal shunt slot in a slotted waveguide array," *IEEE Trans. Antennas Propagat.*, vol. 22, pp. 589–592, July 1974.

[5] R. W. Lyon and A. J. Sangster, "Efficient moment method analysis of radiating slots in a thick-walled rectangular waveguide," *IEE Proc., Part.H*, vol. 128, no. 4, pp. 197–205, August 1981.

[6] P. K. Park, G. J. Stern, and R. S. Elliott, "An improved technique for the evaluation of transverse slot discontinuities in rectangular waveguide,"

IEEE Trans. Antennas Propagat., vol. 31, no. 1, pp. 148–153, January 1983.

[7] G. J. Stern and R. S. Elliott, "Resonant length of longitudinal slots and validity of circuit representation: Theory and experiment," *IEEE Trans. Antennas Propagat.,* vol. 33, no. 11, pp. 1264–1271, November 1985.

[8] L. G. Josefsson, "Analysis of longitudinal slots in rectangular waveguides," *IEEE Trans. Antennas Propagat.,* vol. 35, no. 12, pp. 1351–1357, December 1987.

[9] S. R. Rengarajan, "Compound radiating slots in a broad wall of a rectangular waveguide," *IEEE Trans. Antennas Propagat.,* vol. 37, no. 9, pp. 1116–1123, September 1989.

[10] J. Joubert and D. A. McNamara, "Analysis of radiating slots in a rectangular waveguide inhomogeneously loaded with a dielectric slab," *IEEE Trans. Antennas Propagat.,* vol. 41, no. 9, pp. 1212–1221, September 1993.

[11] J. Joubert, *The Analysis of Radiating Slots in Rectangular Waveguide Inhomogeneously Loaded with a Dielectric Slab,* Ph.D. thesis, University of Pretoria, Pretoria, South Africa, 0002, May 1991.

[12] B. J. Maxum, "Resonant slots with independent control of amplitude and phase," *IRE Trans. Antennas Propagat.,* vol. 8, pp. 384–388, July 1960.

[13] S. R. Rengarajan and E. Gabrelian, "Efficient and accurate evaluation of external mutual coupling between compound broad wall slots," *IEEE Trans. Antennas Propagat.,* vol. 40, no. 6, pp. 733–737, June 1992.

[14] S. R. Rengarajan and A. G. Derneryd, "Application of compound coupling slots in the design of shaped beam antenna patterns," *IEEE Trans. Antennas Propagat.,* vol. 41, no. 1, pp. 59–65, January 1993.

[15] S. R. Rengarajan, "Higher order mode coupling effects in the feeding waveguide of a planar slot array," *IEEE Trans. Microwave Theory Tech.*, vol. 39, no. 7, pp. 1219–1223, July 1991.

[16] R. S. Elliott and W. R. O'Loughlin, "The design of slot arrays including internal mutual coupling," *IEEE Trans. Antennas Propagat.*, vol. 34, no. 9, pp. 1149–1154, September 1986.

[17] R. S. Elliott, "An improved design procedure for small arrays of shunt slots," *IEEE Trans. Antennas Propagat.*, vol. 31, no. 1, pp. 48–53, January 1983.

[18] R. S. Elliott, "The design of waveguide-fed slot arrays," in *Antenna Handbook*, Y. T. Lo and S. W. Lee, Eds., chapter 12, pp. 1–38. Van Nostrand Reinhold, New York, 1988.

[19] C. P. Espino and S. R. Rengarajan, "Longitudinal component of aperture electric field in weakly-excited broadwall slot," *Electron. Lett.*, vol. 28, no. 10, pp. 909–911, May 1992.

[20] D. A. McNamara, J. P. Jacobs, and J. Joubert, "Form of field in small-offset longitudinal slot in broad wall of rectangular waveguide," *Electron. Lett.*, vol. 28, no. 1, pp. 16–17, January 1992.

[21] R. E. Clapp, "Probe-fed slots as radiating elements in linear arrays," Tech. Rep. 455, MIT Radiation Lab., January 1944.

[22] R. Tang, "A slot with variable coupling and its application to a linear array," *IRE Trans. Antennas Propagat.*, pp. 97–101, January 1960.

[23] A. Datta, A. Chakraborty, and B.N. Das, "Analysis of a strip loaded resonant longitudinal slot in the broad wall of a rectangular waveguide," *IEE Proc., Part.H*, vol. 140, no. 2, pp. 135–140, April 1993.

[24] J. S. Ajioka, "Frequency-scan antennas," in *Antenna Engineering Handbook*, R. C. Johnson and H. Jasik, Eds., chapter 19, pp. 22–26. McGraw-Hill, New York, 1984.

[25] S. Hashemi-Yeganeh and R. S. Elliott, "Analysis of untilted edge slots excited by tilted wires," *IEEE Trans. Antennas Propagat.*, vol. 38, no. 11, pp. 1737–1745, November 1990.

[26] Apu Sivadas, "Analysis of probe fed waveguide slot," M.Tech thesis, Indian Institute of Technology, Kanpur, Department of Electrical Engineering, Kanpur, India, 208 016, December 1992.

[27] H. Y. Yee and P. Stellitano, "I-slot characteristics," *IEEE Trans. Antennas Propagat.*, vol. 40, no. 2, pp. 224–228, February 1992.

[28] T. Sphicopoulos, "C-slot:a practical solution for phased arrays of radiating slots located on the narrow side of rectangular, waveguides," *IEE Proc., Part.H*, vol. 129, no. 2, pp. 49–55, April 1982.

[29] Daniel Caer and Jean Le Foll, "Waveguide with noninclined radiating slots excited by flat metal plates," *IEEE Microwave and Guided Wave Lett.*, vol. 6, no. 6, pp. 244, June 1996.

[30] Shung Wu Lee, William R. Jones, and James J. Campbell, "Convergence of numerical solutions of iris-type discontinuity problems," *IEEE Trans. Microwave Theory Tech.*, vol. 19, no. 6, pp. 528–536, June 1971.

[31] Raj Mittra, T. Itoh, and Ti-Shu Li, "Analytical and numerical studies of the relative convergence phenomenon arising in the solution of an integral equation by the moment method," *IEEE Trans. Microwave Theory Tech.*, vol. 20, no. 2, pp. 96–104, February 1972.

[32] M. Leroy, "On the convergence of numerical results in modal analysis," *IEEE Trans. Antennas Propagat.*, vol. 31, no. 4, pp. 655–659, July 1983.

[33] R. E. Collin, *Field Theory of Guided Waves*, chapter 5, pp. 358–362, IEEE Press, New Jersey, second edition, 1991.

[34] S. R. Rengarajan and G. M. Shaw, "Accurate characterization of coupling junctions in waveguide-fed planar slot arrays," *IEEE Trans. Microwave Theory Tech.*, vol. 42, no. 12, pp. 2239–2248, December 1994.

[35] J. P. Mahon, "An alternative representation for green's functions used in rectangular waveguide slot analysis," *J. Electromag. Waves Appl.*, vol. 4, no. 7, pp. 661–672, 1990.

[36] Numerical Algorithms Group, United Kingdom, *Nag Fortran Library Manual, Mark.14*, 1990, Vol.1 Quadrature; Vol.5 Solution of Simultaneous, Linear Equations; Vol.8 Special Functions.

[37] J. Joubert and D. A. McNamara, "Dyadic green's function of electric type for inhomogeneously loaded rectangular waveguides," *IEE Proc., Part.H*, vol. 136, no. 6, pp. 469–474, December 1989.

[38] H. Jin and W. Lin, "Dyadic green's functions for a rectangular waveguide with an E-plane dielectric slab," *IEE Proc., Part.H*, vol. 137, no. 4, pp. 231–234, August 1990.

[39] A. D. Bresler, G. H. Joshi, and N. Marcuvitz, "Orthogonality properties for modes in passive and active uniform wave guides," *J. Appl. Phys.*, vol. 29, no. 5, pp. 794–799, May 1958.

[40] Y. Rahmat-Samii, "On the question of computation of the dyadic green's function at the source region in waveguides and cavities," *IEEE Trans. Microwave Theory Tech.*, vol. 23, pp. 762–765, September 1975.

[41] William H. Press, Saul A. Teukolsky, William T. Vetterling, and Brian P. Flannery, *Numerical Recipes in Fortran*, chapter 9, pp. 359–360, Cambridge University Press, New Delhi, second edition, 1993.

[42] Kôsaku Yosida, *Functional Analysis*, chapter 6, p. 182, Narosa Publishing House, New Delhi, 1974.

[43] A. N. Tikhonov and V. Y. Arsenin, *Solutions of Ill-Posed Problems*, John-Wiley, New York, 1977.

[44] L. M. Delves and J. L. Mohamed, *Computational Methods for Integral Equations*, chapter 12, pp. 299–325, Cambridge University Press, 1985.

[45] Christopher T. H. Baker, *The Numerical treatment of integral equations*, chapter 5, pp. 635–684, Clarendon Press, Oxford, 1977.

[46] Ross A. Speciale, "A generalization of the TSD network-analyzer calibration procedure, covering n-port scattering-parameter measurements, affected by leakage errors," *IEEE Trans. Microwave Theory Tech.*, vol. 25, no. 12, pp. 1100–1115, December 1977.

[47] Hewlett-Packard, *Product Note 8510-8A, Applying the HP 8510 TRL calibration for non-coaxial measurements*, 1992.

[48] R. S. Elliott, "On the design of traveling-wave-fed longitudinal shunt slot arrays," *IEEE Trans. Antennas Propagat.*, vol. 27, no. 5, pp. 717–720, September 1979.

EE- 1996- D- SIV-ANA